CHARACTERIZATION OF MUTATIONS IN THE TERMINAL REPEATS AND CAPSID PROTEINS OF THE ADENO-ASSOCIATED VIRUS TYPE-2

By

SHAUN R. OPIE

A DISSERTATION PRESENTED TO THE GRADUATE SCHOOL
OF THE UNIVERSITY OF FLORIDA IN PARTIAL FULFILLMENT
OF THE REQUIREMENTS FOR THE DEGREE OF
DOCTOR OF PHILOSOPHY

UNIVERSITY OF FLORIDA

2003

This dissertation is dedicated to my family, John, Dona, and Katie, for their love and encouragement.

ACKNOWLEDGMENTS

I would like to express my sincere appreciation to the past and present members of the Muzyczka lab for creating a unique and stimulating environment to work in. I received invaluable scientific discussion and personal encouragment from “Clonemaster” Dr. Ken Warrington Jr.; Dr. “Rowdy” Rodney Brister; “my fraternal lab twin” Dr. Dan Lackner; Dr. Wu Xiao; and Pre-Dr. Hazel Levy who helped to light the path to graduation. I am indebted to Joyce “My Favorite Graduate Secretary” Conners, whose assistance began during arrangements for the initial interview and continued unabated through graduation. I would like to thank Jen Bonjorno from the Lewin lab, and members of The Higher Authority from the Gainesville Rock Gym for their special friendships.

Dr. Sergei Zolotukhin, Micheal Tennant, Marc Potter, Glen and Tina Phillipsberg, Eric Kohlbrenner and the rest of the Vector Core were most helpful lending rotors, reagents, and ridicule. Drs. Mavis and Rob Agbandge-McKenna, Dr. Lakshmanan Govindasamy, and their graduate students helped to guide me through the beauty and complexity of computer modeling. These labs provided me access and assistance to technologies that were instrumental in generating the data for much of this dissertation.

I would like to thank my committee members Dr. Alfred Lewin, Dr. Henry Baker, and Dr. Tom Rowe for their pertinent suggestions and good nature.

Finally, I would like to thank my primary mentor, Nick Muzyczka, for his enduring patience and financial support.

TABLE OF CONTENTS

Page

LIST OF TABLES

LIST OF FIGURES

LIST OF ABBREVIATIONS

AAV	adeno-associated virus
Ad	adenovirus
CAR	coxackie/adenovirus receptor
CBA	chicken β-actin
CHO	Chinese hamster ovary
CMV	cytomegalovirus
EDTA	ethylenediaminetetraacetic acid
EE	early endosome
FACS	fluorescence activated cell sorting
FGF	fibroblast growth factor
FGFR	fibroblast growth factor receptor
GFP	green fluorescent protein
GAG	glycosaminoglycan
GCA	green cell assay
HPI	hours post infection
HSPG	heparan sulfate proteoglycan
HSV	herpes simplex virus
KDa	kilodalton
MBP	maltose binding protein
MOI	multiplicity of infection
NaCl	sodium chloride
NPC	nuclear pore complex
NLS	nuclear localization signal
PEG	polyethylene glycol 8000
PFU	plaque forming units
PI3K	phosphotidylinositol-3-kinase
RBE	Rep binding element
RGD	arginine-glycine-aspartate
RF	replicative form
RIPA	radio-immunoprecipitation assay
RT-PCR	real time PCR
SDS	sodium dodecyl sulfate
TR	terminal repeat
trs	terminal resolution site
VA	virus associated
WPRE	woodchuck hepatitis virus post-transcriptional regulatory element
WT	wild type

Abstract of Dissertation Presented to the Graduate School
of the University of Florida in Partial Fulfillment of the
Requirements for the Degree of Doctor of Philosophy

CHARACTERIZATION OF MUTATIONS IN THE TERMINAL REPEATS AND CAPSID PROTEINS OF THE ADENO-ASSOCIATED VIRUS TYPE-2

By

Shaun R. Opie

May 2003

Chair: Nicholas Muzyczka
Major Department: Molecular Genetics and Microbiology

The adeno-associated virus type-2 (AAV2) has received considerable attention as a gene therapy vector. All current AAV2 vectors share two elements, the terminal repeats (TRs) and the capsid. The TRs are believed to be essential *cis*-DNA elements that participate in the majority of viral intracellular activities including priming DNA replication, transcriptional regulation, directed integration, proviral rescue, and genome packaging. The TRs fold back on themselves in solution forming a stable T-shaped secondary structure that can be endonucleolytically nicked in a strand- and site-specific manner by the Rep protein. Here we produce recombinant viruses with mutations in the TR known to enhance and inhibit nicking and we examine the effects during an infection *in vivo*. We demonstrate that Rep binding and nicking are required for efficient replication from a plasmid template. Importantly, we generated a recombinant virus that is wild type in every respect except that it is unable to integrate into

human chromosome 19. In addition, we show that *in vivo* the p40 Cap proteins are expressed at high levels independent of detectable Rep expression.

The capsid is an icosahedral protein shell (composed of 60 structurally equivalent subunits) that protects the AAV genome from degradation and that physically docks to the cell to initiate a virus infection. Here we identify the specific amino acids on the surface of the capsid that facilitate to binding to the cell surface receptor heparin sulfate proteoglycan (HSPG). Our data indicate that a spatially clustered array of four arginines and one lysine, including residues 484, 487, 532, 585, and 588, are primarily responsible for HSPG binding, and therefore for infectivity. Substituting a six amino acid stretch containing residues 585 and 588 into the HSPG binding-deficient serotype AAV5 conferred heparin binding *in vitro*, suggesting that these are the minimal necessary and sufficient requirements for HSPG binding

CHAPTER 1
INTRODUCTION AND BACKGROUND

Biology of Adeno-Associated Virus Type-2 (AAV2)

The morbidity and mortality that can result from a viral infection has profoundly impacted the direction and pace of modern medicine. Addressing the mechanisms by which viruses enter, replicate and spread to susceptible cells is essential for understanding the complete process of infection, and essential for designing safer gene therapy vectors and vaccines. The adeno-associated virus type-2 (AAV2) has emerged as a versatile model system for exploring these areas. Initially discovered as a contaminant of adenovirus preparations, AAV2 is a small eukaryotic DNA virus with a linear, mostly single-stranded genome that replicates in the host nucleus using cellular factors (38). AAV2 is considered a defective virus as it normally relies upon co-infection with a helper virus, usually adenovirus (Ad), for efficient replication, gene expression, and virion synthesis. Ad proteins do not have a direct role in these processes, but instead induce a productive infection by altering the cellular environment. In the absence of Ad, AAV2 has the ability unique among eukaryotic DNA viruses to persist in the infected cell by targeted integration into the long arm of chromosome 19 in the human genome (16, 46) or as a stable episome (59). The provirus is remarkably stable while maintained in chromatin form. However, upon subsequent helper

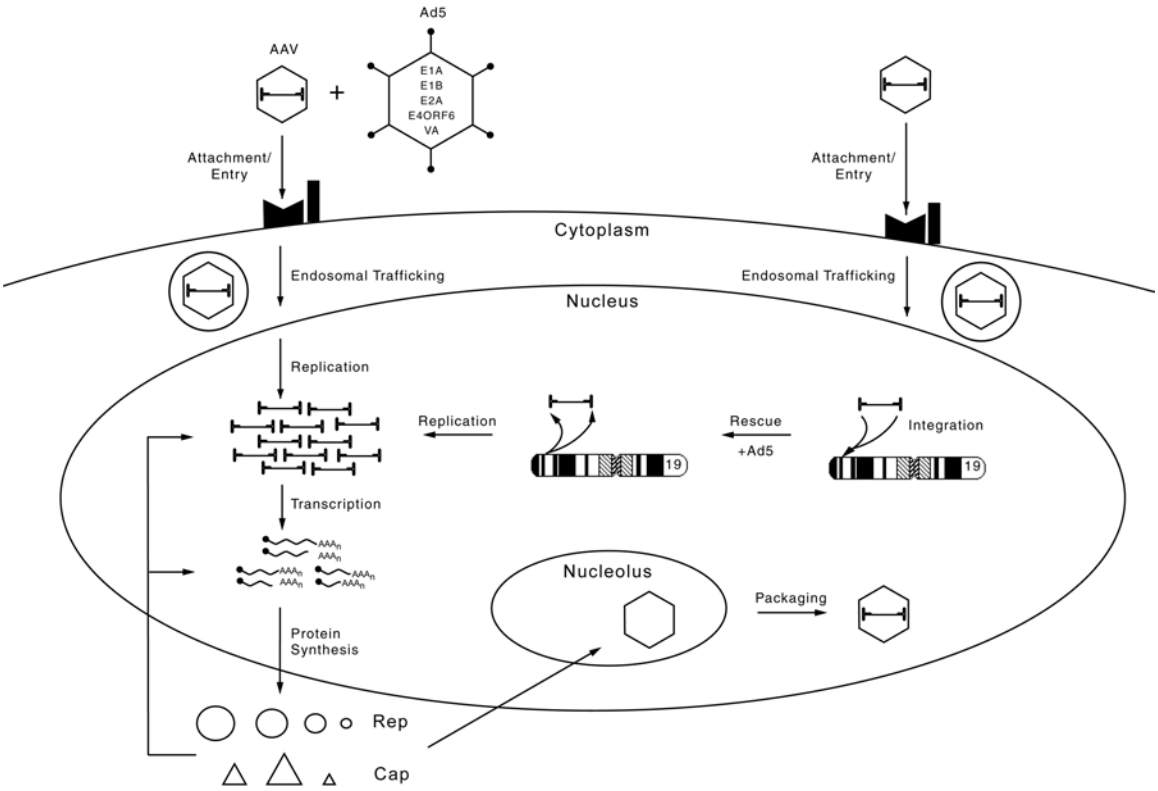

Figure 1-1. The AAV2 life cycle. The lytic and latent pathways of the AAV2 life cycle are shown. Adenovirus gene products are required for efficient replication, transcription, and packaging of single-stranded genomes into for production of infectious virions. In the absence of Ad, AAV2 migrates to the nucleus and integrates preferentially into human chromosome 19. Subsequent adenovirus infection initiates efficient genome reactivation, excision from the host DNA, and synthesis of progeny virus.

Organization of the AAV2 Genome

AAV2 has a remarkably simple genetic structure, condensing its entire coding and regulatory content into 4765 nucleotides of mostly single-stranded DNA (82). Two large open reading frames (Rep on the left half of the genome and Cap on the right) code for regulatory and structural proteins, respectively (37). Flanking each end of the genome is a noncoding sequence containing three internal palindromes able to fold back upon themselves by complementary base pairing to form a stable T-shaped secondary structure called the terminal repeat (TR) (51). The TR plays an integral role in most aspects of the virus life cycle by acting as an origin of DNA replication, as a strong transcriptional promoter, and as a signal element for both DNA packaging and recombination. Three promoter regions (p5, p19, and p40) determined by their position on a genome 100 map-units (m.u.) coordinately regulate the level of Rep and Cap mRNA expression through interactions with viral and cellular proteins. A short intron spanning m.u.s 42-46 can be removed by the cellular splicing machinery to produce six AAV2 mRNAs 4.2kb, 3.9kb, 3.6kb, 3.3kb, 2.3 and 2.25kb in length. These 3'-capped and 5'-polyadenylated transcripts code for Rep78, Rep68, Rep52, Rep40, VP1, VP2 and VP3, respectively (Fig. 1-2).

Rep Proteins of AAV2

The family of Rep proteins regulates nearly every aspect of the AAV2 life cycle including replication, transcription, packaging, integration, and rescue. Four Rep proteins (Rep78, 68, 52 and 40) were originally identified by antisera raised against an AAV2 infection. They were named for their apparent size

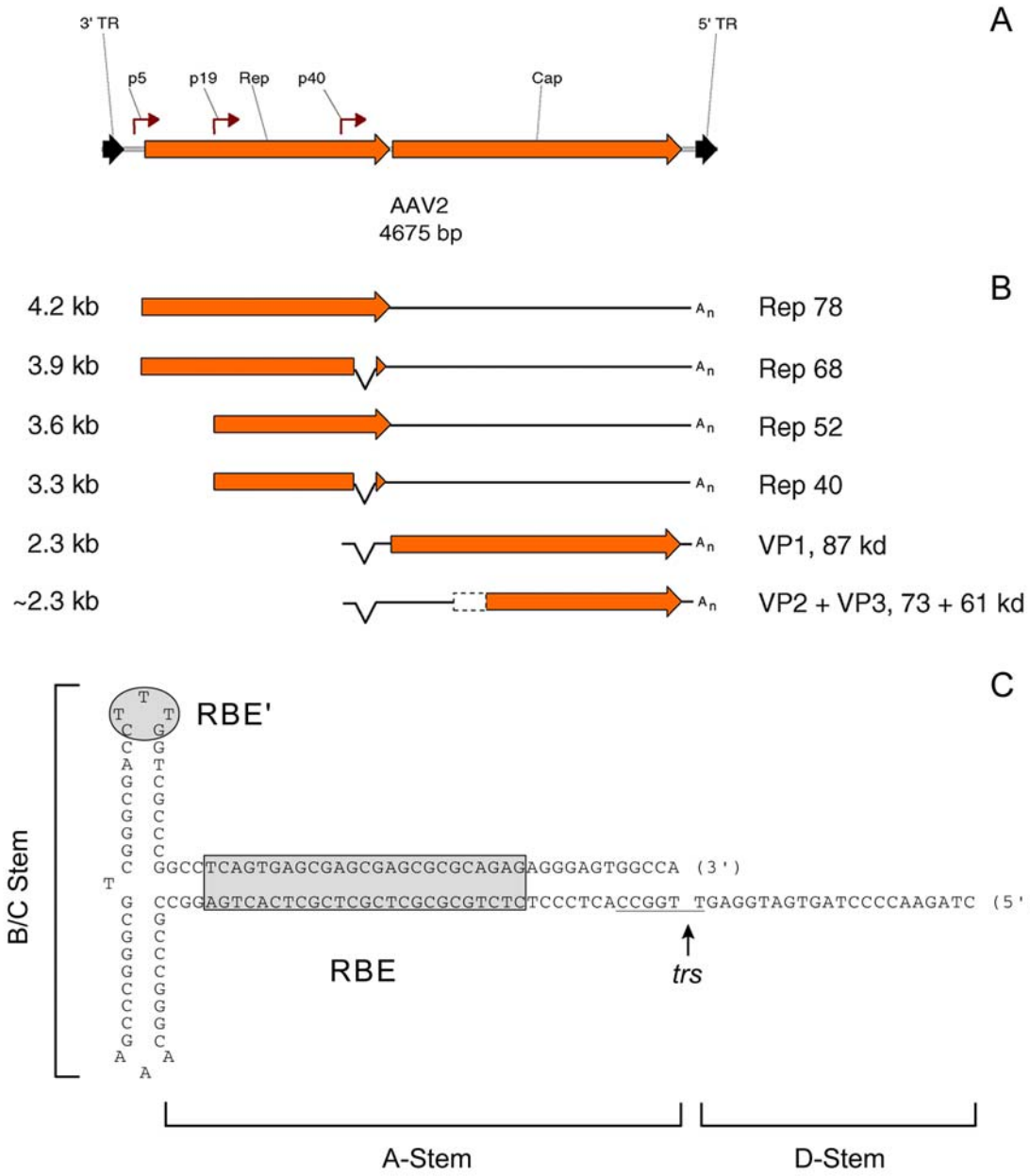

Figure 1-2. Structure of the AAV2 genome. A) The AAV2 genetic map is illustrated with Rep and Cap open reading frames represented as red arrows. Black arrowheads represent the terminal repeat regions. Promoter positions are indicated with bent arrows. B) Primary transcripts and gene products are shown with coding sequence represented as red arrows and non-coding sequence as black lines. The carets indicate spliced regions. C) The AAV2 terminal repeat in hairpinned configuration with internal palindromes is illustrated. The core *trs* site is underlined by a grey bar and the position of the nicked residue by a curved arrow. The RBE and RBE' are shown as a grey box and oval, respectively.

after separation by SDS-PAGE electrophoresis, although their calculated molecular weights are 72, 62, 46 and 34 KDa (87). The p5 and p19 promoters each produce one spliced and one unspliced mRNA that code for the large reps (Rep78/68) and the small reps (Rep 52/40), respectively (34). Understanding of the biology of the rep proteins was facilitated by the production of an infectious AAV2 DNA plasmid clone and by the purification of wild type and mutant forms of Rep protein to near homogeneity (17, 42, 48, 69). The effects of mutations in the Rep gene and the development of *in vitro* protocols contributed to the identification and biochemical characterization of DNA binding, endonuclease (41), ATPase (96, 98, 110), helicase (77, 96, 110), and ligase activities (76) (Fig. 1-3).

Any large mutation in the Rep gene disrupts AAV2 DNA replication. Additionally, AAV2 DNA that contains wild type rep but has deleted TRs is also replication deficient (70, 74). These two early observations linking Rep and the TR to the same activity suggested that a physical interaction occurred between them. Indeed, the amino-terminal 221 amino acids of Rep78/68 constitute a DNA binding domain that can associate with a linear 25 bp DNA sequence within the TR called the Rep binding element (RBE) (17, 61, 68). An intact TR is the optimal substrate for Rep68 binding with a $Kd=2x10^{9}\ M^{-1}$ (63), although other nearly homologous nucleotide sequences in AAV2 DNA and in the human genome can recruit Rep with lower affinities (91, 97). Mutations in the Rep protein that abolish TR binding also disrupt rescue, replication,

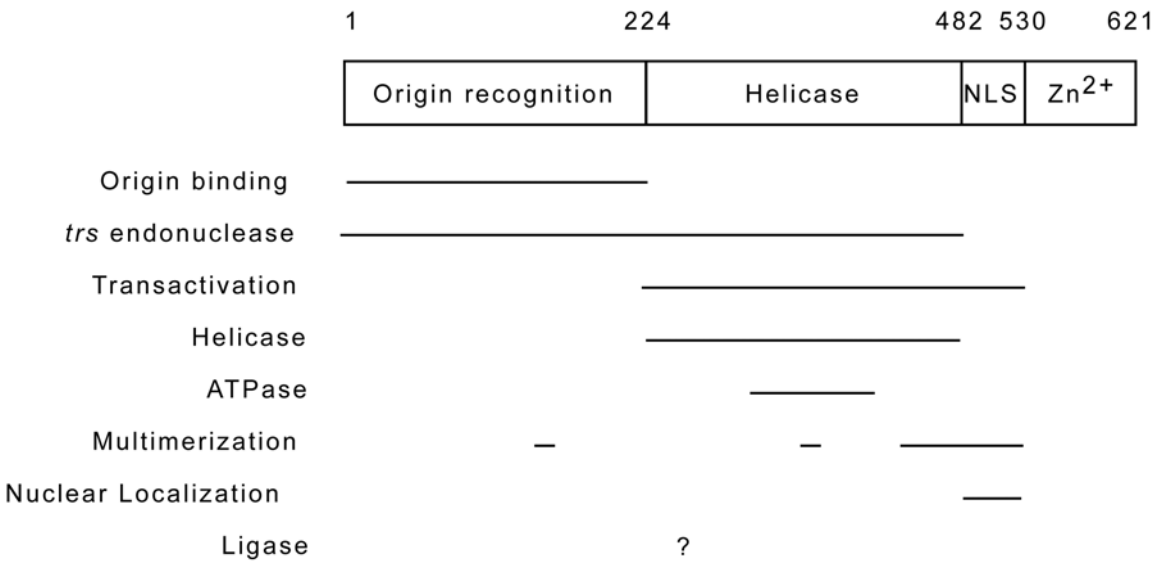

Figure 1-3. Biochemical activities and functional domains of Rep. The rectangles with numbers above them are Rep. Major activities and structural features are shown. Black lines show regions of Rep that have been localized for a particular biochemical activities. The question mark shows activities that have not been mapped. NLS = nuclear localization signal. Zn^{2+} = zinc finger.

transcriptional regulation, and integration. This suggests that binding is the initial and necessary event for regulating multiple pathways.

Rep78/68 possesses an endonuclease activity that can introduce a nick into the AAV2 TR (41). The cut is both strand- and site-specific occurring between two thymidines in the sequence 5'-GT/TGGCC-3' and requires ATP on a double-stranded substrate. These nucleotides constitute the core terminal resolution site (*trs)* and are highly conserved among AAV serotypes (11). In addition, there are specific spacing requirements from the RBE, as even small insertions between them dramatically reduce nicking efficiency (10). As part of the process of terminal resolution, *trs* nicking was originally proposed as a mechanism to explain how parvoviruses duplicate the extreme ends of their DNA during replication. Given the size and complexity of the human genome, it is not surprising that an RBE homolog and core *trs* with appropriate spacing occurs that can be bound and nicked by Rep78 (91, 97).

Detectable by database searches for protein motifs is a nucleoside tri-phosphate binding pocket in the central portion of all the Rep proteins that can capture and promote the hydrolysis of ATP (3). Mutations inside the NTP binding pocket, in particular at the catalytic lysine at amino acid residue 340, completely disrupt replication and transactivation (96). Although not required for TR binding, ATP hydrolysis is thought to provide a necessary source of energy for the fundamental activities in AAV2 life cycle functions performed by Rep.

Rep78, 68, and 52 showed an ATP-dependent ability to unwind double-stranded DNA in a 3'-5' direction (77, 96, 110). Helicase activity of the large

Reps is thought to promote stem-loop formation required for *trs* clevage during DNA replication and may also enable it to participate directly in promoting movement of the polymerase complex along the template. In contrast, Rep52 helicase activity is associated with the physical process of packaging DNA efficiently into the capsid (45). Reps52 lacks the amino-terminal DNA binding domain required for TR binding and nicking which suggests that it is recruited to the capsid through Rep:Rep protein interactions or by direct association with the capsid.

Wild-type AAV2 preferentially integrates into the human chromosome 19q13.3-qter region called AAVS1 when Ad is not present (46). In contrast, recombinant vectors randomly integrate at much lower frequencies suggesting that Rep directly catalyzes this activity. Several lines of evidence support this hypothesis. First, the AAV2S1 region contains a RBE homolog in close proximity to a *trs*-like sequence that can be bound and cleaved by Rep78 (31, 49, 91). Second, the large Reps can multimerize into higher order protein/DNA complexes capable of forming a physical bridge between the AAV2 TR and the AAVS1 sequence (78, 91). Third, Rep is required *in vitro* for the efficient formation of junctions between AAV2 TR sequences and a plasmid construct containing the cloned AAVS1 integration locus (26). Fourth, a purified maltose-binding protein (MBP)-Rep78 expressed from E. coli is able to ligate small oligonucleotides derived from the AAV2 origin of DNA replication in an ATP dependent manner (76). Taken together, these activities describe a possible Rep-mediated mechanism used by AAV2 to achieve site-specific integration.

Subcellular fractionation and immunocytochemsitry of Ad- and AAV2-infected cells show that Rep78/68 are predominantly nuclear proteins while Rep52/40 are distributed equally between the nucleus and cytoplasm (40, 94). It is unclear if Rep52/40 are imported with lower efficiency or if a mechanism exists to cycle between the nucleus and the cytoplasm. Rep is retained in the cytoplasm when a SV40-like nuclear localization signal in the carboxyl-terminus of the protein is mutated and inhibits both replication and transcriptional repression from p5 (106).

Cap Proteins of AAV2

The family of cap proteins are involved in forming the protein shell that protects AAV2 DNA and binds to the cell surface receptor. In purified virions, three structural proteins (VP1, VP2, and VP3 with molecular masses of 87, 73, and 62 KDa respectively) are present in an approximate molar ratio of 1:1:10 (12). Accordingly, the major mRNA originating from p40 is the shortest spliced variant translated from an internal ATG start codon to generate VP3 (33, 34). The comparatively lower amounts of VP1 and VP2 are likely due to a weak ACG start codon for VP2, and to low levels of unspliced VP1 mRNAs. Capsid proteins are translated in the same open reading frame and therefore share an identical 532 carboxy-terminal amino acid domain (5, 6) (Fig. 1-4). In this sense, VP2 and VP3 represent successive amino terminal truncations of VP1.

Immunohistochemistry and subcellular fractionation show that after synthesis in the cytoplasm the capsid proteins are translocated efficiently to the nucleus (94). Four putative nuclear localization signals (NLS) in the capsid coding sequence can be identified by homology searches in protein motif

databases (Fig 1-4). One group observed that truncating the amino terminal 45 residues from VP2 (which deleted the putative nuclear localization signal PARKRLN) prevented nuclear accumulation of VP3, suggesting that VP2 may act as a transport protein for VP3 (39). However, unpublished data from our lab show that infectious virus particles can be recovered when VP3 is expressed alone. This result suggests that VP3 harbors a functional nuclear localization signal and VP3 is sufficient for capsid assembly and DNA encapsidation. The role of the unique region of VP1 is essential. Mutations that span amino acid residues 40 to 100 generally disrupt infectivity but not capsid assembly or packaging (37, 99). Multiple sequence alignments revealed that this region in all densoviruses and parvoviruses contains a phospholipase A2-like domain (107). When the catalytic histidine and aspartate residues are mutated, confocal microscopy shows that trafficking of the virus is blocked at the periphery of the nuclear membrane (32).

AAV2 particles have T=1 icosahedral symmetry with a maximum external radius of 240 angstroms and a molecular weight of about 4×10^6 Daltons. Only recently have crystals of sufficient size and quality been grown for resolving the atomic structure of AAV2. Before this information was available, AAV2 serotype capsid protein sequences were aligned by a least squares fit to the known atomic coordinates of other related parvoviruses to serve as a guide for structural studies. Fortunately, the crystal structure of carboxyl-terminal 518 amino of VP3 (PDB entry: 1LPN) is remarkably consistent with the conclusions reached by

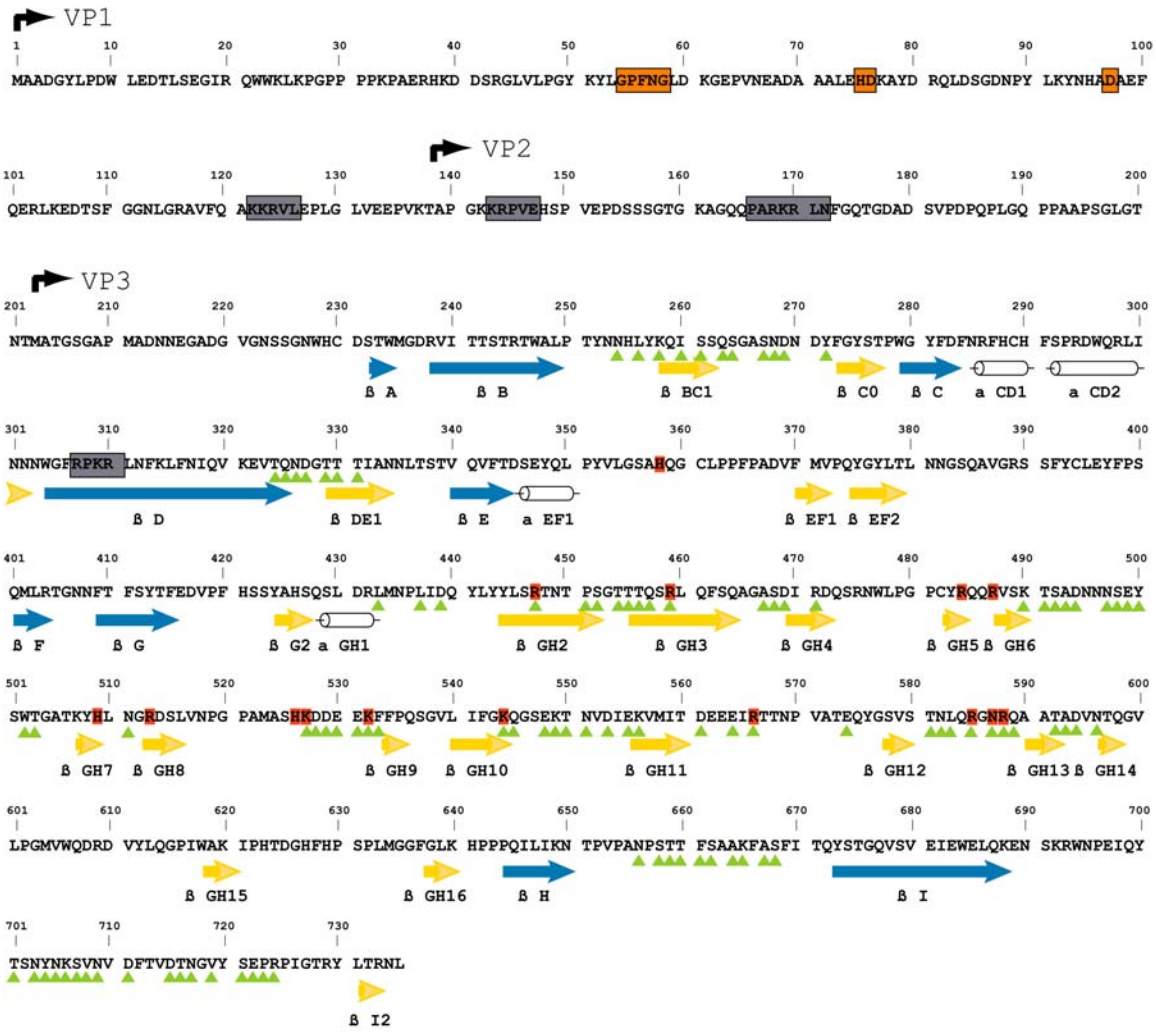

Figure 1-4. Sequence and structure of the AAV2 cap protein. The primary protein sequence for AAV2 VP1 is shown with numbered amino acids. Black arrows identify VP1, VP2, and VP3 start codons. Blue arrows represent core beta strands conserved among parvoviruses. Yellow arrows represent non-conserved beta strands. White cylinders represent alpha helices. Green triangles are surface accessible amino acid residues. Grey boxes represent putative nuclear localization signals. Orange boxes indicate conserved residues required for phospholipase-A2-like activity.

computer modeling and genetic approaches (102). VP1 and VP2 represent about 10% of the assembled capsid and did not provide sufficient electron density to be included in the structural analysis. The core of the subunit is formed by eight highly conserved antiparallel ß-strands that adopt a jellyroll barrel structure and form the capsid interior surface. Connecting the ß-sheets are loops of highly variable length and sequence that extend outward to form the capsid exterior surface (Fig 1-5). The surface of the assembled capsid is contoured with “spikes” found at the 3-fold axis, “dimples” at the 2-fold, and “canyons” at the 5-fold axis (Fig. 1-6). A curious feature of the AAV2 particle is that regions from separate subunits physically overlap at the 3-fold and 5-fold related regions. This intertwining of the peptide subunits is likely to raise the overall stability of the particle consistent with its ability to withstand heating at 70°C for 30 mins, 2 M NaCl, and lysophillization while retaining infectivity.

Model of AAV2 Attachment and Internalization

Incubating cultured cells with a variety of proteases can temporarily abolish infection by most viruses. This early observation for both enveloped and non-enveloped viruses suggested that virus-cell interactions have a protein component found on the cell surface that is required for infectivity. Termed the cell surface receptor, it functions to dock the virus to the cell so that subsequent events permitting membrane penetration and internalization can occur. Although their existence was recognized for decades, until recently receptor identification remained elusive for a large number of viruses.

Summerford and Samulski (86) observed during trial purifications of AAV2 vectors that the virus was efficiently retained on a cellulofine-sulfate column.

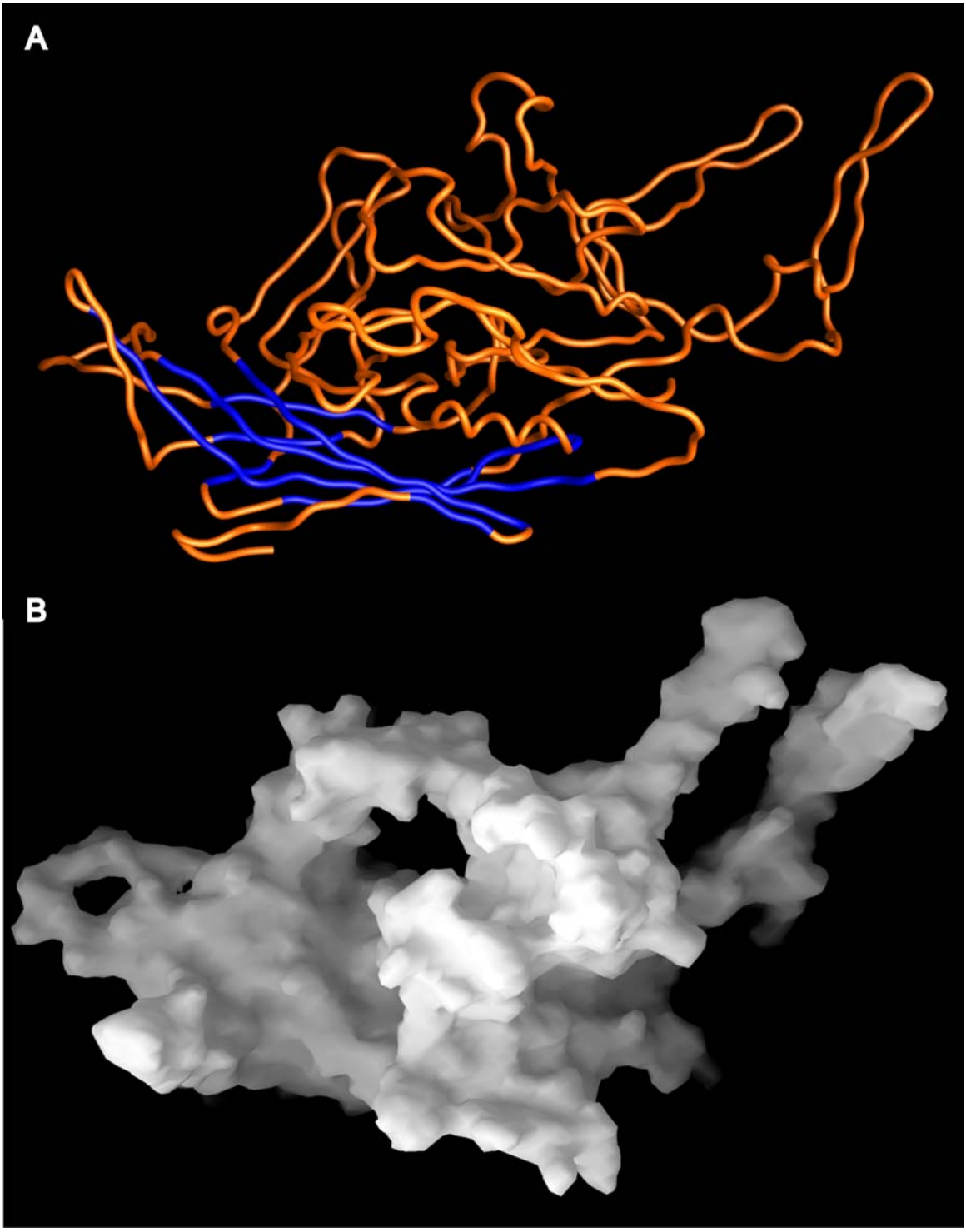

Figure 1-5. AAV2 VP3 structure. A) Ribbon diagram of the VP3 C_{α}-backbone viewed from the side. Conserved β-strands forming the interior surface of the capsid are drawn in blue. B) Surface representation of a VP3 monomer viewed from approximately the same perspective as in (A).

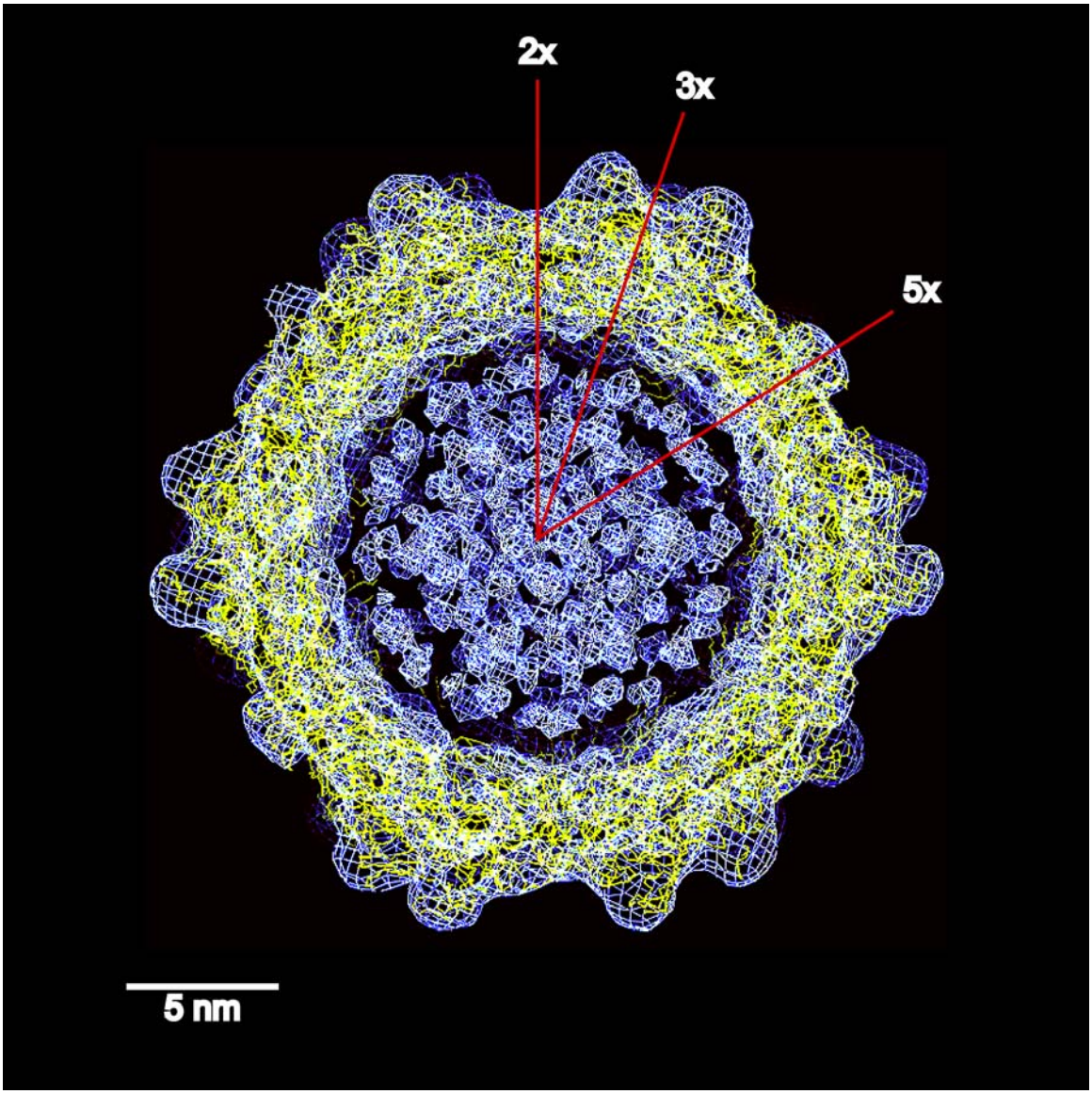

Figure 1-6. Ultrastructure of the parvovirus capsid. A cross section through the center of the parvovirus capsid at 23 angstrom resolution is shown by cryoelectron microscopy reconstruction. Axes of symmetry are indicated by red lines. Electron density is shown as a white grid overlay. The white bar denotes scale = 5 nm.

They suggested that electrostatic attraction between the virus and the highly sulfated affinity matrix might be mimicking the receptor-binding event on the cell surface. Consistent with these predictions, a variety of experiments showed that the heparan sulfate proteoglycan is the primary AAV2 receptor. First, AAV2 transduction in Hela cells is competed by soluble heparin, but not other glycosaminoglycans (GAG) dermatin sulfate, chondroitin sulfate A, or chondroitin sulate C. Second, enzymatic digestion of cell surface GAGs by heparitinase reduced transduction 4-fold. Third, GAG desulfation by sodium chlorate treatment reduced infectivity 5-7 fold. Fourth, soluble heparin inhibited binding of ^{3}H-labeled AAV2 to Hela cells. Finally, five mutant Chinese hamster ovary (CHO) cell lines that have decreased HSPG expression and overall sulfation levels compared to the wt CHO cell line showed corresponding lower levels of binding and infectivity by AAV2. Taken together, these data provide strong evidence that HSPG is the primary cell-surface receptor for AAV2 (65, 86). It is worth noting that complete disruption of AAV2 infection by any of these methods was not observed, suggesting that a secondary attachment receptor or alternative entry pathway may have a role in the AAV2 infectious entry process.

Considerable evolutionary selection pressure exists for non-autonomous parvoviruses to infect the same cell types that Ad infects. Although AAV2 can latently infect a cell without adenovirus, reactivation in a natural environment is dependent on the presence of a co-infecting helper virus. One mechanism to achieve identical tropism would be to share a cell surface receptor. Indeed, there is considerable overlap in receptor usage. At least three cell surface molecules

are involved in Ad5 attachment and internalization. First, similar to AAV2, HSPG functions as a nonspecific attachment molecule and appears not to have any further role in infection (19, 20). Second, the coxackie/adenovirus receptor (CAR) recognizes a pentamer of linear arginine-glycine-aspartate (RGD) motifs in fiber knobs and acts as a high-affinity receptor (8). The AAV2 capsid does not have an RGD sequence so it is unlikely that it is recognized by the CAR receptor (67). Third, the vitronectin-binding integrin $\alpha_V\beta_5$ facilitates adenovirus internalization and membrane permeabilization (92, 93). Internalization of AAV2 is also facilitated by $\alpha_V\beta_5$ and can be efficiently blocked by chelating free calcium ions in cell culture media with 20mM EDTA (85). When mutant cell lines that are defective for $\alpha_V\beta_5$ synthesis are infected with AAV2 the virus is still able to accumulate around the external periphery of the cell, suggesting that integrins are not acting as the primary receptor (85). However, immunoprecipitated $\alpha_V\beta_5$ is detected by AAV2 virions in a virus overlay western assay, suggesting that $\alpha_V\beta_5$ may act as a secondary receptor able to physically interact with AAV2 (85). These data suggest that AAV2 and Ad share at least a primary receptor required for initial docking and another that facilitates membrane penetration.

Heparin sulfate can participate in the formation of a stable heteromeric complex between proteins in the fibroblast growth factor (FGF) and fibroblast growth factor receptor (FGFR) families (21, 83). FGFRs are a family of receptor tyrosine kinases that undergo autophosphorylation and can activate an intracellular signaling cascade upon dimerization with soluble FGF. Given the intimate relationship between FGF and HSPG, Qing et al. (64) hypothesized that

in addition to $\alpha_V\beta_5$, AAV2 might use FGFR as a co-receptor. AAV2 binds poorly to cell lines MO7e and Raji. Neither express HSPG, and Raji cells are also FGFR negative. When HSPG is stably transfected into both cell lines AAV2 efficiently binds and transduces MO7e cells but not Raji cells. Taken together these results suggest that HSPG alone is insufficient for cell attachment, and that a secondary receptor FGFR is required (64).

A new paradigm that implicates a dynamic and multistep process is replacing the classical notion of viral attachment and entry being mediated solely by a single binding event. A growing body of literature concerning virus entry into the cell describes a series of events that begin with a relatively low affinity, nonspecific interaction with common extracellular components as a means for attachment to the cell surface (9, 19, 50, 81). After stable binding to the exterior of the cell, secondary receptor interaction that is specific for particular virus occurs. This is often a high affinity binding event that targets receptor complexes to clathrin-coated membrane invaginations for endocytosis. The remarkable diversity in primary and secondary receptor preferences among viruses is likely to account for their highly variable tropisms.

Model of AAV2 Endosomal Uptake and Trafficking

After an appropriate virus/receptor complex has formed, viruses translocate to the inside of the cell by one of two primary mechanisms: either direct fusion with the cell membrane or internalization into cellular compartments. In general, whereas enveloped viruses undergo fusion with the plasma membrane, non-enveloped viruses use endocytosis as their primary means of entry (75). Endocytic uptake can occur by four independent pathways including clathrin

mediated macropinocytosis, endocytosis, caveolae formation, and novel non-clathrin, non-caveolae endocytosis. Direct visualization of the AAV2 infection process by microscopy shows efficient internalization of virus with a half time less than 10 min followed by rapid perinuclear accumulation (2, 73, 100). The cellular mechanisms and the chronological order of the events that occur during AAV2 endocytosis and during rapid intracellular movement towards the nucleus are currently an area of intensive study.

The formation of clathrin-coated pits from the plasma membrane requires dynamin, a 100KDa cytosolic GTPase that can oligomerize into a ring structure necessary for pinching off coated vesicles. When Hela cells are co-infected with rAAV2 and recombinant adenovirus expressing dynamin K44A, a strong dominant negative mutant of dynamin I, cell surface attachment is unaffected; however transduction is reduced nearly 4-fold (23). Furthermore, by immunohistochemical analysis, rAAV2 is found co-localized with the transferrin and $\alpha_V\beta_5$ integrin proteins, both of which are known to be endocytosed by clathrin-coated pits (23, 71).

Clathrin-coated pit formation can be initiated after phosphotidylinositol-3 kinase (PI3K) is activated by the GTPase rac1. This triggers a signal cascade that ultimately facilitates actin fiber rearrangment surrounding the nascent coated pit. Tracking Cy3-labeled AAV2 capsids by immunofluoresence microscopy showed that transient overexpression of a dominant negative mutant of rac1 leads to AAV2 accumulation on the external surface of the cell membrane. Additionally, a selective inhibitor of phosphoinositide 3-kinase, wortmannin, also

prevented AAV2 endocytosis but not attachment (71). Taken together these data suggest that a primary mechanism of AAV2 entry into the cell is through receptor-mediated endocytosis into clathrin coated pits. Interestingly, transduction was not completely abolished in any of these experiments suggesting that these genetic approaches may be slightly leaky or that an alternative internalization mechanism exists for AAV2. Adenovirus also penetrates the cell membrane through the same coated-pit entry mechanism again highlighting a parallel evolution between Ad and AAV2 (88).

After budding from the cell membrane, the coated vesicle enters the endosomal trafficking pathway. It should be noted that the endosome surrounds an extracellular environment rather than cytoplasmic environment. The endosome is a dynamic vesicle that normally undergoes physiological and structural maturation as it is transported towards the nucleus. The four classes of endocytic vesicles include early endosomes (EE), late endosomes, recycling vesicles, and lysosomes. They have overlapping activities so strict classification is difficult, and they could appropriately be viewed as a cycle. Of particular use are chemical inhibitors that block specific endosomal trafficking activities which helped to partly unravel the components and mechanisms by which AAV2 is translocated towards the nuclear compartment.

A hallmark of the endosomal pathway is the presence of an active vacuolar ATPase that is responsible for translocating protons into the endolysosomal lumen decreasing the pH of vesicles as they progress towards the nucleus. Inhibitors of this activity have been used in a number of virus systems to examine

the requirement for pH change during endosomal trafficking. Inhibition of the vacuolar ATPase with Bafilomycin A1 prevents endosome acidification. When HeLa, 293, and HepG2 cells are treated with bafilomycin A1, AAV2 transduction is reduced in a dose-dependent manner up to 50-fold as measured by luciferase activity (2). Reversible ammonium chloride treatment of cells raises the pH of endosomes as well as other intracellular organelles. As might be predicted, AAV2 transduction was reduced 8-fold in cells exposed to ammonium chloride and was restored after media replacement (2). Taken together, these results suggest that AAV2 infection requires acidification of the endosome for escape into the cytoplasm.

Brefeldin A is an antimycotic that inhibits early to late endosome transition by causing early endosomes to form a restricted tubular network. Pretreatment of HeLa, 293 and HepG2 cells prior to AAV2 infection reduce transduction in a dose dependent manner. (22) Interestingly, adenovirus gene transduction is unaffected by Brefeldin A treatment, consistent with its known ability to escape efficiently from the early endosome in a pH independent manner. These data suggest that trafficking pathways for AAV2 and Ad may diverge at later stages.

In the final stage in endosomal processing, EE's transition into lysosomes that function to degrade and recycle any remaining material. MG-132 is a potent inhibitor of proteolytic activity of the proteosome. When cells are treated with MG-132 AAV2 transduction is increased about 50-fold and the pool of single stranded DNA is increased nearly 10-fold (22). Ubquitinization of the AAV2 capsid prepares it for trafficking to the proteosome. Treating cells with ubquitin

ligase inhibitors results in a 200-fold increase in transduction levels in polarized epithelial cells (25). Taken together, these data suggest that a large proportion of AAV2 capsids are not gaining entry to the nucleus but instead are being trafficked to the proteosome for degradation. This may explain in part the high multiplicities of infection required for robust rAAV2 gene expression.

Classic cytoskeletal disrupting agents, cytochalasin B and nocodazole, destabilize microfilaments and depolymerize microtubules, respectively, and have been studied extensively characterized in several virus systems. Hela cells pretreated with either of these agents prior to AAV2 infection reveal a dispersed pattern AAV2 accumulation throughout the cytoplasm. In addition, there is cytoplasmic accumulation of genomic DNA and low transduction efficiencies under similar conditions. These observations suggest that components of the cytoskeletal architecture are actively involved in transporting endosomes containing AAV2 to the nucleus.

When Adenovirus is present in co-infection studies, a notable change occurs. First, AAV2 can escape prematurely the early endosome and bypass the acidification requirement. This is an interesting observation, as Ad and AAV2 have not been shown to co-localize within endosomes. Clearly, during a co-infection Ad virions will not be replicating at this early stage suggesting that a signal cascade, likely activated by the Ad capsid proteins, rather than a direct mechanism is responsible. Accordingly, empty Ad particles, having no capacity to replicate, are sufficient for this activity (100).

In summary, like many other intracellular parasites, AAV2 relies on the cellular machinery that has evolved for the transport of molecules from the cell membrane to the nucleus and vice-versa. It appears that after binding to cell surface receptors, a regulated, intracellular signal cascade initiates clathrin coated pit to bud for viral uptake into the cell. AAV2 remains inside an endosomal compartment while it is being actively transported along cytoskeletal microtubules and microfilaments. During movement towards the nucleus, the internal pH of the endosome is lowered by a vacuolar ATPase pump and appears necessary for escape at the border of the nuclear membrane.

Model of AAV2 Nuclear Entry and Uncoating

Once released from the endosome AAV2 is still blocked by the nuclear membrane. Clearly, it must be able to transfer its genome past the nuclear envelope so that it can gain access to replication and transcription machinery. There are two primary mechanisms for nuclear entry: either by direct fusion with the nuclear membrane or by transport through the nuclear pore complex (NPC). The most extensively characterized mechanism of nuclear transport involves the NPC. Molecules with a diameter less than 8nm are able to freely diffuse through the NPC, whereas molecules as large as 39nm that possess a nuclear localization peptide sequence can be actively translocated by energy consumption through the NPC (62). Non-enveloped viruses that do not acquire a cell membrane during trafficking are generally thought rely on the NPC in some manner. Transfer of the entire capsid through the NPC may occur, but is not a strict requirement. Electron microscopy showed that Ad docks at the nuclear

pore, partially disassembles, and injects its DNA into the nucleus, whereas the entire hepatitis B virus is actively transported through the nuclear pore (62).

Given that the AAV2 capsid is only 24-26nm in diameter, it is possible that the entire particle can undergo nuclear transport through the NPC. To test this hypothesis, the effects of two NPC inhibitors have been examined. NPC import can be blocked by wheat germ agglutinin (WGA), which binds to O-linked N-actelyglucosamine residues on the NPC, and by thapsigargin, an inhibitor of the endoplasmic reticulum/nuclear membrane calcium pump required for NPC activity. Confocal microscopy of Cy3-fluorophore conjugated AAV2 capsids showed that neither inhibitor prevented AAV2 nuclear entry suggesting that the virus can gain access to the nuclear compartment by an NPC independent or a novel transport mechanism (100).

Data concerning the kinetics of nuclear import results have been variable leading to conflicting conclusions. In one paper, laser scanning confocal microscopy of Cy3-fluorophore conjugated AAV2 capsids detected nuclear localization in 2 hrs (71). In contrast, by immunohistochemistry capsids were not detected in the nucleus until 24-48 hours post-infection (100). Additional DNA hybridization analysis of nuclear and cytoplasmic fractions also supported a delayed nuclear entry. It should be noted that capsid protomer subunits are likely recognized by the A20 antibody used in these studies, and that free Cy3 label can be present in stocks due to degradation. As such, conclusions reached about the physical structure of the capsid as it enters the nucleus should be viewed accordingly. Further improvement in virus labeling and visualization

protocols will certainly help to elucidate apparent contradictions. Interesting, Xiao et al. (100) reported that when Ad was present, AAV2 nuclear entry happened as early as 30 min in either the absence or presence of thapsigargin. These data suggested that the signal cascade initiated by adenovirus has a profound effect on the trafficking and expression of the AAV2 genome.

AAV2 uncoating and genome received little attention primarily due to a lack of technical methodologies. As such, several intriguing questions remain unanswered: Where does uncoating occur? What is the extent of capsid disassembly required for genome release? Do adenoviral or cellular components assist during uncoating? What, if any, is the role of Rep? More sensitive visualization techniques or novel indirect approaches will be necessary before these questions can be answered.

Model of AAV2 DNA Replication

The single strandedness of AAV2 DNA renders the genome transcriptionally silent after nuclear entry. In a normal infection, AAV gene expression requires at least a single round of DNA replication. An exception to this is positive and negative strand re-annealing. However this occurs only at artificially high MOIs. In addition to the host cell polymerase complex, two AAV2 genetic elements are required for virus DNA synthesis. The first is a 145bp TR that acts as the viral origin of replication. The second is the Rep gene. The current model, originally proposed by Hauswirth and Berns (36), predicts that the TR forms a stem-loop structure by folding back upon itself as a result of complementary base pairing to expose a free 3' OH. The double stranded hairpin region and terminal 3' OH serve as a primer for synthesis of a duplex linear DNA

molecule that is covalently joined at one end. The large p5 Rep proteins simultaneously bind to a 26bp Rep binding element (RBE) within the A-stem and a small loop in the tip of the B/C-stem of the TR catalyzing a site-specific and strand-specific nick that exposes a new 3'OH (41, 53, 54, 68). DNA repair synthesis from this priming site generates a complementary full length duplex DNA. After the TR sequence renatures forming another hairpin primer, strand displacement synthesis from the second priming site generates a replicative form (RF) and a single stranded progeny molecule (Fig. 1-7). Progeny DNA is packaged into capsids to form an infectious virion.

Accumulation of Rep the protein alone although necessary, is insufficient for replication. A productive infection is generally associated with Ad. However, herpes simplex virus (HSV) I and II, cytomegalovirus (CMV), and pseudorabies virus are also serve natural helpers (4, 55, 72). The genetic regions of Ad that stimulate AAV2 replication have been well characterized by deletion mutants and include E1a, E1b, E2a, E4 ORF-6 and Virus Associated I(VA_I) RNA (13, 14, 47, 66, 89). E1a is a general transactivating protein and is also able to transform primary cells.

E1b is a transforming protein and like E4-ORF6 is required for the efficient accumulation of AAV2 mRNA. E2a is the adenovirus DNA binding protein and increases the overall processivity of AAV DNA replication (89). The VA_I RNA is a translational control RNA and along with E2a also aids in the timely accumulation of AAV2 RNA and enhances translation of these messages (43). HSV can also

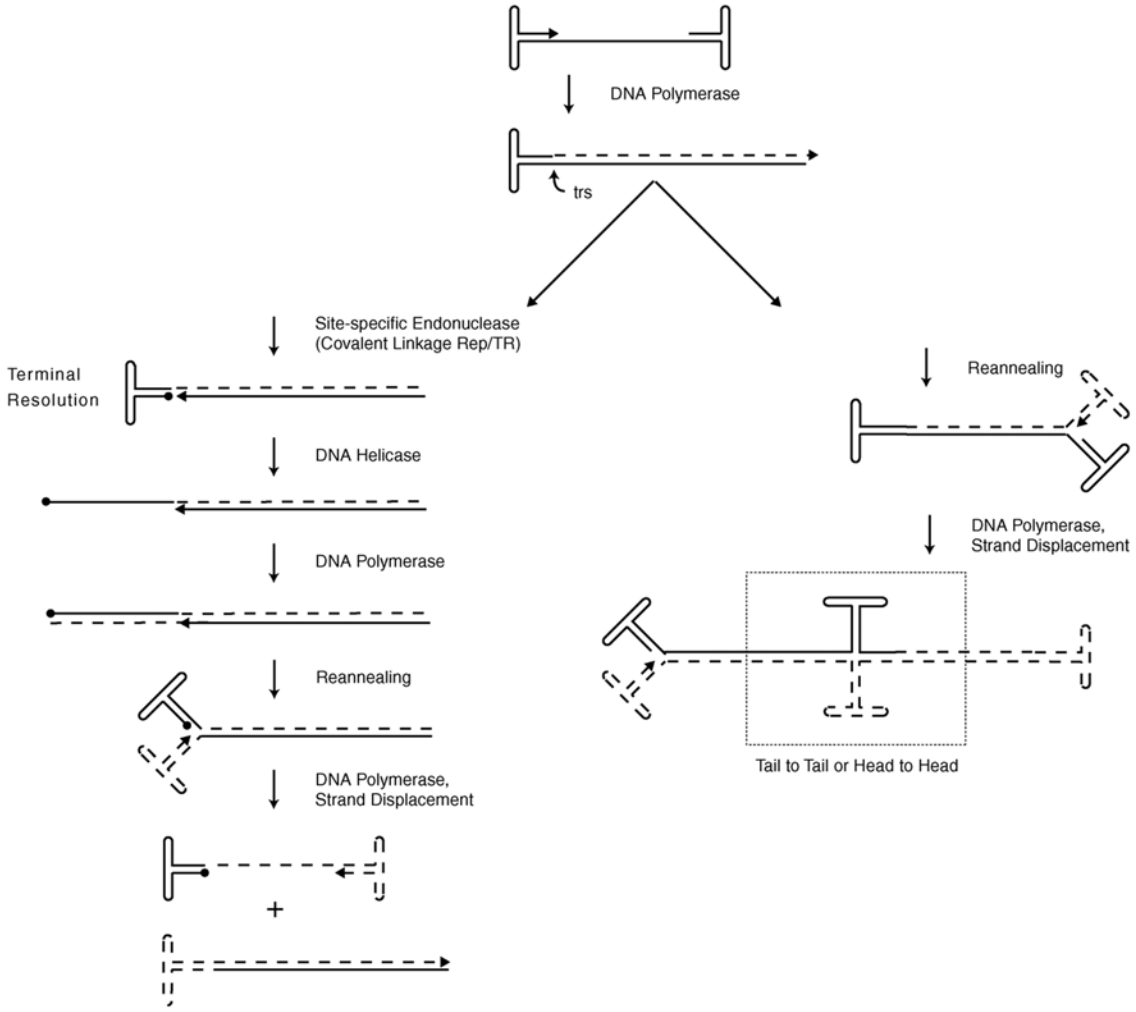

Figure 1-7. Model of AAV2 DNA replication. Two potential replication pathways and the AAV2 DNA intermediates are shown. The single stranded AAV2 genome self-primes by hairpin formation and is extended by cellular DNA polymerases. The left pathway illustrates monomer DNA synthesis initiated by Rep nicking. The right pathway illustrates formation of concatameric products generated in the absence of Rep nicking. The viral 3' end and Rep are indicated by the filled arrowhead and circle, respectively. Dashed lines indicate newly replicated DNA.

provide the gene functions necessary to produce infectious AAV2 particles (56). The genetic regions that are required include UL5, UL8, UL52, and UL29, which encode the HSV helicase primase complex and the major DNA binding protein, respectively. Interestingly, neither adenovirus nor herpesvirus gene products appear to an absolute requirement for AAV2 replication as cells can be rendered permissive for DNA synthesis by growing cells to high density prior to extract preparation or by treatment with toxic agents or UV irradiation (1, 60, 103, 108).

Model of AAV2 Capsid Assembly and DNA Packaging

Newly replicated genomic viral DNA and RNA are highly susceptible to degradation by intracellular nucleases if left unprotected. To maintain intra- and extracellular genomic integrity, viruses have evolved a proteinaceous coat that assembles around the nucleic acid protecting it from insult. The process is remarkably well organized, using only one or a few proteins to form a defined and stable structure, making viruses excellent model systems for studying macromolecular assembly.

Early *in vivo* pulse chase experiments showed that capsid proteins synthesis begins between 10-12 hours post-infection. They relocate to the nucleus and rapidly associate to form empty particles that mature into infectious virions over several hours (58). The large proportion of empty capsid particles produced during infection suggests that DNA is not required for capsid assembly. Indeed, recombinant baculoviruses containing AAV2 capsid proteins expressed in SF9 insect cell cells in the absence of a DNA packaging construct are still able to form virus-like particles composed of the three capsid proteins in the expected

ratios. Analysis of soluble cytoplasmic and nuclear proteins separated by sucrose cushion gradients showed that at early times during infection the majority of newly synthesized capsid proteins were found the cytoplasm across the 5S-30S sedimentation range encompassing VP monomers through tri- and pentameric subunits (94, 95). Relatively low levels of mostly empty capsids were in found the nucleus. In contrast, at later times during infection the majority of the capsid proteins were located in the nucleus. Interestingly, capsid components found in the nucleus sedimented between 30S-160S. The lack of detectable monomers in the nucleus suggests that they are unable to pass through the nuclear membrane or that after import they rapidly complex with other capsid monomers to form protomers or larger structures. Taken together these results indicate that capsid assembly has significant temporal, spatial, and stoichiometric regulation.

Nuclear import of capsid proteins after translation in the cytoplasm is thought to require a nuclear localization signal (NLS). In one report, a mutated VP2 containing a 45 residue amino terminal truncation disrupted VP3 nuclear localization. This suggested that VP3 uses VP2 as a shuttle protein for nuclear import. Unpublished work from our lab indicates that this is not the case. Using a plasmid that expresses only VP3 and a packaging construct, we are able to recover infectious particles after iodixanol gradient purification and heparin-affinity chromatography. Although it is possible that capsids may have formed in the cytoplasm, the infectious nature of the viruses suggests that capsid proteins must have been in the nucleus to acquire DNA. Also, one of the four Simian

Virus 40 (SV40)-like putative nuclear localization signals is located in the amino terminus of VP3. Using site-directed mutagenesis to modify this putative NLS, Wu et al. (99) was unable to recover virus particles from a standard virus preparation method. Nuclear and cytoplasmic fractionation of virus preparations was not examined so a formal block to nuclear import was not determined. However, this putative NLS is common to each VP protein and suggests that independent mechanism of transport of AAV2 capsid proteins is possible. It does not exclude the possibility for larger complex import. This additional evidence suggests that cytoplasmic assembly is at best inefficient and that cellular nuclear components are likely to have a role in particle formation.

DNA packaging is the process of inserting AAV DNA into a preformed capsid. It is thought to occur in the nucleoplasm where there are pools of replicated DNA. The AAV2 capsid can package either positive or negative strand DNA shown by isolation and purification using density centrifugation (84). The only required *cis*-packaging signals are the 145 bp terminal repeats located at each end of the viral genome (101). This property has been exploited by all AAV vector technologies because foreign DNA upwards of 4.3kb can be inserted between the TRs and can be packaged to high titers. Efficient DNA packaging was reconstituted *in vitro* and has multiple requirements including DNA replication, terminal repeats, $MgCl_2$, Rep, and an adenovirus infected HeLa cell extract (109). DNA between 50%-75% of full length can be packaged in the absence of Rep, albeit inefficiently, suggesting that DNA can associate with the capsid however Rep is required for complete encapsidation. Expression of individual rep proteins

in an in vivo packaging model system showed that Rep52 was the main AAV rep protein involved in DNA packaging. Further analysis showed that the helicase acitivity of Rep52 and Rep40 were essential for DNA packaging (45). Neither Rep52 nor Rep40 have the amino-terminal DNA binding domain suggesting that they first associate with the capsid or a large Rep protein already bound to genomic DNA. Indeed, soluble nuclear Rep protein co-immunoprecipitates with capsid proteins sedimenting between 60S-110S using capsid specific antibodies (95).

Although no cellular proteins or adenoviral proteins have been identified to have a direct role in AAV DNA packaging, successful *in vitro* reconstitution requires an Ad-infected nuclear extract (109). It could be that cellular proteins are activated by Ad, that cellular proteins have no direct role, or that a complexes of Ad, AAV and cellular factors are required. A 110 KDa nuclear shuttle protein, nucleolin, co-purifies with AAV during CsCl density centrifugation and co-localizes in the same subcellular compartments. No specific function has yet been associated with nucleolin, but its DNA binding activity, protein shuttling ability, and co-localization with AAV capsid proteins during capsid formation suggests that could act as a mediator during DNA packaging.

The AAV2 Vectors

Although several virus families have demonstrated sustained transgene expression and phenotypic correction in susceptible cells, AAV2 has several properties that make it extremely attractive as a mammalian vector. First, infectious plasmid clones have been produced that allow relatively easy genetic manipulation and mutant analysis (69). Second, established protocols exist that

generate high-titer, stable, contaminant-free stocks (35). Third, AAV2 vectors can efficiently infect a broad range of non-dividing tissue types including lung (7, 18, 29), CNS (15, 30, 52), liver (79, 90), pancreas (28), and muscle (27, 44, 80); and demonstrate transgene expression for over a year. Finally, and importantly, AAV2 has not been associated with any pathology (57). Using AAV2 as a vector has one distinct disadvantage in that its capacity for packaging DNA is limited to 4.3 kb of foreign DNA. Although this is sufficient for many genetic targets, unless cumbersome bicistronic vector approaches are used, (24, 104, 105) corrective genes must be relatively short.

All current AAV2 vectors share two components, the TRs and the capsid. Several important considerations have arisen during AAV vector development for clinical trials. First, how safe is DNA – is it capable of insertional mutagenesis into active genes? Second – will the TR affect regulation of the transgene. Third, will immune system responses from the high capsid particle titers preferred in clinical studies prevent vector re-administration? Fourth, can the natural preference of the virus to infect $HSPG^{+}$ cells be altered?

The possibility of a retargeting a virus to a novel cell, tissue, or organ type is appealing because it may broaden the therapeutic target range and reduce potential vector toxicity. Preliminary studies with AAV2 using a genetic approach to insert foreign ligands into the capsid showed vector retargeting to normally non-permissive cell populations. However the virus still bound to HSPG. These experiments have shown that modification of virus tropism has the potential to expand the therapeutic scope of AAV2 vectors, but the system requires

additional development. In order to examine the selectivity and efficiency of a recombinant AAV2 targeted to a novel cell type it will be necessary to interfere with the natural viral affinity for HSPG. In essence, a recombinant viral vector that is deficient in HSPG binding is needed in order to accurately study the effectiveness of retargeted virions *in vivo.*

CHAPTER 2
MATERIALS AND METHODS

Plasmids

Plasmid pIM45 (previously called pIM29-45) contains the Rep and Cap coding sequences from AAV with expression controlled by their natural promoters (7). It was used as the parent template for construction of all the AAV2 mutant vectors.

Plasmid pXX6 supplies the adenovirus helper gene products in *trans* to allow rAAV production in an adenovirus free environment (10).

Plasmid pTR2-UF5 supplies the recombinant AAV DNA to be packaged. It contains a cytomegalovirus promoter driving expression of a green fluorescent protein (GFP) reporter gene flanked by AAV2 terminal repeats (6). Plasmid pTR5-UF11 was constructed using an expression cassette consisting of a strong constitutive chicken β-actin (CBA) promoter (11), green fluorescent protein (GFP) reporter gene (13), woodchuck hepatitis virus posttranscriptional regulatory element (WPRE) (4) and bovine growth hormone gene polyadenylation signal. The cassette was assembled using standard molecular biology techniques and substituted for the lacZ cassette in the plasmid backbone of pAAV5RnlacZ containing AAV5 terminal repeats (2).

Plasmids pXYZ1, pXYZ5 contain the AAV1 and AAV5 Cap coding sequences, respectively, in addition to AAV2 Rep coding sequence with an ACG

start codon under control of the AAV2 p5 promoter (14). Plasmid pAAV5-2 contains the AAV5 nucleotides 260 to 4448 without terminal repeats (2).

Construction of Mutant Capsid Plasmids

Quickchange site directed mutagenesis (Stratagene) was performed on plasmid pIM45 as per the manufacturers instructions. For each AAV2 mutant, two complementary PCR primers that contained alanine or lysine substitutions in addition to a silent change for restriction endonuclease screening purposes were used to introduce changes into pIM45. For construction of AAV5-HS, pAAV5-2 was used as the parental template. Sequences for the oligonucleotides used are available upon request. PCR products were digested with DpnI to remove methylated template DNA, phenol:cholorform:isoamyl (25:24:1) extracted, ethanol precipitated, and transformed into electrocompetent JM109 cells. Miniprep DNA was extracted from overnight LB/amp cultures and screened with the appropriate restriction enzyme. All mutants were sequenced prior to use. Transfection quality plasmid DNA was produced by standard alkaline lysis method of a 1-liter TB culture followed by polyethylene glycol 8000 (PEG) precipitation and cesium chloride gradient purification. A list of the sequences of oligionucleotides used for mutagenesis is provided in Table 3-1.

For construction of AAV5-HS, pXYZ5 was used as the parental template for mutagenesis using the following primer pair: AAV2-HepS 5'-ATGGCCACCAACAACCAGAGCAGAGGCAACAGACAAGCAGCGACCGGTACGTACAACCTC-3' and 5'-ATCCGGTGGTTGTTGGTCTCGTCTCCGTTGTCTGTTCGTCGCTGGCCATGCATGTTGGAG-3'.

Cell culture

Human embryonic kidney 293's and cervical carcinoma HeLa C12's, a gift from Dr. Phil Johnson (3) were grown in Dulbecco Modified Eagle Medium (Gibco-BRL) supplemented with 100U/ml penicillin, 100U/ml streptomycin, 10% bovine calf serum, sodium pyruvate and L-glutamine. Cells were incubated at 37°C in a 5% CO_2 atmosphere.

Production of rAAV2 Particles

To produce AAV2 virions, low passage 293's were seeded so that they were approximately 75% confluent at transfection time. A triple plasmid transfection protocol (10) was followed that included pIM45 to supply Rep and mutated capsid genes, pTR2-UF5 (6) to supply recombinant DNA with AAV2 terminal repeats and a CMV driven GFP reporter gene, and pXX6 (10) to supply the adenovirus helper functions in *trans*. A total of 60 µg of plasmid DNA in a 1:1:1 molar ratio was transfected by lipofectamine (Invitrogen).

To produce pseudotyped rAAV1 and rAAV5 particles, a total of 60 µg of pXYZ1 or pXYZ5 (14) was co-transfected with pTR2-UF5 plasmid DNA in a 1:1 molar ratio as above. pXYZ1 and pXYZ5 are AAV/adenovirus hybrid plasmids consisting of the AAV2 Rep and the AAV1 or AAV5 Cap gene, respectively, and the adenoviral helper genes required to pseudotype AAV2 TR-containing expression cassettes into AAV1 and AAV5 capsids. To produce rAAV5 and rAAV5-HS virions a total of 60 µg of pAAV5 or pAAV5-HS was co-transfected with pTR5-UF11.

Purification of rAAV has been described previously (12, 14). Briefly, seventy-two hours after transfection, cells were harvested by centrifugation and

the pellets were resuspended in lysis buffer (.15M NaCl, 50mM Tris-Cl pH=8.5). Virus was released by three cycles of freezing and thawing. Benzonase (Sigma) was added to the cell lysate to a final concentration of 140 U/ml and incubated at 37°C for 30 min. Cell debris was pelleted by centrifugation at 3,700 x g for 30 min and the supernatant was loaded onto a 15%-25%-40%-60% iodixanol (5,5'[2-hydroxy-1,3-propanediyl)bis(acetyl-amino)] bis[N,N'-bis(2,3dihydroxypropyl-2,4,6-triiodo-1,3-benzenecarboxamide] step gradient (Nycomed). The 40% fraction was collected after centrifugation at 69,000 x g for 1 h and stored at -80°C until further use.

Western Analysis of Virus Stocks

Equal volumes of iodixanol virus stocks were boiled for 3 mins in 1X SDS polyacrylamide gel loading buffer. Denatured samples were loaded onto a 10% SDS polyacrylamide gel and separated by electrophoresis at 6-10V/cm. Proteins were transferred to nitrocellulose in western transfer buffer at either 1000mA for 4 hours or 100mA for 18 hrs. Nitrocellulose was rinsed in PBS/.05% Tween-20 and blocked for 1 hour with rocking in 5%BSA/PBS/.05% Tween-20. Optimal primary and secondary antibody dilutions were 1:3000.

Virus Titer Determination

To determine the concentration of intact capsid particles the A20 ELIZA (American Research Bioproducts) was used. The A20 antibody detects intact, fully assembled particles, both full and empty (9). Iodixinal purified stocks were serially diluted and processed by the manufacturer's recommended protocol. Only readings within the linear range of the kit standard were used.

To determine the concentration of DNA containing particles, real-time PCR (RT-PCR) was performed using a Perkin Elmer-Applied Biosystems (Foster City, CA) Prism 7700 sequence detector system. Equal volumes of iodixanol purified virus stocks were treated with 600 U/ml benzonase in 50mM Tris-CL pH=7.5, 10mM $MgCl_2$, 10mM $CaCl_2$ at 37°C for 30 min. 280 U/ml proteinase-K was added to reactions adjusted to 10mM EDTA and 5% SDS, and then incubated at 37°C for 30 min. Reactions were extracted with phenol/chloroform/ isoamyl-alcohol (25:24:1) and undigested DNA was precipitated overnight with ethanol and glycogen carrier. Precipitated DNA pellets were resuspended in 100 ul of water. Five µl was used for RT-PCR analysis in a reaction mixture that included 900 nM each of GFP forward (5'-TTCAAAGATGACGGGAACTACAA-3') and reverse (5'-TCAATGCCCTTCAGCTCGAT-3') primers, 250 nM Taqman probe (5'-6FAM-CCCGCGCTGAAGTCAAGTTCGAAG-TAMRA-3'), 1X Taqman universal PCR master mix in a total volume of 50 µl. Cycling parameters were 1 cycle each of 50°C, 5 mins, and 95°C, 10 mins, followed by 40 cycles of 95°C, 15 sec and 60°C, 1 min. Only values within the linear portion of a standard curve having a coefficient of linearity greater than .98 were accepted. The average RT-PCR titer was calculated from virus preparations assayed three times.

To determine the infectious titer of the wild-type (WT) and mutant virus stocks we performed a green cell assay (GCA) essentially as previously described (12). Briefly, HeLa C12 cells were seeded in a 96 well plate so that they were approximately 75% confluent at infection time. Cells were infected with 10-fold serial dilutions of iodixanol purified mutant viruses and Ad5 at a

constant multiplicity of infection (MOI) = 10. Cells were incubated at 37°C in a 5% CO_2 atmosphere for 24 hours and examined by fluorescence microscopy. The average GCA titer was calculated by averaging the number of green cells counted in individual wells from two or three virus preparations each assayed three times. Particle to infectivity ratios were calculated by dividing the average RT-PCR titer by the average GCA titer. In some figures, this number was expressed as a $\log_{10}$ value with rAAV2 arbitrarily set to one. See figure legends.

In Vitro Heparin Binding Assay

Bio-Rad microspin columns were treated with silicon dioxide to minimize non-specific binding of the virus to the column wall. A 500 µl heparin-agarose (Sigma H-6508) gravity column was prepared by washing with 3 column volumes each of 1X TD (137nM NaCl, 15mM KCl, 10mM Na_2PO_4, 5mM $MgCl_2$, 2mM KH_2PO_4, pH=7.4), 1X TD + 2M NaCl and 1X TD. Approximately equal numbers of virus particles were added to 1X TD to a final volume of 600 µl and loaded onto the column. The column was washed with 7 column volumes of 1X TD. Bound virus was eluted with 1X TD + 2M NaCl. The entire volume of the flow through, wash, and eluate fractions were pooled separately, denatured by boiling in SDS, and slot blotted onto nitrocellulose (Osmonics) for immunoblot analysis. The membrane was blocked in PBS (137mM NaCl, 2.7 mM KCl, 10 mM Na_2PO_4, 2 mM KH_2PO_4)/0.05% Tween-20 + 5% dry milk, and incubated with B1 antibody (8) at a 1:3000 dilution for 18h at 4°C. Anti-mouse IgG-horse radish peroxidase was used to detect bands by enhanced chemiluminesence (Amersham-Pharmacia).

Fluorescence Activated Cell Sorting (FACS)

HeLa C12 cells were seeded in 6 well plates so that they were approximately 75% confluent at infection time. Cells were infected with a rAAV MOI=500 based on the genomic titer as determined by DNA dot blot assay (12). Adenovirus type-5 was used at an MOI=10 plaque forming units (pfu). Twenty-four hours postinfection, cells were washed, trypsinized, and fixed in 2% paraformaldyhede. FACS analysis for GFP expression was done in the ICBR Flow Cytometry lab of the University of Florida on a Becton-Dickinson FACScan.

Cell Attachment Assay

10^6 Hela C12 cells were infected with rAAV2 or R585A/R588A at a genome containing particle MOI = 1000 as determined by RT-PCR. Cells were incubated at 37°C in a 5% CO_2 atmosphere until harvesting. At indicated time points, the infection media were removed and saved and the cells were washed four times with PBS before being scraped. Low molecular weight DNA from the infection media and the cell pellet was extracted by the Hirt procedure (5). DNA pellets were resuspended in 0.2M NaOH, incubated at 37°C for 20 mins, and slot blotted onto nitrocellulose. DNA was UV cross-linked to the nitrocellulose and probed at 65°C for 18h with [α-^{32}P]-dATP labeled GFP probe in hybridization buffer (7% SDS, 10mM EDTA and .5M Na_2HPO_4). Membranes were washed twice in 2X SSC (.3M NaCl, .03M NaOAC)/0.1%SDS, 0.2XSSC/0.1%SDS, 0.1X SSC/0.1%SDS, and rinsed with water. The membranes were then exposed to film and quantitated using a BAS-1000 phosphor imager (Fuji).

Production of Viruses With Mutant Terminal Repeats (TR)

Ligation of synthetic oligonucleotides was done as previously described. (1) Briefly, two complementary A-stem oligonuceotides were annealed and then ligated to a B-C stem oligonucleotide. Correctly sized ligation products were visualized with UV light after denaturing polyacrylamide gel electrophoresis, excised, and eluted overnight in Oligonucleotide Elution Buffer (50mM Tris-Cl pH=7.5, 10mM EDTA, 0.1% SDS, .3M NaOAC). Purified synthetic terminal repeats were then ligated to the XbaI fragment of pIM45 to create no-end (NE) substrate DNA. Non-covalently closed DNA was removed with exhaustive digestion with Exonuclease III In order to produce virus we used a three-plasmid system. The first plasmid was the NE substrate with mutations in the TR. The second was pIM45. This plasmid was included to achieve the boost molar ratio of DNA for efficient $CaPO_4$-DNA precipitation, as well as to express the appropriate regulated levels of Rep and Cap proteins. The third plasmid was pDG and supplied both Ad helper and AAV proteins eliminating adenovirus contamination. To produce AAV2 virions, low passage 293's were seeded so that they were approximately 75% confluent at transfection time. Approx. 500ng of NE substrate was co-transfected with 15µg pIM45 and 20µg pDG by $CaPO_4$ transfection. Medium was replaced 48 hpi. Cells were washed, scraped and resuspended in PBS-MK (137nM NaCl, 15mM KCl, 10mM Na_2PO_4, 5mM $MgCl_2$, 2mM KH_2PO_4, pH=7.4, 1mM $MgCl_2$). Three freeze-thaw cycles were performed to release virus particles. Crude virus lystates were stored at -80°C until needed.

Titering of Viruses With Mutant Terminal Repeats

Equal volumes of crude lysates were treated with 600 U/ml benzonase in 50mM Tris-CL pH=7.5, 10mM $MgCl_2$, 10mM $CaCl_2$ at 37°C for 30 min. 280 U/ml proteinase-K was added to reactions adjusted to 10mM EDTA and 5% SDS, and then incubated at 37°C for 30 min. Reactions were extracted with phenol/chloroform/ isoamyl-alcohol (25:24:1) and undigested DNA was precipitated overnight with ethanol and glycogen carrier. DNA pellets were resuspended in 0.2M NaOH, incubated at 37°C for 20 mins, and two fold serial dilutions were slot blotted onto nitrocellulose (Hybond-N). DNA was UV crosslinked to the nitrocellulose and probed at 65°C for 18h with [α-^{32}P]dATP labeled GFP probe in hybridization buffer (7% SDS, 10mM EDTA and .5M Na_2HPO_4). Membranes were washed twice in 2X SSC/0.1%SDS, 0.2XSSC/0.1%SDS, 0.1X SSC/0.1%SDS, and rinsed with water. The membranes were then exposed to film and quantitated using a BAS-1000 phosphor imager (Fuji).

Random Primed Probe Labeling

50ng of gel purified pIM45 XbaI fragment was denatured by boiling for 10 mins and then quick chilled on ice. Denature DNA was added to a reaction mixture containing 50 µCi of ^{32}P-dATP and synthesis of the complementary strand by Klenow was performed as per the manufacturers recommended protocol (Roche).

Hirt DNA Extraction

Cells were harvested, washed with PBS and the cell pellet was saved. The pellet was resuspended in solution A (10mM Tris-HCl, pH=7.5, 10 mM EDTA,

100µg/ml proteinase K). An equal volume of solution B (10mM Tris-HCl, pH=7.5, 10 mM EDTA, 1.2% SDS) was added and the mixture was incubated for 1hr at 37°C. NaCl was added to a final concentration of 1M. One drop of chloroform was added and the mixture was incubated overnight at 4°C with constant rotation. The chromosomal DNA/protein/SDS complex was pelleted by centrifugation a 14K x g for 30 mins. The supernatant was saved, extracted once with phenol, once with phenol:chloroform:isoamyl alcohol (25:24:1), once with chloroform, and precipitated with ethanol. DNA was washed with 70% ethanol and resuspended in TE.

Mutant TR Virus Infections

293 cells seeded in 15cm dishes so that they were approximately 75% confluent at infection time infected with the mutant panel with an MOI=5 and with or without adenovirus MOI=1. See text for details. Cells were harvested 4, 25, 48, and 72 hours post-infection, pelleted and stored at –80°C until further use.

RNA Extraction and Northern Hybridization

RNA from 1 x 10^7 cells was extracted using the Qiagen RNeasy mini-column isolation protocol as recommended by the manufacturer. RNA was checked by examining the ribosomal RNA integrity prior to denaturing and slot blotting 15µg of total RNA onto nitrocellulose. Hybridization was carried out at 65°C for 18 hours in 5X SSPE (.75M NaCl, .5M NaH_2PO_4, .005M EDTA), .1% SDS, 5X Denhardts (1% w/v Ficoll 400, 1% w/v polyvinylpyrrolidone, 1% w/v bovine serum albumin), and 100 µg/ml denatured, sonicated salmon sperm DNA. Membranes were washed twice in 2X SSC/0.1%SDS, 0.2XSSC/0.1%SDS, 0.1X

SSC/0.1%SDS, and rinsed with water. The membranes were then exposed to film and quantitated using a BAS-1000 phosphor imager (Fuji).

PCR Integration Assay

Integration reactions were carried out in a 50ul volume and contained 100mM KCl, 100mM Tris-Cl, 5mM $MgCl_2$, 200μM dATP, 200μM dTTP, 200μM dCTP, 200μM dGTP, 200ng each of primers #80 and #81, and 200 ng of total cellular DNA. The primer sequences are: #81 D-stem: 5'-AGGAACCCCTAGTGATGGAGT-3'. #80 AAV-S1 5'-GGAGGATGGGCTCAGAGG-3'. The cycling parameters were: 94°C for 3 mins, followed by 35 cycles of 94°C for 1 min, 55°C for 1 min, 72°C for 1 min. Cycling was completed by a final extension step of 72°C for 10 mins and held at 4°C. PCR products were analyzed by directly slot blotting onto nitrocellulose (Hybond-N) or separated on 1.0% agarose gels. Agarose gels were denatured with three changes of Southern Denaturing Solution. (1.5M NaCl and 0.5M NaOH), neutralized with three changes of Southern Neutralization Solution (1.0M Tris-Cl pH=7.4 and 1.5M NaCl.), and then transferred to nitrocelullose with 20X SSC by capillary action. DNA was UV crosslinked to the nitrocellulose and probed by Southern hybridization.

Mixed Micelle Assay

Wild-type AAV2 capsids were incubated for 2 mins at 70°C in 150mM Tris-Cl pH=8 in a final volume of 20ul. Denatured capsids were added to 50mM Tris-Cl pH=8, 1mM $CaCl_2$, 100mM NaCl, 1mM Triton-X 100, 6μM phosphotidylcholine in final volume of 50μl. Reactions were incubated for 30 minutes at 37°C, and products were extracted with chloroform:methanol:4M KCl (2:1:1). After

centrifugation 10 minutes at 14K, the aqueous phase was saved and spotted onto silica gel thin layer chromatography plates. Products were separated in a closed, pre-equilibrated chromatography chamber with chloroform:methanol:water (65:35:4) as a running solvent. Plates were air dried, and exposed to film for autoradiography.

CHAPTER 3
IDENTIFICATION OF CRITICAL AMINO ACID RESIDUES IN THE CAPSID PROTEINS OF THE ADENO-ASSOCIATED VIRUS TYPE-2 THAT CONTRIBUTE TO HEPARIN SULFATE PROTEOGLYCAN BINDING.

Introduction

The adeno-associated virus type 2 (AAV2) is a small, non-enveloped parvovirus that has received considerable attention as a gene therapy vector [reviewed in ref. (83)]. The capsid has a diameter of approximately 24nm formed by an icosahedral lattice with T=1 symmetry (60 structurally equivalent subunits) (66, 151). In purified virions three structural proteins, VP1, VP2, and VP3 with molecular masses of 87, 73, and 62 KDa, respectively, are present in a molar ratio of 1:1:10 (13). mRNAs encoding capsid proteins are synthesized from a single open reading frame and use alternative splicing and start codons to produce three VP proteins that share an identical 532 carboxyl-terminal amino acid domain (7, 8), with VP2 and VP3 containing successive amino terminal truncations of VP1.

The atomic structure of the AAV2 capsid has been determined to a resolution of 3.0 Å (151). In this model, sixty copies of VP3 minus 14 amino terminal residues are present in an icosahedral arrangement. The VP3 protein contains 8 anti-parallel ß-strands that adopt a barreled structure similar to capsid proteins of other non-enveloped viruses (103). Loops of variable length connect the interior ß-barrel scaffold and extend outwards to form the capsid surface. Cryo-electron microscopy of empty AAV2 particles generated a surface density

map that described depressions, spikes, and canyon features similar to those found in other parvoviruses (66) Before the crystal structure was available, several alternative methods were utilized in attempts to localize specific functional regions of the capsid. Neutralizing antibody screening of peptide sequences derived from VP1 found multiple antigenic determinants distributed on the capsid exterior in both linear and conformation dependent forms (81). Computer modeling of AAV structure based on the known atomic structure of the related canine parvovirus coupled with genetic modification of the capsid identified several positions that were on the surface of the capsid and could tolerate insertions and substitutions (45, 89, 100, 102, 115, 147, 157).

Cell membrane binding and entry initiate all viral infections. Non-enveloped viruses rely on membrane bound extracellular receptors for attachment to the cell membrane. AAV2 has evolved a dynamic and multistep infectious entry pathway that utilizes the abundantly expressed heparan sulfate proteoglycan (HSPG) as its primary target (127). Two co-receptors, αVβ5 integrin and basic fibroblast growth factor receptor (bFGFR) have been identified, which act as secondary receptors that may stabilize virus attachment or participate during internalization (29, 94, 126). HSPG is a macromolecule expressed by many cell types and is a component of the extracellular matrix of most tissues [reviewed in refs. (51, 82)]. Attached to the core protein are glycosaminoglycan side chains heparin and heparin sulfate (HS). These carbohydrate polymers are formed by disaccharide repeats consisting of alternating N-acetylglucosamine and iduronic acid residues in a α1,4 linkage. The saccharides can be modified by N-sulfation as well as 2-O

and 6-O-sulfation to impart a dense overall negative charge at physiological pH. As a result, HS interacts with an extensive range of proteins primarily by electrostatic attraction between the electron dense sulfate groups and a cluster of positively charged amino acids. Two linear HS consensus-binding sequences, XBBXBX and XBBBXXBX, and a conformation dependent sequence, TXXBXXTBXXXTBB, (where B is any basic amino acids including His, Lys or Arg and X is any hydropathic amino acid and T is a turn) have been reported (51). Although HSPG is thought to participate in attachment during the infectious process of numerous human viruses (71), information about the molecular mechanisms of these interactions is limited. A report describing the atomic structure of the foot and mouth disease virus co-crystallized with a HS pentasaccharide is available and serves as the only model defined at the atomic level that describes the molecular interaction between a non-enveloped icosahedral virus and HS (37).

Several laboratories have attempted to retarget AAV vectors to non-permissive cell types by inserting sequences coding for short foreign peptides into VP3. Interestingly, insertions at position 587 including an L14 integrin binding peptide, a myc tag, an IgG binding domain truncation of protein A and an endothelial cell targeting peptide abolished the natural heparin binding ability of virus capsids with these alterations (41, 45, 89, 102, 115). Similarly, an alanine repeat insertion at position 509, an L14 peptide insertion at position 520, a hemagluttinin tag insertion at positions 522 and 591, and peptides derived from the human luteinizng hormone receptor and the bovine papilloma virus at

inserted positions 520 and 584, respectively, have been reported to disrupt heparin binding (115, 147). Curiously, alanine substitutions of acidic residues between 561 and 565 also reduced heparin binding, suggesting that nearby basic residues were affected (147). Finally, a substitution mutation of two arginines and a glutamine at positions 585, 588, and 587, respectively, binds poorly to heparin-agarose (147). Taken together, these genetic modifications suggested two potential heparin-binding loci that cluster between positions 509-522 and 561-591(147).

In this study, charged-to-alanine substitution mutants were made to analyze the effects of single and combinatorial mutations in the capsid gene. We have discovered new point mutants that result in assembly, packaging, and receptor binding deficiencies. Importantly, we identified five amino acids, arginines 484, 487, 585, and 588, and one lysine at position 532 that appear to mediate the natural affinity of AAV for HSPG. Our observations contribute to the current map of the AAV capsid and provide a reagent for the discovery of novel, heparin independent targeting ligands.

Results

Selection and Generation of AAV Mutants

A considerable body of information regarding the determinants of HS-protein interactions suggests that association is driven mainly by electrostatic attraction between acidic sulfate groups on the polysaccharide and basic R-groups on amino acids in the target protein (49, 51). We hypothesized that similar electrostatic interactions would govern HSPG-AAV2 association. In order to evaluate the role of particular amino acids in receptor binding, we generated a

panel of mutants by site directed mutagenesis of selected residues. We confined our selection primarily to basic amino acids (His, Lys, Arg) in VP3 as AAV-like particles composed only of VP3 proteins have been purified by heparin affinity chromatography in our laboratory (manuscript in preparation) and by others (100). Any basic amino acid substitution mutant that previously had demonstrated capsid instability or efficient purification by heparin affinity chromatography (147) was excluded from our pool of mutants.

Seven AAV serotypes have been reported (2, 38, 53, 92, 105). Several groups have shown that rAAV2 and rAAV3 bind efficiently to heparin sulfate (98, 115, 147). A single report concerning rAAV1 suggests that it binds with low affinity if at all to heparin (98). In contrast, rAAV4 and rAAV5 do not bind heparin and instead recognize 2,3 O-linked and 2,6 N-linked sialic acid moieties (59). Indeed, this may account for their different cellular tropisms. We reasoned that residues conserved among all five serotypes were probably not participating directly in receptor discrimination and binding and were excluded from further consideration. Additionally, we had previously isolated a number of charge to alanine substitution mutants in the AAV capsid and these had been characterized for their ability to bind heparin sulfate columns (147) and amino acid positions that did not affect heparin binding or had been shown to be assembly mutants were excluded from further study. Using a Clustal W algorithm, we then generated a sequence alignment of capsid proteins from serotypes 1-5, and identified 9 basic residues in AAV2 that were conserved in AAV3 and/or AAV1 but were uncharged or acidic in AAV4 and AAV5, and had not previously been

Table 3-1. Oligonucleotides used for mutagenesis.

Oligo name[a]	*Oligo sequence (5' to 3')*[b]
H358A-EagI+	cccgtacgtcctaggctcggcg**GCG**caaggatgcctcccgccgttcccagcag
H358A-EagI-	ctgctgggaacgccgggaggcatccttg**CGC**cgccgagcctaggacgtacggg
R447A-AflII+	cagtacctgtattacttaagc**GCG**acaaacactccaagtggaac
R447A-AflII-	gttccacttggagtgtttgt**CGC**gcttaagtaatacaggtactg
R459A-EagI+	accaccacgcagtca**GCG**cttcagttttctccggccggagcg
R459A-EagI-	cgctccggccggagaaaactgaag**CGC**tgactgcgtggtggt
R484A-SpeI+	cctggaccctgttac**GCG**cagcagcgagtatcaaagactagtgcgcataacaac
R484A-SpeI-	gttgttatccgcactagtctttgatactcgctgctg**CGC**gtaacagggtccagg
R487A-SpeI+	cctggaccctgttacgcgcagcag**GCG**gtatcaaagactagtgcgcataacaac
R487A-SpeI-	gttgttatccgcactagtctttgatactcgctgctg**CGC**gtaacagggtccagg
H509A-EagI+	ggagctaccaagtag**GCG**atcgatggcagagactc
H509A-EagI-	gagtctctgccatcgat**CGC**gtacttggtagctcc
R513A-SpeI+	cacctcaatggc**GCG**gactcactagtgaatccg
R513A-SpeI-	cggattcactactgagtc**CGC**gccattgaggtg
K532A-AflII+	agccacaaggacgacagcgaa**GCG**ttttttcctcag
K532A-AflII-	ctgaagaaaaaa**CGC**ttcgctagcgtccttgtggct
K544A-EspI+	gcggggttctcatctttggg**GCG**caaggctcagcgaaaacaaatg
K544A-EspI-	catttgttttcgctgagccttg**CGC**cccaaagatgagaaccccgc
R566A-MscI+	gaagaggaaatc**GCG**acaaccaatcccgtggccacggagcag
R566A-MscI-	ctgctccgtggccacgggattggttgt**CGC**gatttcctcttc
R585A-SpeI+	gtatctaccaacctccag**GCG**ggcaacagactagtagctaccgcagatgtc
R585A-SpeI-	gacatctgcggtagctactagtctgttgc**CGC**cctggaggttggtagatac
N587A-SpeI+	gtatctaccaacctccagagaggc**GCG**agactagtagctaccgcagatgtc
N587A-SpeI-	gacatctgcggtagctactagtct**CGC**gcctctctggaggttggtagatac
R588A-SpeI+	gtatctaccaacctccagagaggcaac**GCG**ctagtagctaccgcagatgtc
R588A-SpeI-	gacatctgcggtagctactag**CGC**gttgcctctctggaggttggtagatac
R585K-SpeI+	gtatctaccaacctccag**AAA**ggcaacagactagtagctaccgcagatgtc
R585K-SpeI-	gacatctgcggtagctactagtctgttgcc**TTT**ctggaggttggtagatac
H526A/K527A+	gcccggccatggcaagc**GCAGCG**gacgatgaag
H526A/K527A-	cttcatcgtc**CGCTGC**gcttgccatggccgggc
R585A/R588A-SpeI+	gtatctaccaacctccag**GCG**ggcaac**GCG**ctagtagctaccgcagatgtc
R585A/R588A-SpeI-	gacatctgcggtagctactag**CGC**gttgcc**CGC**ctggaggttggtagatac
R585K/R588K-SpeI+	gtatctaccaacctccag**AAA**ggcaac**AAA**ctagtagctaccgcagatgtc
R585K/R588K-SpeI-	gacatctgcggtagctactag**TTT**gttgcc**TTT**ctggaggttggtagatac
AAV5-HS-AgeI+	atggccaccaacaaccagagc**AGAGGCAACAGACAAGCA**gcgaccggtacgtacaacctc
AAV5-HS-AgeI-	gaggttgtacgtaccggtcgc**TGCTTGTCTGTTGCCTCT**gctctggttgttggtggccat

[a] Each oligonucleotide is named by its mutant position, the restriction site engineered at the site of the mutation and the polarity of the oligonucleotide strand (+ or -).
[b] The bold capital letters indicate the specific substitutions made in the parental wild type sequence.

tested for heparin-agarose binding (Table 3-2). In addition to these 9 amino acids, Wu et al. (147) described a virus deficient for heparin binding with alanine substitution mutations at positions 585, 587, and 588. Finally, during the course of these studies, the atomic structure of AAV2 was solved (151) and suggested that residues 484, 513, and 532 might participate in a heparin-binding pocket as they were located close to residues 585, 587, and 588. We included these six extra residues to complete our mutant panel (Table 1).

Mutant Virus Production and Physical Characterization

We generated a series of single and combinatorial capsid mutants from our pool of candidate residues in the AAV2 capsid gene (Table 3-2). To designate the mutant viruses we used the number of the mutated amino acid based on its position in VP1. Iodixanol purified virus stocks were checked by western blot using the monoclonal antibody B1. The B1 antibody recognizes a linear epitope in the extreme carboxyl terminus of all three VP proteins from AAV serotypes 1, 2, 3 and 5 (98, 143). With the exception of H358A, capsid proteins were detected in all virus stocks (Fig. 3-1).

To confirm that we had purified assembled capsids, rather than subunits or assembly intermediates, we measured the particle concentration with an A20 antibody ELISA (Table 3-3). The A20 antibody recognizes a structural epitope that is found only on assembled capsids with or without packaged DNA (46). Although there was some variability between stocks due to different transfection efficiencies and purification recoveries, only the H358A mutant was negative by A20 ELISA assay. Excluding H358A, we determined a particle concentration

Table 3-2. Residues chosen for mutagenesis

	AAV serotype [b]				
VP residue [a]	2	3	1	4	5
358	H	H	H	Q	T
447	R	R	R	S	S
459	R	R	D	T	G
484	R	R	R	K	R
487	R	R	R	G	G
509	H	H	H	T	E
513	R	R	R	R	A
526	H	H	H	A	N
527	K	K	K	G	N
532	K	K	K	K	N
544	K	K	K	P	S
566	R	R	K	A	Q
585	R	S	S	S	S
587	N	N	S	S	T
588	R	T	T	N	T

[a] Residues selected for mutagenesis were generated by a sequence alignment of the VP1 capsid protein from each serotype using the Clustal W algorithm (Vector NTi 5.2, Informax).

[b] Amino acids are represented by their one letter abbreviation. Blue letters represent positively charged, basic amino acids. Red letters represent any other amino acid.

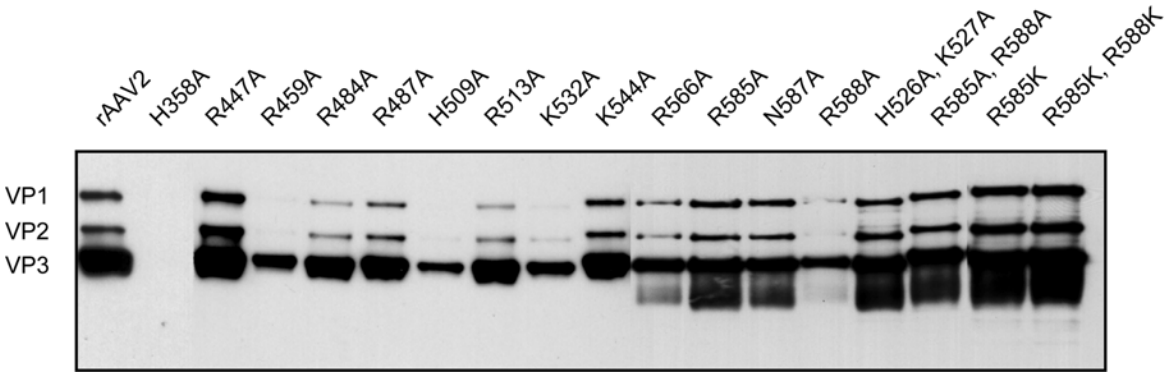

Figure 3-1. Western blot of iodixanol virus stocks. Equal volumes of virus stock were separated by 10% SDS-PAGE and analyzed by western blot using the B1 antibody.

range that spanned 1.5 logs and correlated reasonably well with the B1 antibody results (Fig. 3-1 and Table 3-3). Several possibilities may account for this range of particle titers including that capsid subunits containing these mutations (i) form intact particles inefficiently, (ii) are unstable during purification or, (iii) formed a particle with a partially disrupted A20 epitope. Since none of our mutations fell within the antigenic regions that have been mapped for A20 (143) these results suggested that the A20 epitope had probably not been modified but rather the stability or assembly of some of the mutants was altered so that fewer particles were recovered after iodixanol centrifugation (Fig. 3-1 and Table 3-3).

To determine whether any mutations affected DNA packaging, the titer of DNA containing virions was determined by real-time (RT)-PCR (21, 130) (Table 3-3) and confirmed by DNA dot blot hybridization (data not shown). Although there was variation between preparations, the majority of the capsid mutants were able to package detectable DNA (Table 3-3). As expected, H358A was negative for

DNA packaging, as it did not produce virus particles. We concluded that none of the capsids in our mutant panel that made A20 positive particles were completely defective for DNA packaging. However, by comparing the A20 ELISA and PCR titers we noted that stocks of mutant R459A contained 40-fold more empty particles than rAAV2. Thus R459 could have a role in DNA packaging. Although less dramatic, mutants R447A, R566A, R587A, R585K, and R585K/R588K had approximately 10-fold more empty particles than rAAV2. The remainder of the virus preparations packaged DNA at levels comparable to AAV2 (Table 3-3).

Table 3-3. Summary of mutants.

Mutant virus [a]	Particle titer [b]		Infectious titer [c]	Particle to Infectivity [d]	Heparin binding [e]	Empty/ Full [g]
	A20/ml	Genome/ml	(IU/ml)			
rAAV2 (WT)	1.5×10^{12}	4.6×10^{11}	1.8×10^{10}	25	+	3.4
H358A	$<1.0 \times 10^{8}$	$<1.0 \times 10^{6}$	$<1.0 \times 10^{4}$	N/D [f]	N/D	N/D
R447A	1.2×10^{12}	3.4×10^{10}	1.3×10^{9}	25	+	35.9
R459A	9.1×10^{10}	7.2×10^{8}	$<1.0 \times 10^{4}$	>72500	+	126.3
R484A	1.5×10^{11}	3.0×10^{10}	$<1.0 \times 10^{4}$	>2976667	+/-	5.1
R487A	5.4×10^{11}	2.2×10^{11}	2.3×10^{8}	954	+/-	2.5
H509A	4.6×10^{10}	2.3×10^{9}	6.9×10^{5}	3285	+	20.3
R513A	2.9×10^{11}	1.7×10^{10}	1.6×10^{8}	106	+	17.9
K532A	1.1×10^{11}	3.6×10^{10}	$<1.0 \times 10^{4}$	>3633333	+/-	3.0
K544A	2.0×10^{11}	1.7×10^{10}	8.3×10^{8}	20	+	11.9
R566A	5.1×10^{11}	1.6×10^{10}	7.4×10^{8}	21	+	32.6
R585A	5.0×10^{11}	4.8×10^{10}	1.7×10^{7}	2812	-	1.4
N587A	4.4×10^{11}	1.3×10^{10}	7.7×10^{7}	165	+	34.7
R588A	2.4×10^{11}	5.6×10^{10}	3.0×10^{6}	18521	-	4.2
H526A, K527A	1.4×10^{11}	8.2×10^{10}	5.5×10^{7}	1489	+	1.8
R585A, R588A	1.2×10^{12}	9.2×10^{11}	1.9×10^{7}	48421	-	1.2
R585K	1.3×10^{12}	3.7×10^{10}	4.0×10^{8}	92	+	35.4
R585K, R588K	1.4×10^{12}	3.9×10^{10}	8.9×10^{7}	436	+	34.9
AAV1	N/D	3.7×10^{10}	1.1×10^{9}	37	+/-	N/D
AAV5	N/D	3.4×10^{10}	3.2×10^{6}	10692	-	N/D
AAV5-HS	N/D	8.0×10^{8}	$<1.0 \times 10^{4}$	>80000	+	N/D

[a] Two letters flanking a number designate each mutant. The first letter is the one letter abbreviation for the wild type amino acid followed by its numerical position in VP1 followed by the one letter abbreviation for the amino acid to which it was mutated.
[b] A20 particle titers were determined as described in Materials and Methods using the A20 ELISA assay. Genomic titers were determined by RT-PCR.
[c] Infectious titers were determined by green cell assay as described by counting GFP fluorescent cells.
[d] Particle to infectivity ratio was calculated by dividing the average genomic titer as determined by RT-PCR by the average green cell assay titer.
[e] Determined by heparin-agarose binding assay. +, >95% virus recovered in the eluate; +/-, >50 recovered in the eluate; -, <5% of virus recovered in the eluate.
[f] N/D, not determined.
[g] Empty to full ratio was determined by dividing the A20 particle titer by the average genomic titer.

In Vitro Heparin Binding of Capsid Mutants

To assess the ability of mutant capsids to bind heparin sulfate, we used a modification of an assay previously described by Wu et al. (147). Virus preparations that had been purified by iodixanol step gradients were loaded on heparin agarose columns and the entire volume of the flow through, wash, and eluate fractions were pooled separately, denatured, and slot blotted onto nitrocellulose for immunoblot analysis with B1 antibody. A representative western analysis for each mutant is shown in Fig. 3-2. As expected, wild type AAV2 was not observed in the flow through or wash fractions and most of the virus bound to the column was recovered at the elution step. Eight other mutants, R447A, R459A, H509A, R513A, K544A, K566A, N587A, and H526A/K527A, had a heparin-agarose binding phenotype indistinguishable from wild type. The results with R513A confirmed a previous report by Wu et al, (147) in which a double mutant at positions 513 and 514 was positive for heparin binding. In marked contrast, we observed that any capsid harboring a non-conservative mutation at position 585 or 588 was detected only in the flow through and wash. We also detected intermediate heparin-agarose binding phenotypes in mutants R484A, R487A and K532A with approximately equal levels of signal detected in the flow through, wash, and eluate. The results with K532A were inconsistent with our previous results in which a mutant containing alanine substitutions at positions 527 to 532 was found to be positive for heparin binding (147). These data suggested that at least five amino acids had the potential to contribute to the electrostatic attraction between AAV and heparin

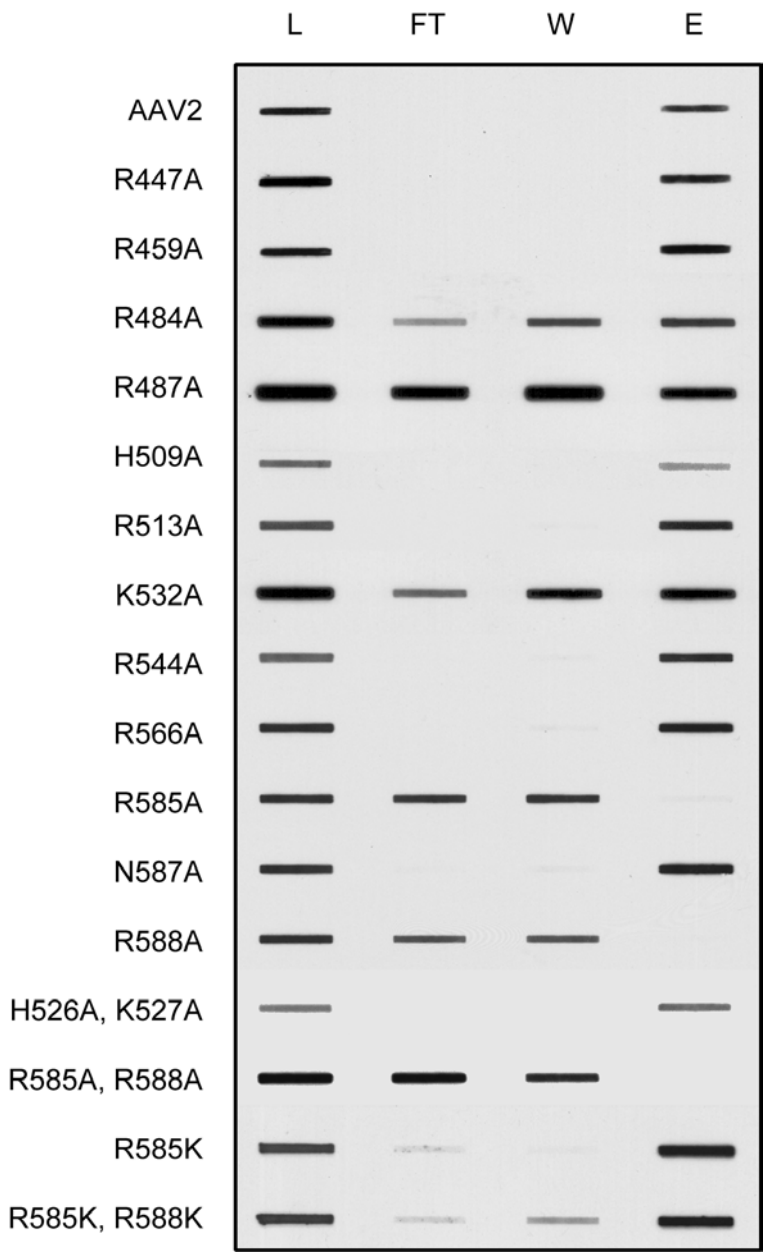

Figure 3-2. Heparin-agarose binding profiles of mutant capsids. Approximately $5x10^{10}$ particles were applied to 500 ul of heparin-agarose affinity matrix at a 100 mM NaCl concentration, washed extensively with the loading buffer, and bound capsids were eluted with 2M NaCl. Pooled fractions were denatured and slot blotted onto nitrocellulose for immunodetection with mAb B1. For each mutant, L is the total amount of iodixanol purified virus that was loaded onto the heparin agarose column; FT is the total virus that flowed through the column, W is the wash; E, eluate. See Materials and Methods for details.

sulfate. These included predominantly R585 and R588, and to a lesser but detectable extent, R484, R487, K532.

To confirm that the charge at R585 and R588 was primarily responsible for heparin interaction, we generated two viruses with conservative mutations, R585K and R585K/R588K, and tested them in the *in vitro* heparin binding assay. Both lysine and arginine residues are positively charged, however, the two amino acids have a different architecture due to the extra methylene group in lysine and a guanidium rather than an amino group in arginine. We found that both of these capsids bound to heparin-agarose almost as well as wild type virus (Fig. 3-2). In each case, most of the virus was recovered in the eluate; however, the flow through and wash fractions also contained minor amounts of virus. This result suggested that both localized negative surface charge and the relative position of the changes in this region of the capsid are responsible for mediating the interaction with heparin-agarose.

Finally, as a control for our experiments and to validate the heparin binding assay, we compared the ability of wild type rAAV2, rAAV1, and rAAV5 to bind to heparin-agarose. For this purpose, we produced and purified recombinant viruses by using a pseudotyping protocol developed to package AAV2 terminal repeat containing genomes into alternative serotype capsids (Fig. 3-3A) (98, 165). Approximately equal amounts of input virus as determined by western blot signal intensity were applied to a heparin-agarose column, and fractions from the column were slot blotted onto nitrocellulose for immunodetection using the B1 antibody (Fig. 3-3B). As expected, rAAV2 was

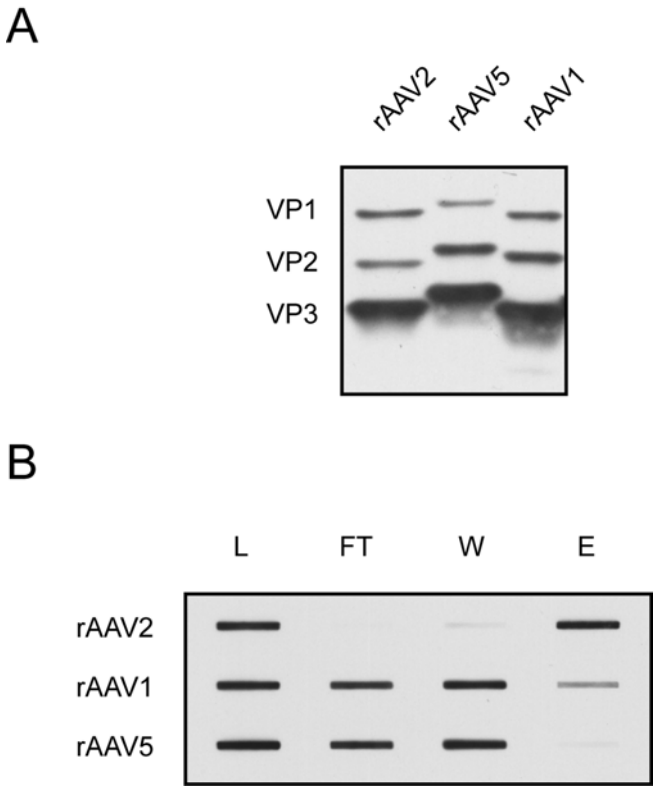

Figure 3-3. Production and purification of AAV serotypes. A) Equivalent amounts of iodixanol purified AAV1, AAV2 and AAV5 were separated by 10% PAGE and analyzed by western blot using the B1 antibody. B) Heparin-agarose binding properties of AAV2, AAV1 and AAV5. Abbreviations are the same as Fig. 3-2.

efficiently retained by heparin-agarose under low ionic conditions but the majority of rAAV1 and all of rAAV5 was seen in the flow through and wash. A low amount of AAV1 was detected in the eluate. These data were consistent with previous observations by Rabinowitz et al. (98).

Multiple Mutations in the AAV2 Capsid Effect Viral Transduction

To determine how the heparin-agarose binding phenotypes correlated to infectivity, iodixanol stocks were tested for their ability to transduce HeLa C12 cells by performing a green cell assay (GCA). Cells in a 96 well plate were co-infected with Ad5 at a constant MOI=10 pfu/cell and mutant AAV virus stocks in a 10-fold dilution series (see Materials and Methods). Twenty-four hours post-infection (hpi) the number of GFP expressing cells in individual wells were counted and a GCA titer was calculated (Table 3-3). The detection limit of this assay was approximately 10^4 transducing units/ml. The GCA titers were then normalized to genome containing physical particles by calculating a particle to infectivity (P/I) ratio. This ratio is equivalent to the number of genomes required to transduce one cell (Table 3-3). To get a measure of the relative impact of a particular mutation on viral infectivity, the P/I ratio of each mutant was divided by the wild type capsid P/I ratio and the $\log_{10}$ of this value was plotted in Fig. 3-4. This provided a simple comparison of how many genome-containing particles of each mutant were required to achieve the same number of transduced cells as the wild type virus.

Several phenotypes emerged from this analysis. Mutants R477A, K544A, and K566A were virtually identical to wild type, and mutants R513A, N587A, R585K, and R585K/R588K were only slightly defective (approximately 1 log).

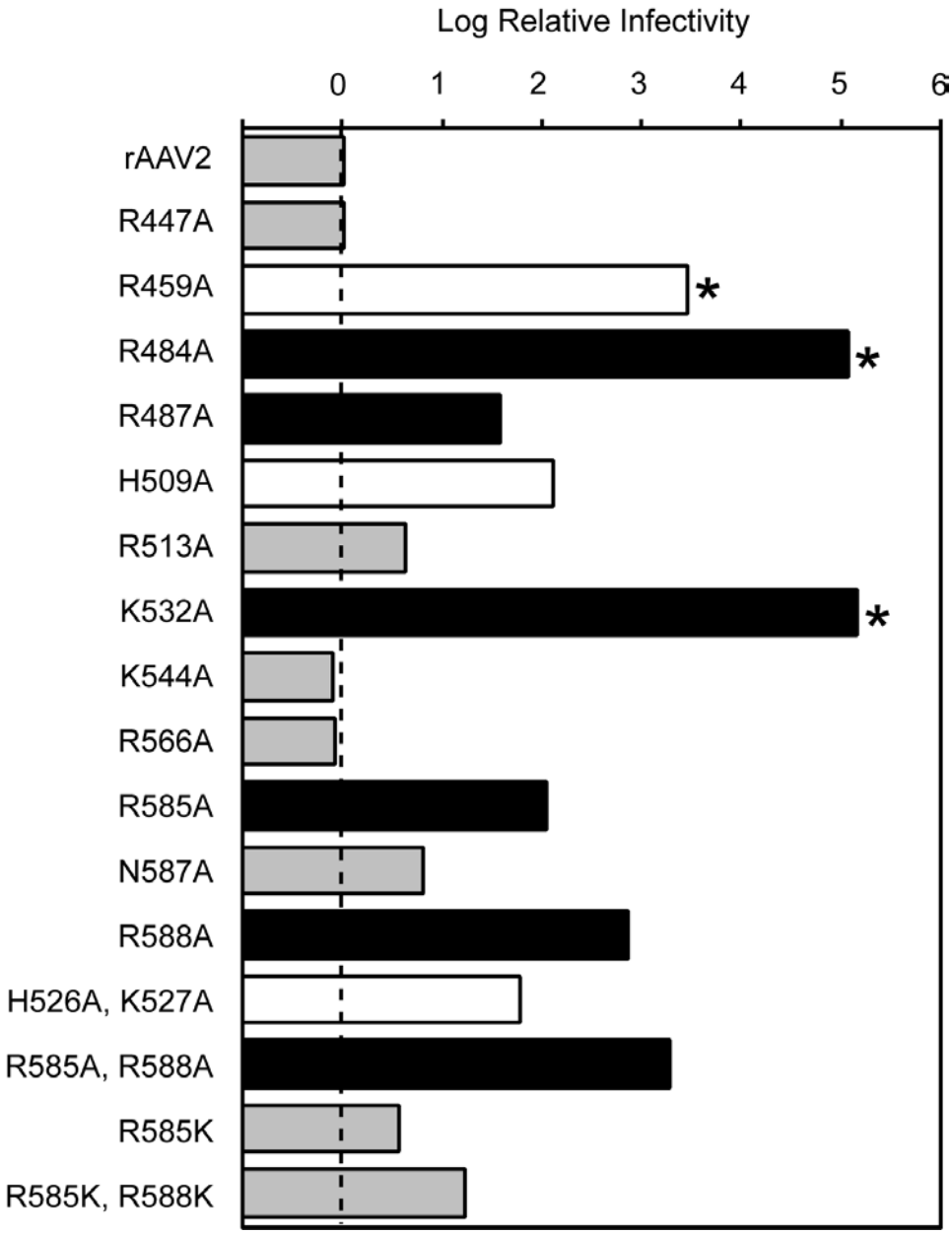

Figure 3-4. Particle to infectivity ratios of mutants relative to wild type. The particle to infectivity ratio for each mutant was calculated by dividing the average genomic titer by the average green cell assay titer (see Materials and Methods and Table 3-3). The P/I ratio of each mutant was then normalized to wild type by dividing the P/I of each mutant by the P/I of wild type rAAV2, and the $\log_{10}$ value of the ratio was plotted. Wild type therefore equals one and is indicated by the dashed line. Grey bars, mutant viruses with infectivity comparable to wild type; Black bars, mutant viruses that are heparin binding deficient; White bars, mutant viruses with an undetermined block to infectivity; Asterisks indicate those mutants for which no green cells were scored. For these mutants the green cell assay titer used was the limit of detection in the assay. Thus, the log difference is a minimum estimate.

These seven mutants were found previously to bind heparin sulfate to the same extent as wild type rAAV2 (Fig. 3-2).

Three of the mutants R459A, R484A, and K532A produced virus that was essentially non-infectious with P/I ratios between 7.2 x 10^4 and 3.6 X 10^6 compared to the wild type ratio of 25 (Table 3-3, Fig. 3-4). The P/I ratios for these mutants were minimum estimates based on the GCA assay sensitivity of 1 x 10^4 IU/ml. In fact, no transduction events were seen with any of these mutants.

R459A was the most severe example of three mutants (R459A, H509A, and H526A/K527A) that were essentially wild type for heparin binding but defective for transduction (Fig. 3-4). These mutants were presumably defective in some late stage of viral infection.

Finally, all five of the mutants that were defective or partially defective for heparin binding (R484A, R487A, K532A, R585A, and R588A) were defective for transduction. However, the loss of infectivity did not correlate completely with the loss of heparin binding. (Compare Figs. 3-2 and 3-4). Two of these mutants (R484A and K532A) were only partially defective for heparin binding but severely defective (>5 logs) for transduction, suggesting that some other step in viral infection was defective in these mutants in addition to heparin binding. The remaining heparin binding mutants (R487A, R585A, and R588A) had defects in transduction that approximately correlated with their ability to bind heparin.

Evaluation of R585A/R588A Cell Attachment *In Vivo*

As mentioned earlier, alanine substitutions at either position 585 or 588 were the only mutations that completely abolished binding to heparin agarose (Fig. 3-2), suggesting that these two arginines were primarily responsible for

heparin binding. Moreover, the extent to which mutation of either or both of these residues inhibited transduction (Fig. 3-4, 1.5-3 logs) was approximately the same when soluble heparin sulfate is used to inhibit wild type rAAV2 infection (47) and data no shown. We therefore examined these mutants in more detail.

To see if the defect in transduction of R585 and R588 mutants could be overcome by using higher input MOI's, cells were co-infected with rAAV2 or the mutant viruses at an MOI=500 genome containing particles/cell. Twenty-four hours post infection cells were examined by fluorescence microscopy and counted by fluorescence activated cell sorting (FACS). The data from three independent experiments and representative histograms are shown in Fig. 3-5. As expected the defects in transduction of the single mutants, R585A and R588A, could be overcome by higher MOI's (56% and 25% transduction for R585A, and R588A, respectively). Predictably, the level of recovery of the double mutant, R585A/R588A, was lower (10% transduction). However, it was clear that the fluorescence intensity profile for the heparin binding mutants was quite different from wild type, suggesting a significant delay in the onset of GFP expression by 24 hours. In contrast, the level of transduction of the conservative double mutant, R585K/R588K, and the heparin positive mutant, N587A, was indistinguishable from wild type.

As a more direct assay for cell attachment, we infected Hela C12 cells and tracked the location of viral DNA. Cells were infected with rAAV2 or R585A/R588A at an MOI=1000 genome containing particles as determined by

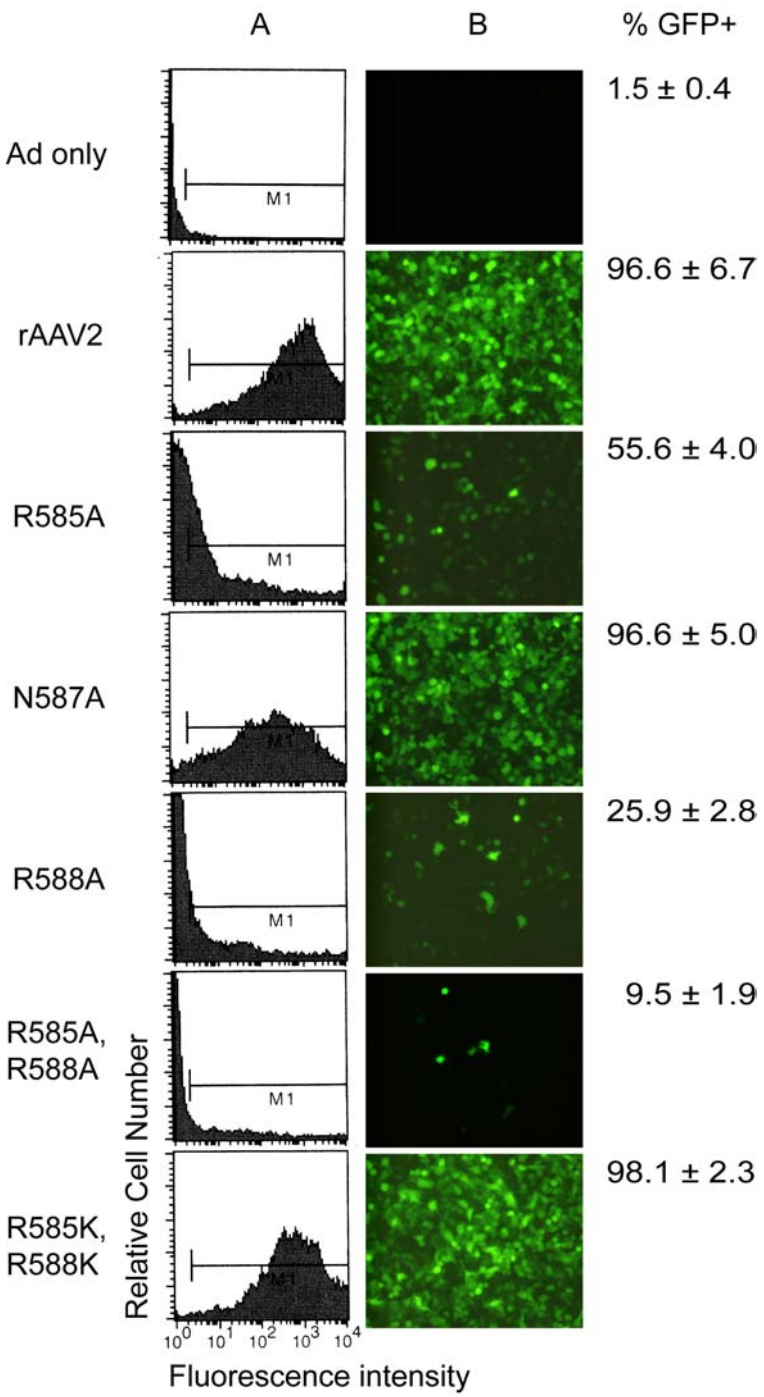

Figure 3-5. GFP transduction ability of mutants in HeLa C12 cells. A) Cells were infected with wild type rAAV or mutant virus at an MOI = 500 genomic particles and an Ad5 MOI = 10 pfu per cell. Twenty-four hours post infection cells were fixed with 2% paraformaldehyde and the number of GFP positive cells was determined by FACS analysis. B) Representative GFP fluorescence microscopy image.

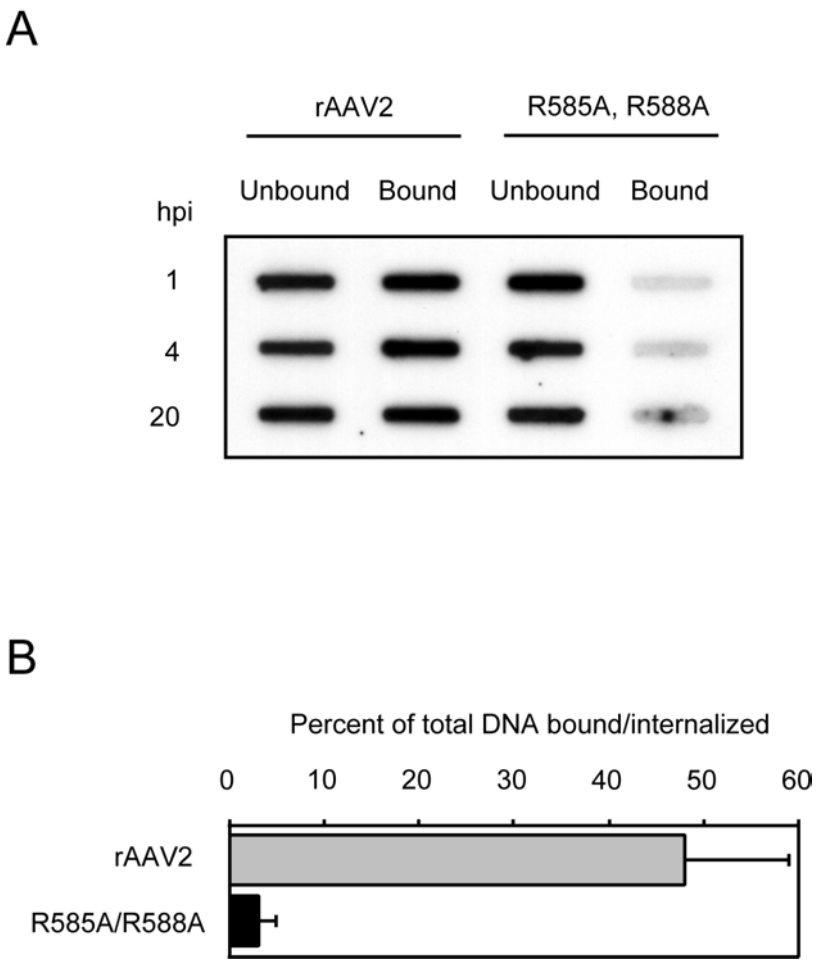

Figure 3-6. Binding and uptake of rAAV2 and R585A/R588A in Hela C12 cells. (A) 10^6 cells were infected with rAAV2 or R585/R588A at an MOI = 1000 genome containing particles per cell. At the indicated times, infection media was removed and saved. The cells were washed and harvested, and Hirt DNA was extracted from both the infection media and the cell pellet. Southern analysis was performed using an [α-^{32}P]-dATP labeled GFP probe. (B) The percent bound/internalized DNA was calculated by dividing the total DNA present in both the media and the cell pellet by the amount bound/internalized for each time point. The average of three determinations is shown. Error bars indicate a standard deviation.

RT-PCR. At 1, 4, and 20 hpi, the infection media was removed and saved, and the cells were washed extensively to remove any residual unbound virus. The cells were then harvested and low molecular weight DNA was extracted from both the infection media (Unbound) and the cell pellet (Bound or internalized) by the Hirt procedure and transferred to nitrocellulose for Southern hybridization with an [α-^{32}P]-dATP labeled GFP probe (Fig. 3-6).

We saw that at all time points rAAV2 DNA was detectable both bound/internalized and in the infection media. In contrast, cells infected with 10-fold more genomic copies of R585A/R588A showed the vast majority of the signal only in the unbound fraction (Fig. 3-6A). Phosphor imager analysis determined that at each time point approximately one third of the total rAAV2 DNA was attached or internalized compared to only 1-3% of R585A/R588A (Fig. 3-6B and data not shown). As these infections were performed at 37°C, the process of internalization should not have been prevented. This result demonstrated that the block in infection for mutant R585A/R588A occurred at the cell attachment stage or internalization stage, and correlated to heparin sulfate binding *in vitro*.

Loop Swapping Confers Heparin Binding to AAV5

Although the primary amino acid sequences are moderately divergent, the architectural position of ß-sheets and loops is predicted to be very similar among AAV serotypes (99). We hypothesized that if R585 and R588 were the critical residues involved in HSPG binding, then it should be possible to substitute that region of AAV2 into AAV5 to create a hybrid virus capable of interacting with heparin-agarose. To achieve this, we generated a recombinant virus, designated

rAAV5-HS by replacing a short loop containing residues 585 through 590 from AAV2 into a region predicted to be structurally equivalent in AAV5 (Fig. 3-7A). Loop substitution rather than point mutagenesis was done to account for the possibility of additional Van der Waals interactions or hydrophobic contributions from nearby amino acids.

Production and purification of rAAV5-HS was unaffected by the six amino acid substitution (Fig 3-7B, Table 3-3). When we tested rAAV5-HS in the *in vitro* heparin-agarose binding assay, it was indistinguishable from wild type rAAV2 (Fig. 3-7C). These data suggested that this region of AAV5 was surface accessible, and that heparin-agarose binding could be artificially conferred by the six amino acids containing R585 and R588.

To compare the infectivity of rAAV5 and rAAV5-HS, we generated packaged viruses that contained a recombinant AAV5 genome in which the GFP reporter gene was flanked by AAV5 terminal repeats. (See Materials and Methods). The infectivity of these viruses was compared to rAAV2 in a GCA assay and particle to infectivity ratios were calculated as before (Fig. 3-7D). rAAV5 was able to transduce Hela C12 cells at a low efficiency, approximately 2.5 logs lower than AAV2. However, no transduction was seen with AAV5-HS ($<1 \times 10^4$ IU/ml) (Table2, Fig. 3-7D). Given the minimum sensitivity of the GCA assay this meant that the P/I ratio of AAV5-HS was at least 3.5 logs higher than rAAV2 and at least 1 log higher than wild type rAAV5. We concluded that although substitution of these five heterologous amino acids into the AAV5

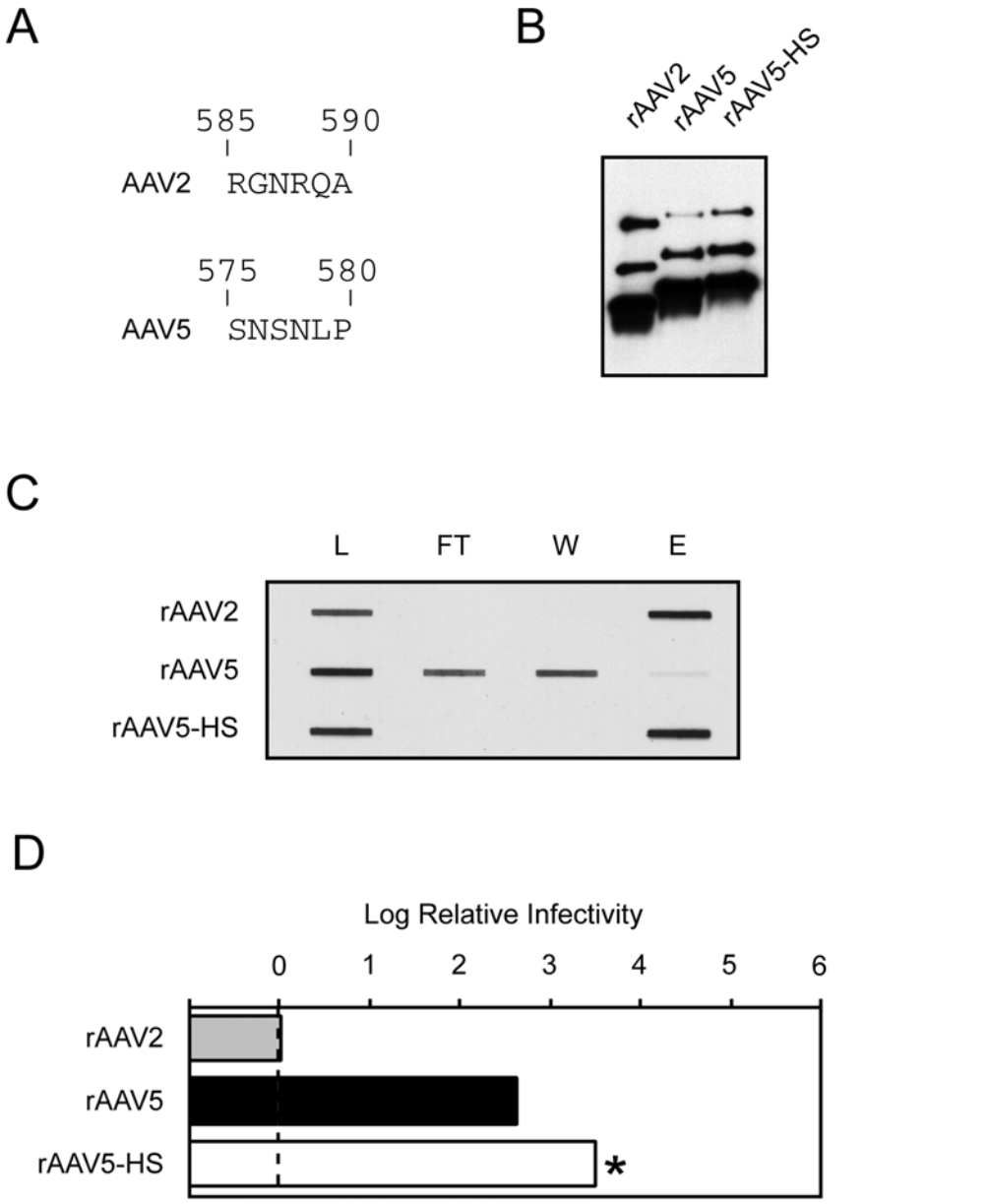

Figure 3-7. Modifying the heparin binding properties of AAV5. A) Alignment of AAV2 amino acid residues 585 through 590 to residues predicted by amino acid alignment to be structurally equivalent in AAV5. B) Western blot of iodixanol virus stocks. Equal volumes of virus were separated by 10% SDS-PAGE and analyzed by western blot using the B1 antibody. C) Novel heparin binding properties of AAV5-HS. Heparin-agarose binding was performed as described in Fig 3-2. See Fig. 3-2 for abbreviations. D) The log of the particle to infectivity ratio of the rAAV5 variants normalized to wild type rAAV2 as described in Fig. 3-4.

capsid restored heparin binding to the level of AAV2 capsids, it was not sufficient to produce AAV2 levels of infectivity in a cell line normally permissive for AAV2.

Discussion

The aim of this study was to identify amino acids in the capsid of AAV2 that mediate binding to heparin sulfate proteoglycans. Several lines of evidence suggest that HSPG serves as the primary receptor for AAV2. Inhibition of AAV2 infection can be demonstrated by competition with soluble analogs, GAG desulfation by sodium chlorate treatment, antibody competition, enzymatic removal of heparin, and use of mutant cell lines that express varying levels of HSPG (47, 96, 127, 147). Binding to heparin sulfate is usually the result of electrostatic charge interactions between basic amino acids (R, K, or H) and negatively charged sulfate residues (51, 82). During the course of our previous mutagenesis studies, we were able to eliminate many of the basic amino acids in the AAV2 capsid that could potentially contribute to heparin sulfate binding (147). In this study we examined the remaining basic residues by looking at their conservation in AAV serotypes 1-5. Those that were present in all five serotypes were not likely to contribute significantly to heparin binding. Those that were conserved in the heparin binding serotypes, AAV1-3, but not in the remaining serotypes were targeted for mutagenesis. Finally, we also took advantage of the fact that we had previously identified R585 and 588 as potential heparin binding amino acids (147) and that these amino acids were located in a cluster of basic residues at the three fold axis of symmetry (151). All of the basic amino acids in this cluster were also targeted for mutagenesis. This approach yielded a total of 15 amino acids that could have been involved in heparin binding and we

characterized alanine mutations at all of these positions. We note that this approach does not necessarily identify all possible heparin binding amino acids. For example, R484, which is basic in all five serotypes was tested because of its proximity to R585 and R588 and subsequently proved to be involved in heparin binding.

Heparin Binding and Infectivity

Our studies indicated that capsids with mutations at residue 484, 487, 532, 585 or 588, were partially or completely defective for heparin-agarose binding. The most severe defect was found with mutations in R585 and R588. No binding to heparin sulfate columns could be detected with either mutant (Fig. 3-2), and both mutations reduced the particle to infectivity ratio by two to three logs (Table 3-3). Mutants that contained substitutions at both positions had even lower infectivity.

The phenotypes of R487A, R585A, and R588A, were probably largely due to defective heparin binding. For example, the double mutant R585A/R588A was approximately 10-50 fold more defective in cell binding and internalization than wild type (Fig. 3-6B) at artificially high MOI's (500-1000), and essentially undetectable at lower MOI's (1-10) (data not shown). This was consistent with the approximately 2000 fold lower infectivity of R585A/R588A (Table 3-3), as judged by the change in particle to infectivity ratio. Another indication that heparin binding was primarily responsible for the defects in R585 and R588 was the fact that conservative mutations at these two positions (R585K and R585K/R588K) produced virus particles with properties similar to wild type (Figs. 3-2, 3-4, 3-5, and Table 3-3). Results from the conservative lysine substitutions

at R585 and R588 are reasonably consistent with electrostatic attraction being the primary mediator for AAV-heparin interaction. R585K, the least defective heparin binding mutant (Fig. 3-2), had transduction levels nearly equal to rAAV2 (Fig. 3-4), and R585K/R588K was only slightly more defective for heparin binding (Fig. 3-2) and transduction (Fig 3-4), and within one log of wild type. Furthermore, when cells were infected at a high MOI, robust transduction was observed for both mutants (Fig. 3-5). Finally, substitution of a six amino acid sequence containing R585 and R588 imparted heparin binding to AAV5 that was comparable to that seen with AAV2 (Fig. 3-7). Although similar experiments were not done with the R487 position, it was clear that mutation of R487 produced virus with a more modest defect in heparin binding (Fig. 3-2) and in infectivity (Fig. 3-4).

In addition to R487A, R585, and R588, two other mutants were found that were defective for heparin binding, R484A and K532A. R484A and K532A, like R487A had a more modest effect on binding to heparin sulfate, but unlike the other heparin binding mutants, these two mutations had a dramatic effect on transduction efficiency. Both R484A and R532A were more than 5 logs less infectious than wild type capsids (Table 3-3, Fig. 3-4). This severe defect is presumably due to a different block in the infection process that is unrelated to heparin binding, but as we have not identified the defect yet. The result from K532A is consistent with our earlier study that identified a mutant (mut 37) that contained six amino acid substitutions that included K532A (147). Mut 37 had a phenotype identical to K532A in that it produced full virus particles that were non-

infectious and more recently has been shown to have a modest defect (approximately 5 fold) in heparin binding and internalization (Xiao and Muzyczka, unpublished). Taken together these observations potentially map this defect to a single amino acid.

Computer Visualization of the AAV2 Structure

We took advantage of the recently published atomic structure of AAV2 (PDB ID code: 1LP3) (151) and examined the positions of the heparin binding mutations (Fig 3-8). Symmetry transformation operations from the original PDB file were applied to generate a VP3 trimer arrangement in the context of an icosahedron. When viewed directly down a three-fold axis, residues R484, R487, R532, R585 and R588, represented in CPK format, are located in a linear formation lining one side of each three-fold related spike (Fig 3-9 and Fig. 3-12C). When viewed across the top surface of the trimer, residues R585 and R588, which are contributed by one of the peptides in the trimer, are positioned above a linear arrangement of R484, R487 and K532 (Fig 3-10 and Fig. 3-12D), which are contributed by a second peptide in the trimer. Thus, it appears that a heparin binding motif is formed from some combination of these five amino acids using amino acids from two different polypeptides. We also generated an electrostatic potential surface map of a VP3 trimer (Fig. 3-12A and 3-12B), in which areas of positive and negative charge are represented as blue and red, respectively. When viewed perpendicular to the three fold-axis, the five amino acids mapped by these studies appear to contribute collectively to a basic patch on one side of each three-fold related spike (Fig. 3-12B). The charge, clustering, and surface presentation of these residues are all consistent with a model

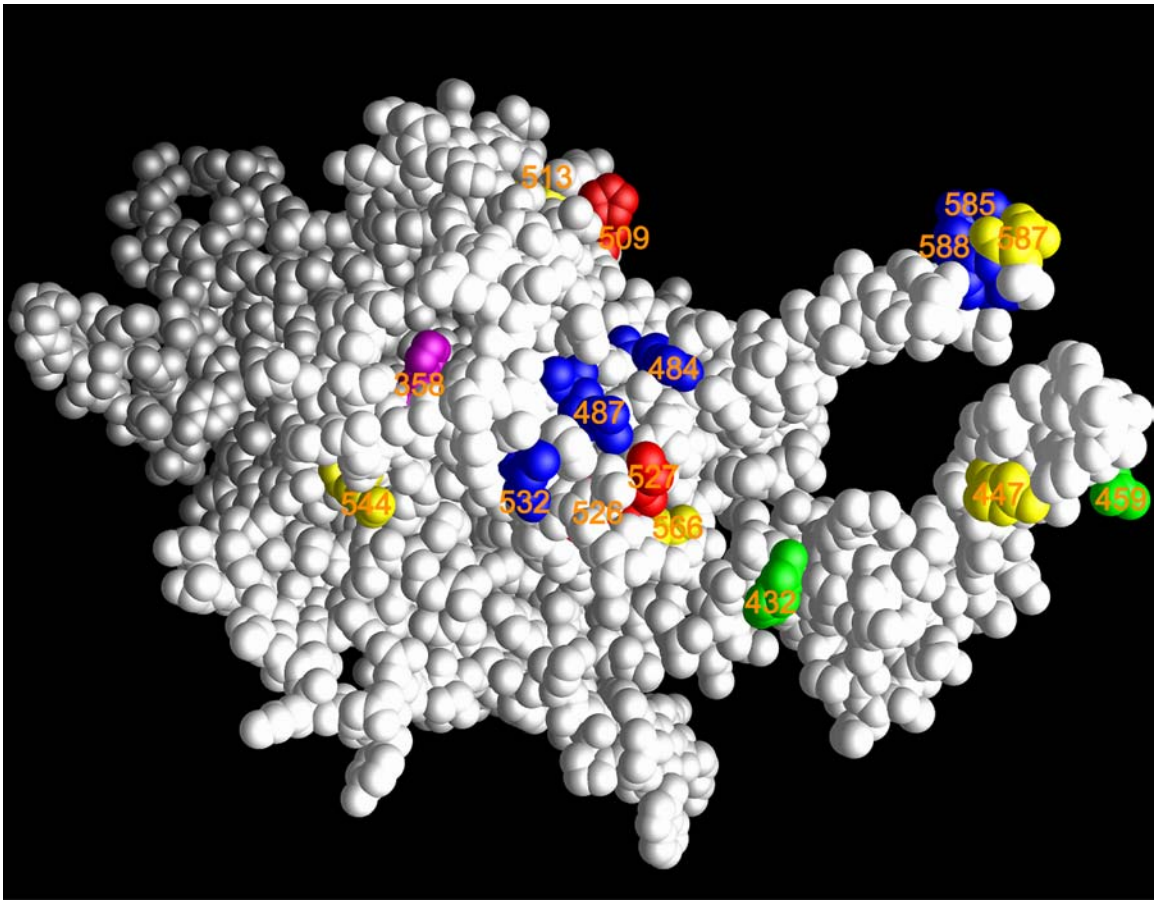

Figure 3-8. Location of mutations in VP3 monomer. The atoms composing the VP3 monomer are rendered in CPK format. The residues mutated in this study are labeled by their numerical position and color-coded for clarity. White, residues that were not mutated; Yellow, wild-type; Blue, infectivity and heparin binding mutants; Red, infectivity mutants; Green, DNA packaging mutants; Magenta, Assembly mutants.

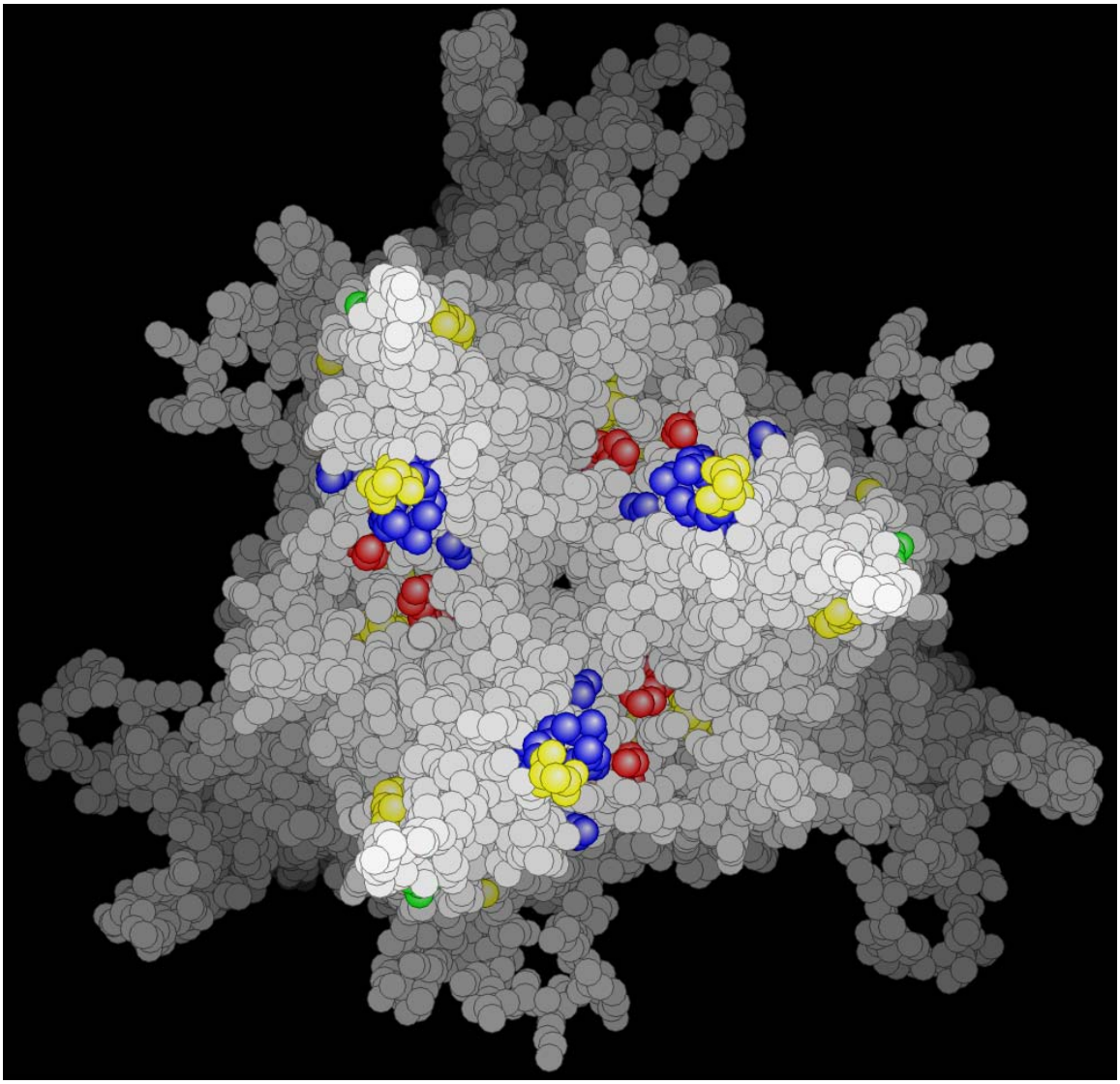

Figure 3-9. Location of mutations in a VP3 trimer viewed down a 3-fold axis of symmetry. Atoms composing the VP3 trimer are rendered as shaded balls. The residues mutated in this study are color-coded by their phenotype. White and grey, residues that were not mutated; Yellow, wild-type; Blue, infectivity and heparin binding mutants; Red, infectivity mutants; Green, DNA packaging mutants; Magenta, Assembly mutants.

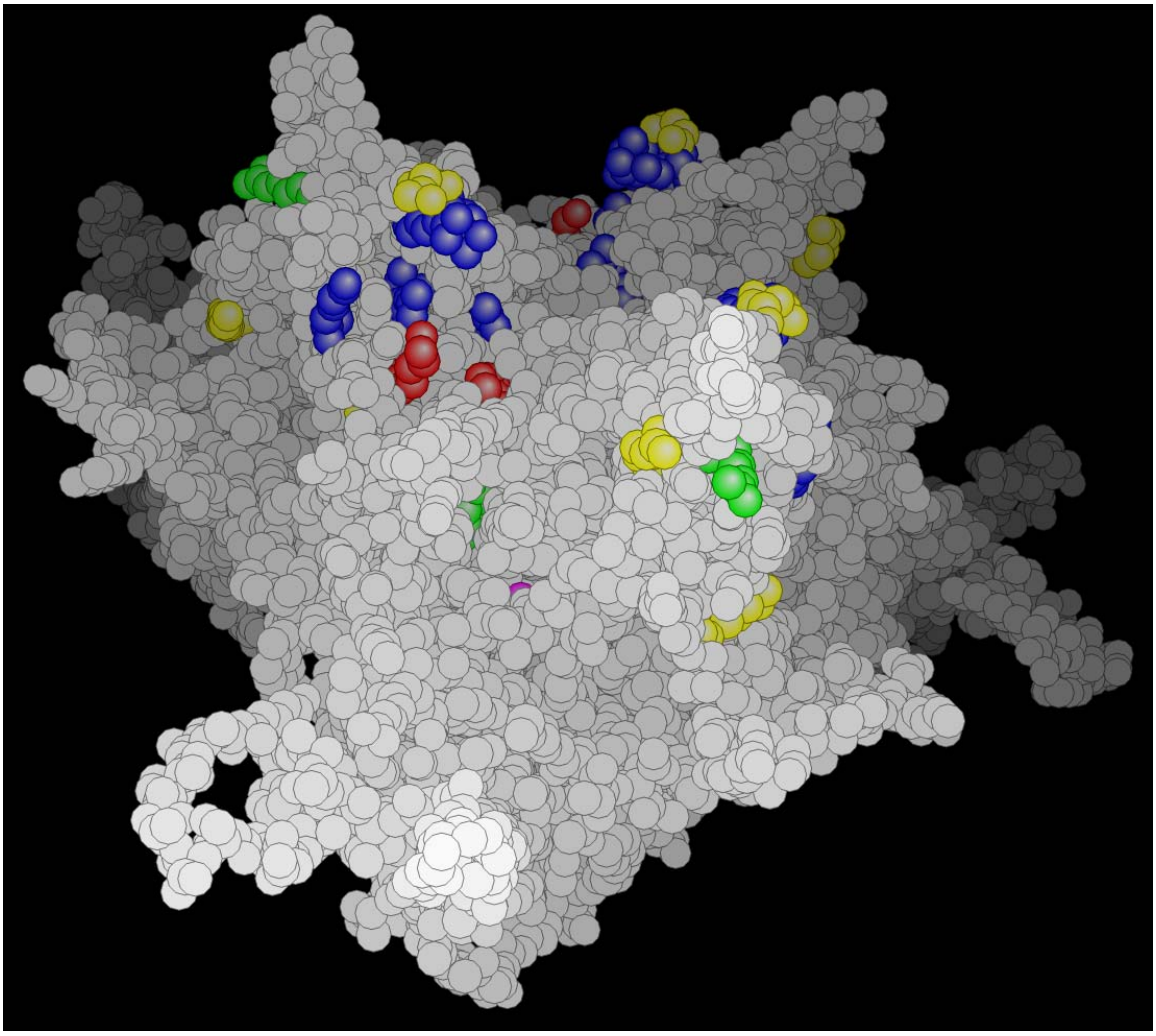

Figure 3-10. Location of mutations in a VP3 trimer when viewed across the 3-fold axis of symmetry. Atoms composing the VP3 trimer are rendered as shaded balls. The residues mutated in this study are color-coded by their phenotype. White and grey, residues that were not mutated; Yellow, wild-type; Blue, infectivity and heparin binding mutants; Red, infectivity mutants; Green, DNA packaging mutants; Magenta, Assembly mutants.

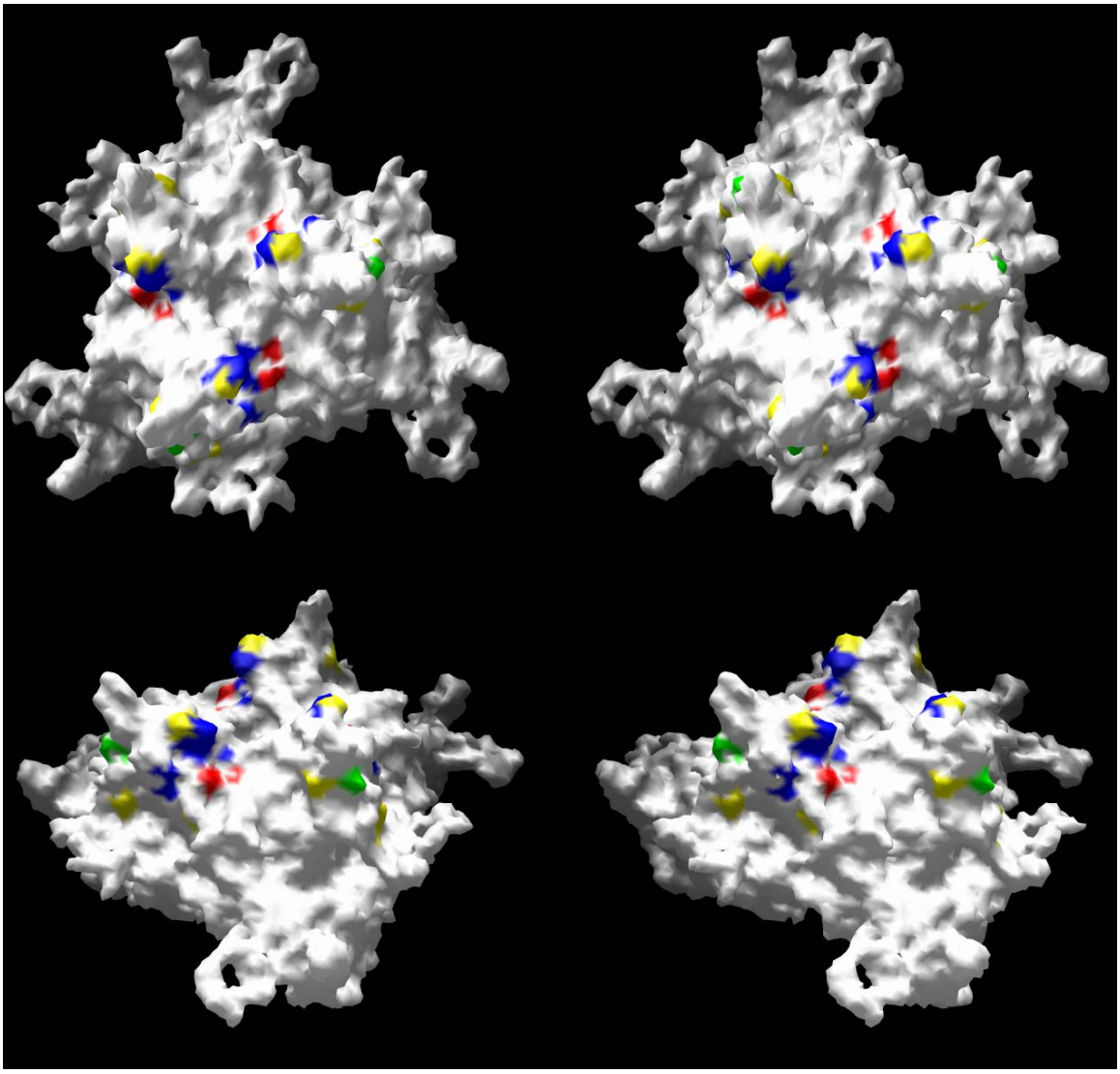

Fig 3-11. Stereodiagram of the top surface of a VP3 trimer. The residues mutated in this study are color-coded by their phenotype. White and grey, residues that were not mutated; Yellow, wild-type; Blue, infectivity and heparin binding mutants; Red, infectivity mutants; Green, DNA packaging mutants; Magenta, Assembly mutants.

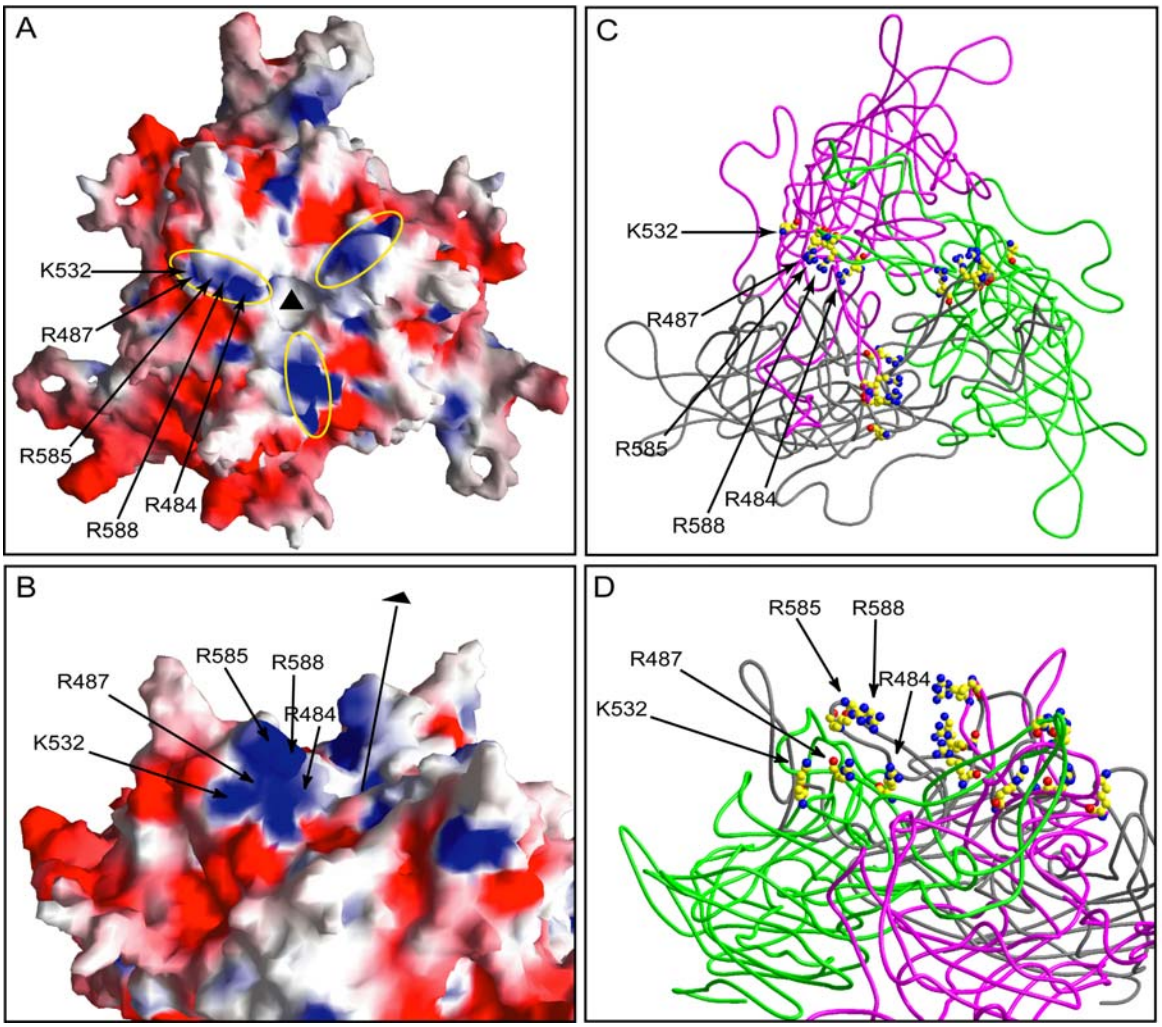

Figure 3-12. Surface and ribbon and diagrams of the atomic model of an AAV2 trimer. A) Electrostatic surface potential of the VP3 trimer viewed down a three-fold axis (black triangle) calculated with GRASP (88) running from –12 (red) to +12 (blue). B) Electrostatic surface potential of VP3 trimer viewed from the side perpendicular to the three-fold axis indicated by a black line and triangle. Labeled arrows indicate the position of residues involved in heparin binding. C) VP3 trimer viewed down a threefold axis. C_α-backbones for individual monomers are rendered as pink, gray and green ribbons. Residues that contribute to heparin binding are shown in CPK representation with atoms in conventional colors: Yellow, carbon; blue, nitrogen; red, oxygen. These images were generated in Bobscript/Raster3D (65, 79). D) VP3 trimer viewed from approximately the same vantage point as in Fig 3-8B. Features are as described above in (C).

of electrostatic attraction. Residue K527 is surface accessible, unlike its direct neighbor H526, and although it contributes to the base basic cluster at the three fold spike K527 does not appear to be required for heparin binding (Fig. 3-2). A stereodiagram of the surface of a VP3 trimer providing a three-dimensional visualization of the positions of the mutations is shown in Fig. 3-11.

The five mutations that affected heparin binding were located in the large loop IV region, which among AAV serotypes has low overall sequence conservation and includes all of the previously identified insertion and substitution mutations that affect heparin binding. Interestingly, with the exception of N587, the stretch of amino acids encompassing 585 to 590 is unique to AAV2 and is not present in AAV3, which is the other AAV serotype that has been shown to bind efficiently to heparin sulfate. Mutation of N587 had no effect on heparin-agarose binding and only minor effects on transduction. Conceivably residues R484, R487 and K532 could be the dominant residues involved in heparin sulfate binding for AAV3.

The apparent dissociation constant (Kd) of AAV2 and heparin sulfate was determined by competition analysis to be $2x10^{-9}$ M (96). Although this is higher than some heparin-protein interactions, it is sufficiently strong to suggest cooperative binding by one heparin sulfate glycosaminoglycan chain to multiple attachment points. We were unable to address in this study whether heparin sulfate could form a bridge between basic residues in one of the threefold spikes to those in another (yellow ovals in Fig. 3-12A). However, as the average chain length of heparin glycosaminoglycans varies between 50-200 disaccharide

repeats that adopt a helical conformation 40-160 nm in length, it is conceivable that a heparin sulfate chain could wrap around the exterior of the capsid through cooperative binding of multiple spikes at the threefold axis of symmetry. Although we did not undertake a rigorous computational docking analysis, we were able to manually superimpose a heparin molecule (PDB ID code 1NTP) in several orientations that placed multiple reactive sulfate and amine groups within accepted electrostatic attraction distances on pairs of residues spanning the spikes (data not shown). This approach, however, does not account for either the flexibility of heparin or for the possibility of additional molecular interactions. Co-crystallization studies of AAV2 and heparin sulfate are needed to clarify this issue.

Mutants That Bind Heparin But Are Still Defective

Several new mutants were found that bound heparin sulfate as well as wild type but still produced defective particles. H538A was defective for particle assembly. There are a number of reported examples of mutations that disrupt AAV2 particle formation, several of which are located in the conserved β-strand regions (100, 115, 147). H358 is neither surface accessible nor in a conserved β- strand, and instead is internally located in a subunit situated at the base of a loop from another subunit that forms the tall outer peak of the spike. In this position it may function to stabilize or orient the extensive subunit interdigitation that occurs during capsid assembly in this region. Mutants R459A, H509A, and H526A/K527 bound heparin-agarose efficiently but had particle to infectivity ratios that were two to more than three logs higher than wild type. Like K532A

and R484A, these mutants are presumably defective in some stage of the infectious entry pathway between secondary receptor binding and uncoating. H509 is located at the base of the valley between each spike and does not contribute to the basic heparin binding patch. Ongoing studies in the laboratory are examining the block in infectivity for these mutants.

DNA Packaging

The process of DNA packaging is thought to occur by an active process requiring NTP consumption coupled to the helicase activity of the small Rep proteins (61). Although none of the mutations that assembled an A20 positive particle were completely deficient for DNA packaging, mutant R459A produced a 40-fold excess of empty capsid particles compared to rAAV2. Other studies have reported that short insertions at positions 323, 339, 466, 520, 540, 595, 597 that did not interfere with capsid formation still reduced DNA packaging to levels detectable only by PCR amplification (115). In addition, a point mutant R432A prevents DNA packaging (147). R459 points away from the three-fold axis on the outside of the spike slightly below the level of R585 and R588 and is highly accessible. Although the relationship between these mutations and their mechanism of action is unclear, it is possible that they disrupt protein-capsid or DNA-capsid interactions. It is tempting to speculate that some of these residues might act as a binding site for Rep or a cellular protein. In particular, nucleolin, a 110KDa nuclear shuttle protein, binds specifically to the AAV2 capsid both *in vitro* and *in vivo* and is found co-localized with the capsid in the cytoplasm and nucleus of infected cells (95). It has also been shown to bind ssDNA of a related parvovirus, the minute virus of mice (3).

In summary, we have reported an analysis of the HS binding ability and transduction potential of mutants at fifteen positions within the capsid of AAV2. We identified residues that affect capsid assembly, DNA packaging, and mediate heparin sulfate binding. In particular, mutants with the combined mutations in R585 and R588 should be valuable reagents for the development of heparin independent retargeted virus vectors.

CHAPTER 4
THE EFFECTS OF MUTATIONS IN THE TERMINAL REPEAT REGIONS OF THE ADENO-ASSOCIATED TYPE-2 VIRUS *IN VIVO*

Introduction

The 145 bp inverted terminal repeats (TR) located at each end of the AAV genome are *cis*-acting sequences required for efficient virus rescue (23, 24), replication, transcription, packaging, and integration. In solution, three GC rich, internal palindromes fold back upon themselves via extensive hydrogen bonding to form a highly thermostable secondary structure with a $\Delta G = -114$ kCal/Mol^{-1} (21). The ordered "T" shaped TR is composed of four discreet regions, the AA' palindrome forming the stem-arm, the BB' and CC' palindromes forming the cross-arms, and the D stem, a 20nt single stranded region not involved in hairpin formation (Fig 4-1) (27).

All of the functions associated with the TR are believed to require interactions with the p5 Rep proteins. Correspondingly, a 16 bp core sequence called the rep binding element (RBE) is sufficient for Rep binding *in vitro* (22). The RBE is located within the A-stem and is composed of four continuous 5'-GAGC-3' repeats. The interaction between Rep and the TR is thought to be more complex than a single linear binding site, however, as methylation interference studies showed that the tip of the C-stem (RBE') also interacts with the large Rep to increase its affinity about 100-fold. Additional RBE's are located in the p5, p19 and p40 promoter regions although the affinity that Rep associates

with each element varies (1, 10, 19, 22, 35). Multiple RBE homologs exist in the human genome and are bound efficiently by the large Rep proteins (33). Interestingly, Rep can form a physical bridge between the terminal repeat and a RBE homolog. As might be expected, Rep mutants that fail to bind the TR are deficient in proviral rescue, genome replication, transcriptional regulation, DNA packaging and integration into the host DNA (7).

Although not a necessary co-factor for binding, when ATP is present in a binding reaction, Rep can introduce a strand- and site-specific nick between two thymidines in the core *trs* sequence 3'-GGT/TGA-5'. This results in a covalent 5'-phosphotyrosyl linkage of Rep to the parental template, and exposes a 3'-hydroxyl group on the nicked strand. Newly replicated D-stem DNA and the free 3'-OH are believed to act as a primer for DNA polymerase re-initiation in a mechanism used by AAV and other linear genomes to prevent successive shortening of the DNA during replication. Rep mutants that are deficient in endonuclease activity fail to undergo proviral rescue and DNA replication (6) linking nicking to AAV DNA synthesis.

The TR has been extensively mutagenized and characterized with respect to Rep binding and nicking *in vitro*, but results about the effects of similar mutations *in vivo* have been impeded by three major obstacles encountered during cloning and virus production. First, the TRs are highly recombinogenic and susceptible to deletion and/or modification during plasmid propagation in E.coli. Second, the high thermal stability of the TR prevents efficient polymerase read-though which hinders PCR mediated oligonucleotide mutagenesis and

sequencing. Third, attempts to produce viruses with relatively large modifications in the TR result in non-infectious virus stocks composed of empty capsids.

The aim of this study was two-fold: first, to develop a method for synthetically producing AAV genomic templates with specific point mutations in the TR for generating infectious virus stocks. Second, to examine how *cis*-mutations in the TR affect the functional activities of proteins that bind to the TR during the AAV lifecycle *in vivo*. To achieve this we examined the stages of rescue from a plasmid template, DNA replication, RNA transcription, protein expression, DNA packaging, and site-specific integration.

Results

Characterization of Rep68 Nicking Efficiency on Mutant TR Substrates

The model of AAV DNA replication suggests that endonucleolytic cleavage of the terminal repeat by the Rep protein is an absolute requirement for synthesis of full-length, monomeric, progeny DNA strands. Somewhat paradoxically, the inability to cut its own DNA leads to progressively shorter defective-interfering (DI) genomes. Reliable and reproducible *in vitro* reactions that examined the TR binding and *trs* cleavage activities of Rep78/68 thought to occur *in vivo* have been developed by a number of labs (1, 3, 4, 12, 13, 18, 20, 22, 34). Five synthetic TR's were produced on a preparative scale for the purpose of analyzing Rep nicking, as well as downstream virus production. To achieve this, microgram quantities of oligonucleotides that contained either the wild type sequence or specific transversion mutations in their sequences were annealed, ligated, and gel purified in the form of a complete TR (Fig. 4-1A). With the exception of MutD, the mutations were engineered into locations known to alter

the Rep binding or nicking activity on the TR (2, 22). MutE replaces the nicked nucleotide located in the core *trs* site and decreases Rep nicking nearly 10-fold. MutY is located in a spacer sequence between the RBE and the core TRS and stimulates artificially high nicking. MutR is in the central region of the RBE and is a 2 bp transversion that decreases the affinity of Rep68 the RBE 10-fold (22). MutD contains mutations in the 5' RBE that has minimal effects of Rep activity, and in what might constitute the core binding nucleotides of the single stranded D-Stem binding protein (ssDBP). ssDBP is thought to be a cellular phosphoprotein called the FK506 binding protein-52 (FKBP-52), and in its phosphorylated form represses AAV DNA replication.

In vitro Rep-mediated endonuclease cleavage reactions the five synthetic TRs was performed using baculovirus expressed Rep68 under normal conditions and the products were resolved on a 10% denaturing polyacrylamide gel (26). The fraction of the total input substrate cleaved during the reaction was calculated by phosphor image analysis and plotted compared to wild type. A histogram comparing the nicking efficiencies of these substrates to wild type is shown in (Fig 4-1B). Consistent with previous work, mutation of the core nicked nucleotide in MutE reduced accumulation of the nicked product almost 10-fold, whereas MutY had enhanced accumulation of nicked product. Since binding is a prerequisite to nicking, it was anticipated that MutR reduced nicking to a level one third of wild type. Finally, MutD was nicked at about the same level as MutR. The reasons for this remain unclear but it suggests that sequences outside the

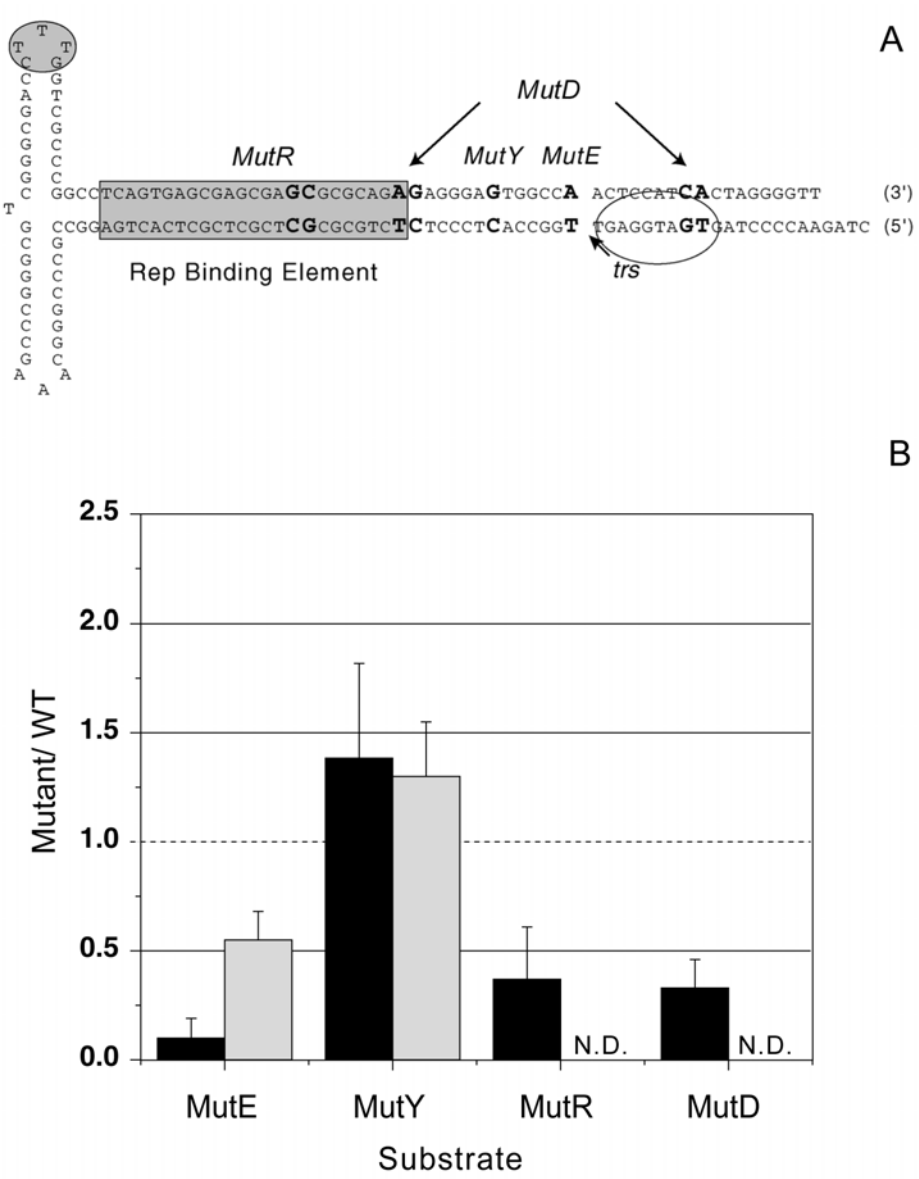

Figure 4-1. Nucleotide sequence and functional activities of wild type and mutant TRs. A) The wt AAV TR is diagrammed in hairpin conformation. The RBE and RBE' are indicated with a gray box and oval. The trs is indicated with an arrow. The ssDBP binding site is indicated with a transparent oval. Boldface lettering indicates the positions of the transversion mutations. B) Nicking and *in vitro* DNA replication reactions were performed as described previously (1, 2). Black boxes indicate the relative nicking activity for each mutant expressed as a fraction of wt. Bars indicate the standard deviation a minimum number of three separate assays performed on each substrate above. Grey columns indicate the relative *in vitro* replication activity for each mutant no-end construct expressed as the amount of mutant substrate DpnI resistant DNA synthesis divided by the amount of wild-type substrate DpnI resistant DNA synthesis.

core RBE and *trs* contribute possibly by interfering with the formation of a predicted stem-loop structure. Nonetheless, the results from this experiment confirmed previous observations which identified specific TR nucleotides that contribute to Rep binding and *trs* cleavage activity (1, 2).

The effects of WT and mutant TRs were tested in a well-characterized *in vitro* DNA replication assay (Fig. 4-3) (16, 17). In order to produce the substrate for this assay, synthetic TR's were ligated to the XbaI fragment of pIM45 (AAV2 genome without TR's) and gel purified to produce No End (NE) DNA. The double-stranded, covalently closed ligation products were purified by exhaustive exonuclease III digestion and recovered from a 0.7% agarose gel. Unlike the wild type genome, NE is double stranded and having no free 3' end generates a single stranded covalently closed circle upon denaturation.

Substrates were incubated with an Ad infected 293 extract and purified Rep68. Radiolabeled products were digested with DpnI to removed unreplicated plasmid DNA and were separated a 0.7% agarose gel. The amount of DNA synthesis was quantitated by phosphorimager analysis (Fig 4-1B). Consistent with predictions, the mutation that stimulated Rep68 nicking in MutY also enhanced AAV DNA replication compared to the NE constructs containing wild-type TRs. Additionally, the mutation that reduced Rep68 nicking, MutE, inhibited replication although not to the same extent as nicking. We concluded that Rep nicking activity directly influences *in vitro* DNA replication.

Generation of AAV Viruses With Mutations in the TR

In order to accurately measure the kinetics of rescue, replication, and integration *in vivo* it was necessary to produce infectious virus stocks. Early

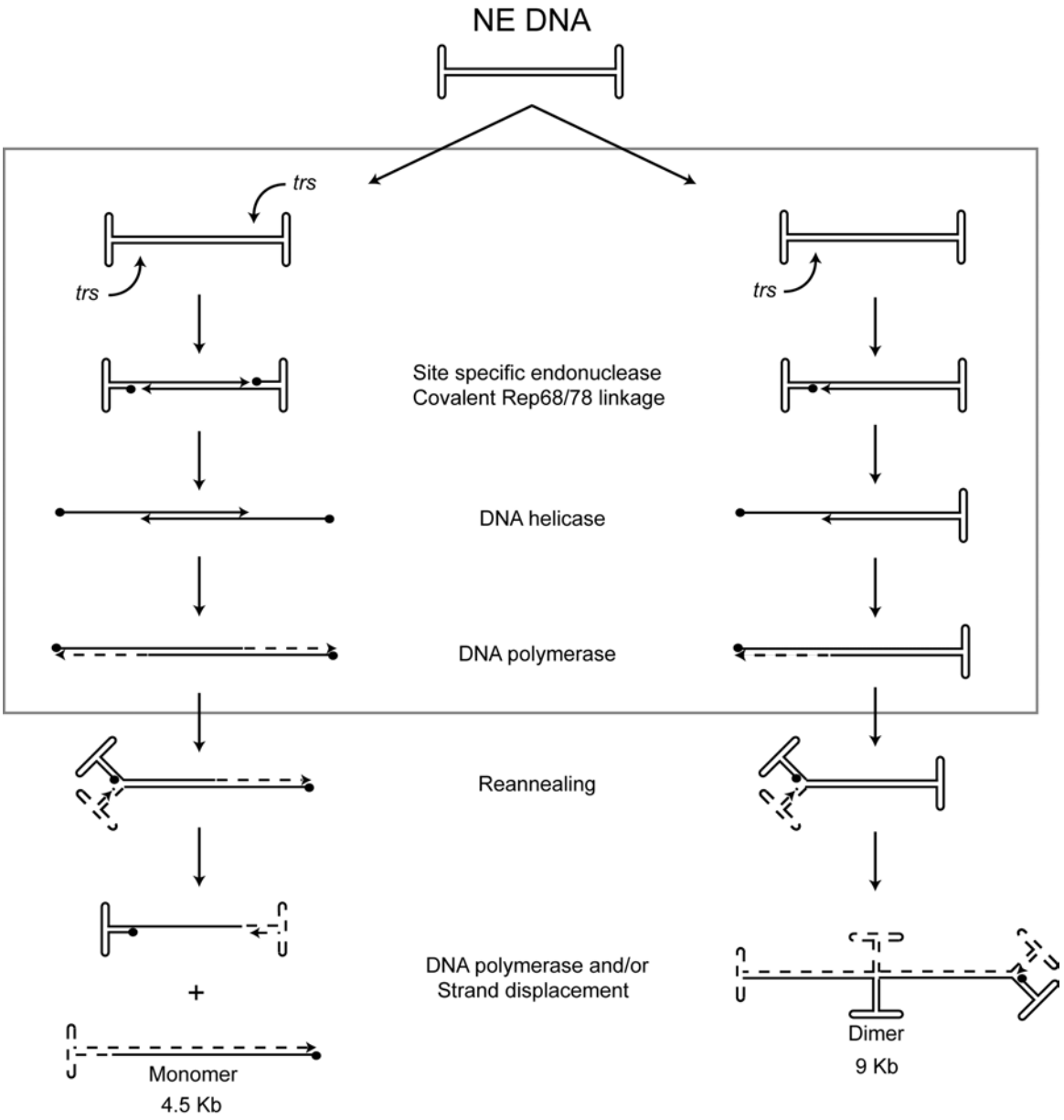

Figure 4-2. Schematic of the intermediates and products formed in an AAV *in vitro* DNA replication assay. No End (NE) DNA substrate has no free 3' OH and requires Rep nicking activity in order to be replicated. The sequence redundancy of the TRs permits Rep to introduce one or two nicks into the NE substrate ultimately leading to different replication products, left and right pathway, respectively. The gray box indicates step that occur during terminal resolution. Filled balls, covalently linked Rep 68/78; Dashed lines, newly replicated DNA; Solid lines, unreplicated, parental DNA.

studies in AAV genetics showed that plasmids containing an AAV genome with deleted TRs resulted in the production of non-viable, empty virus capsids (14, 24). We predicted that by introducing minor point changes in the TR, rather than longer deletions, DNA packaging would not be significantly affected enabling us to generate infectious virus stocks. Using the same NE substrates for the *in vitro* DNA replication assay, we generated virus stocks using a triple transfection protocol.

To avoid the potential for altered transcriptional regulation from the mutant templates, pIM45 plasmid was included in 100-fold molar excess over the mutant NE substrate to ensure constant Rep and Cap protein expression. Because it does not have AAV terminal repeats it should not package. Although the possibility of recombination with another mutant template exists, the packaged product would still have mutant TRs.

AAV normally requires Ad helper functions to initiate a productive infection, however, downstream integration studies must be done in the complete absence of Ad. In order to produce AAV in an Ad free environment, we included plasmid pDG. This plasmid supplies the Ad helper genes E1a, E1b, E2a, and the VA RNA in *trans* to facilitate productive AAV replication, but cannot generate infectious Ad.

Rescue and Replication From Duplex DNA Is Linked To Rep Nicking Activity

The results from the *in vitro* studies suggested that the reduced nicking efficiencies might impede excision from the plasmid backbone and DNA

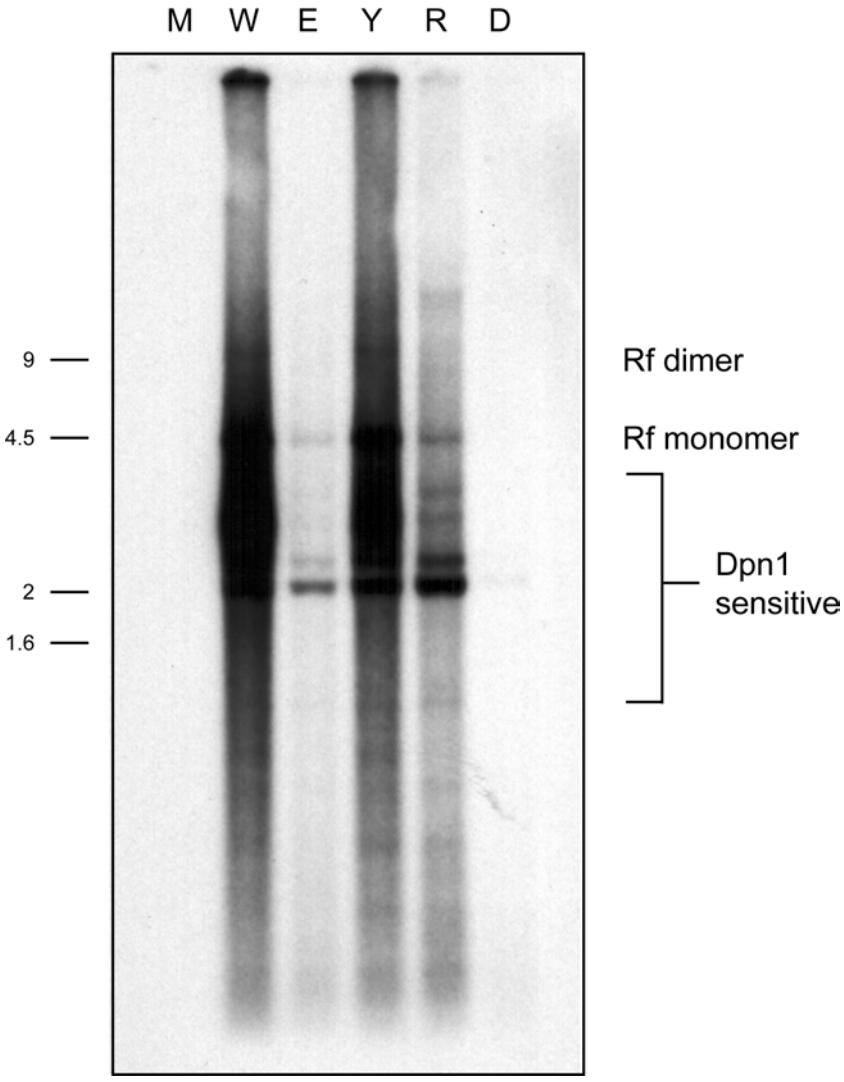

Figure 4-3. Replication of transfected wild type and mutant no-end constructs. HEK 293 cells were transfected with equal molar amounts of wild type and no-end constructs, 100-fold molar excess of Ad helper plasmid pDG and pIM45. Cells were harvested 48 hours post transfection and low molecular weight DNA was extracted by Hirt method. Equal DNA volumes were digested with DpnI, separated on a 0.7% agarose gel, transferred to nitrocellulose, and probed by Southern analysis with an [α-^{32}P]dATP random primed pIM45 XbaI fragment. Monomer and dimer virus DNA replication forms are indicated. M, mock transfected cells; W, wt; E, MutE, Y; MutY; R, MutR; D, MutD.

replication *in vivo*. To compare the efficiency of rescue and replication from a plasmid template, low molecular weight DNA from crude virus stocks was prepared by Hirt extraction (8). Isolated DNA was digested with DpnI to remove residual methylated plasmid DNA and separated on a 1% agarose gel. DNA was transferred to Hybond-N and examined by Southern analysis with an [α-^{32}P]-dATP labeled pIM45 XbaI fragment probe (Fig. 4-3). This blot revealed a correlation between Rep nicking activity and AAV DNA synthesis. Compared to wild-type virus MutR and MutE had markedly reduced accumulation of replication products. Interestingly, MutY and MutD replicated at lower rates than those predicted by *trs* cleavage assays. Binding assays detected only slight differences in Rep:TR complex formation (approx 2-fold, data not shown) between WT, MutY, and MutD and suggest that these mutations disrupt association with other cellular factors that enhance Rep nicking, AAV DNA synthesis or both.

Physical Characterization of Mutant Virus

Carter and Myers originally proposed that during a productive AAV infection capsid protein monomers rapidly associate to form an empty capsid that matures over several hours by insertion of the genome into the virion (15). Deletion of the TR from either wild type or recombinant AAV during production results in empty capsid preparations suggesting that it is a necessary DNA packaging signal. In accord with this view, cellular or unrelated plasmid DNA has not been observed as packaging substrates for the capsid. In one *in vitro* packaging study, AAV DNA without TRs was found associated with the capsid. But it was susceptible to DNaseI digestion, suggesting that the binding was non-specific (38). A

plasmid consisting of a single TR flanked by two D-stem sequences can be rescued, replicated, and packaged further supporting the TR as the crucial encapsidation signal and replication origin (36).

To assess the ability of mutant TRs to direct DNA packaging into the capsid, virus stocks were treated with and without DNaseI prior to Hirt DNA extraction. Recovered DNA was denatured and slot blotted onto nitrocellulose for hybridization analysis using an [α $^{-32}$P]-dATP labeled pIM45 XbaI fragment probe (Fig 4-4). Phosphorimager quantitation shows that all virus preparations were able to package DNA to some extent. As expected, the amount of total DNA was greater than the amount of DNaseI protected DNA (Fig 4-4). The percentage of packaged DNA never exceeded 25%, suggesting that template availability was not rate limiting and that encapsidation is a relatively inefficient process. By generating a standard curve from the pIM45 control plasmid band intensities, the titer of each virus preparation was determined so that we could accurately infect tissue culture cells.

Mutations in the TR Affect The Kinetics Of AAV DNA Accumulation

Given that nicking appeared to be important for efficient replication from a covalently closed duplex molecule, we sought to determine whether this nicking requirement remained when replicating from a linear genomic template. 293 cells were infected with the mutant panel at an MOI=5 and an Ad5 MOI=1. Infected cells were harvested at 4, 24, 48 and 72 hours post infection and total cellular DNA was extracted. Equal amounts of DNA were separated on a 1% agarose gel, transferred to nitrocellulose and probed with an [α-^{32}P]-dATP labeled pIM45 XbaI fragment probe (Fig. 4-5). Consistent with the transfection

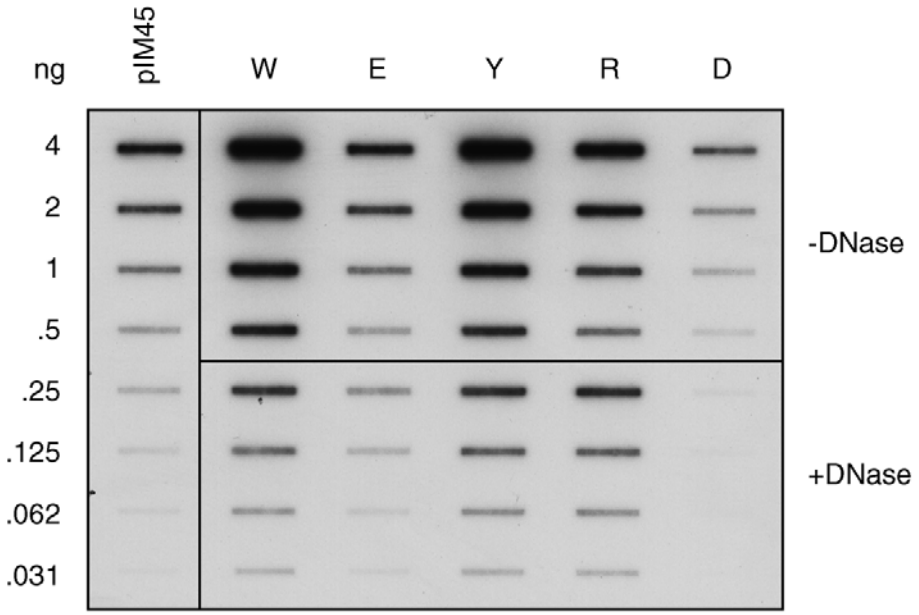

Figure 4-4. Virus titer determination. Equal volumes of virus stocks were incubated with and without DNaseI and DNA was extracted by Hirt method. Two-fold serial dilutions were slot blotted onto nitrocellulose and analyzed by hybridization with an [α^{32}P]-dATP random primed pIM45 XbaI fragment probe. The amounts of viral DNA were quantitated by phosphor imager analysis. Two-fold serial dilutions of pIM45 DNA were included to serve as a hybridization control and a DNA standard curve. W, wild type; E, MutE; Y, MutY; R, MutR; D, MutD.

experiments, MutY rapidly accumulated more DNA than wild type. In addition, MutD revealed a 24 hour lag period and accumulated much less DNA than any other mutant. In contrast to the results from transfection, MutE and MutR, replicated at levels that were equal to or exceeded wild type, respectively. The results for MutR and MutE were inconsistent with what we observed during transfection studies. This suggested that AAV DNA synthesis from a linear genome was no longer linked to trs cleavage.

Hirt DNA was extracted from a second infection and the amounts of packaged and unpackaged AAV DNA was determined DNaseI I resistance. The overall pattern of DNA replication was qualitatively similar to the previous infection. With the exception of MutD, the remaining viruses accumulated significant levels of genomic DNA (Fig. 4-6A). Virus stocks treated with DNaseI I to remove residual plasmid or capsid associated DNA that may been retained from the transfection. With the exception of MutD, which did not package DNA within our range of sensitivity, the remaining viruses packaged significant amounts of DNA similar to the results from virus production (Fig. 4-6B). Interestingly, when we measured the amount of packaged to unpackaged DNA at 24 and 48 hours post infection, wild type AAV was found to have packaged all of the available genomic templates. In this particular case, it is not possible to determine whether capsid availability or second-strand synthesis is the rate-limiting step in virus production. Although, inducing abnormally high p40 expression by down-regulation of Rep protein expression leads to 10-fold higher levels of packaged DNA (11), suggesting that sufficient replicated DNA is

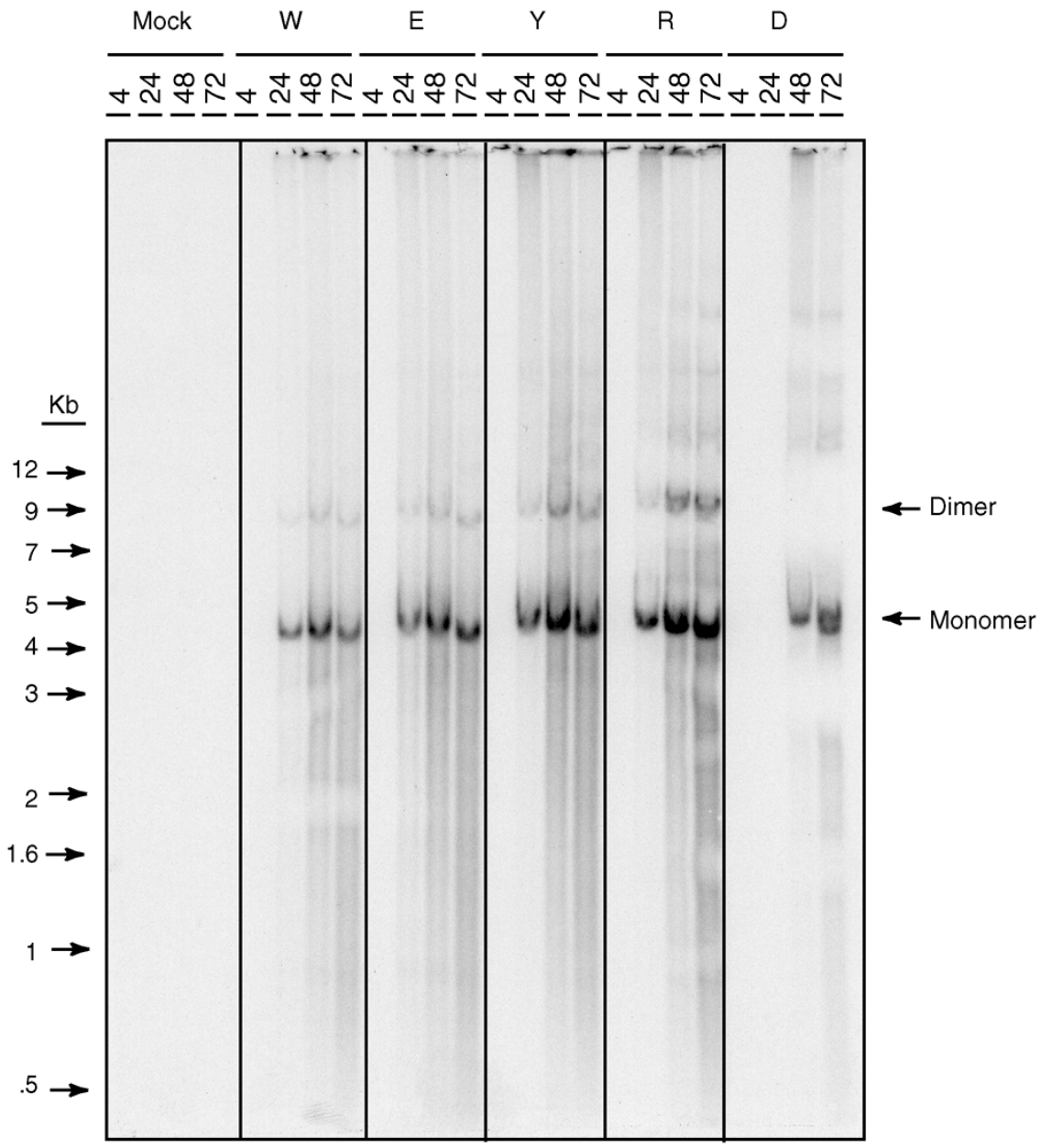

Figure 4-5. *In vivo* replication of wt and mutant virus panel. HEK 293 cells were infected with wild type and mutant viruses (MOI=10) and Ad5 (MOI=5). Cells were harvested at 6, 24, 48, and 72 hours post infection and low molecular weight DNA was extracted by the Hirt method. Equal volumes of DNA were separated on a 0.7% agarose gel, transferred to nitrocellulose, and analyzed by Southern method with an [α^{32}P]-dATP random primed pIM45 XbaI fragment probe. W, wild type; E, MutE; Y, MutY; R, MutR; D, MutD.

available for more efficient packaging. With the exception of MutD, the remaining viruses packaged variably less DNA, but their overall packaging efficiency was significantly higher when compared to the transfection studies. The excess of free genomic DNA for MutE, MutY and MutR suggest that in these cases template concentration is not limiting for virus maturation.

Rep and Cap Protein Expression Correlate To Early Template Levels

Although it was possible that mutations engineered into the TR disrupted the normal process of DNA packaging it was also conceivable that an altered transcription pattern led to reduced capsid accumulation. To examine the kinetics of accumulation of the Rep and Cap protein levels, radio-immunoprecipitation assay (RIPA) extracts were prepared and analyzed by western blotting using the 1F (anti-Rep) and B1 (anti-Cap) monoclonal antibodies (Fig. 4-7). As expected, no Rep or Cap proteins were detected in mock infected or AAV only infected cells. We concluded that all of the mutant viruses were still absolutely dependent on adenovirus for a productive infection. When cells were co-infected with adenovirus, with the exception of MutD, the remaining virus extracts contained detectable amounts of the four rep proteins. At 24 hours post infection, the level of Rep expression correlated well to the amount of genomic template (Compare Fig. 4-5, Fig. 4-6, and Fig 4-7). In contrast, at 48 hours post infection although the genomic template concentrations of MutE and MutR were higher than the other viruses, less Rep protein was observed than would be predicted if copy number alone determined expression levels. The positive transcriptional effects exerted when the large Reps bind to the TR is well

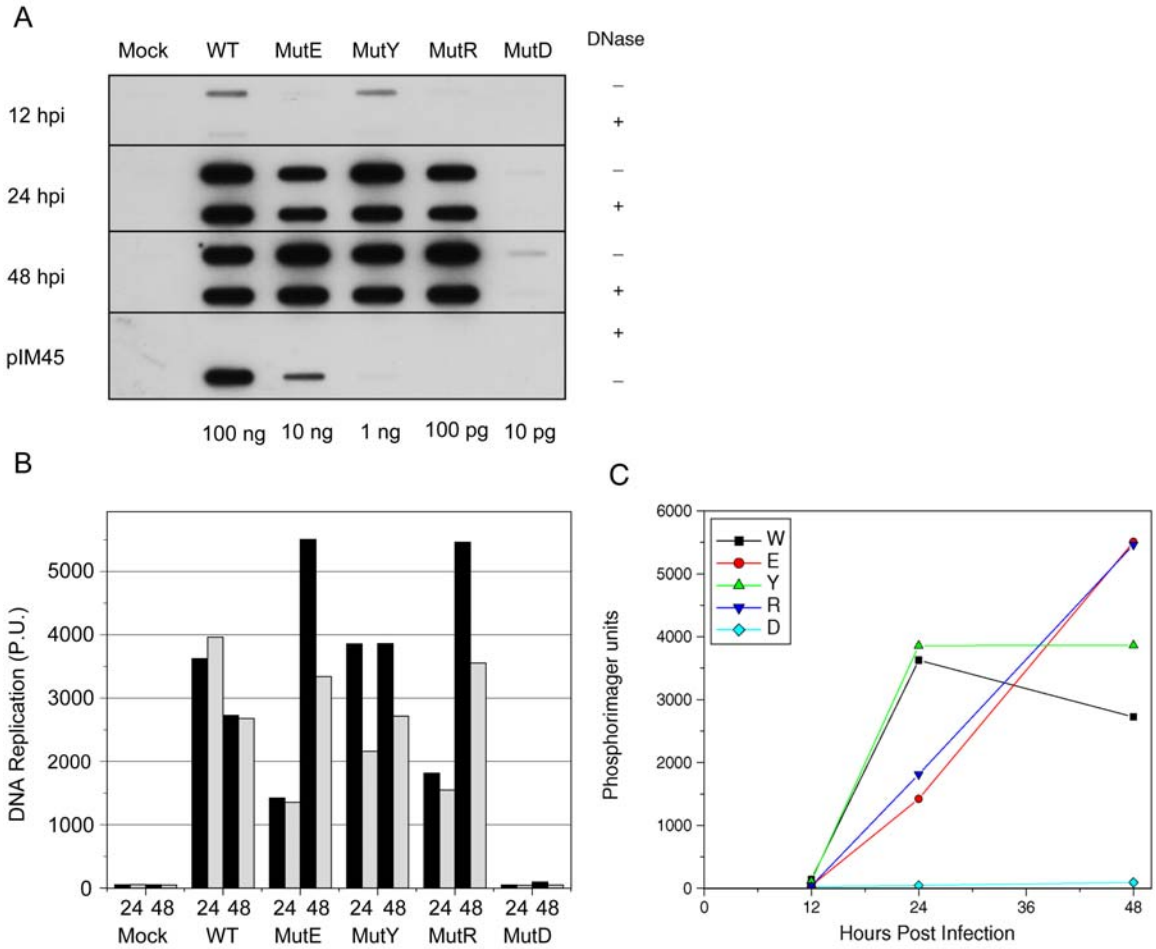

Figure 4-6. Quantitation of the *in vivo* DNA replication and packaging levels of viruses with mutations in their TR. A) Southern blot of total and encapsidated DNA from virus preparations. Total DNA (-DNaseI I) and packaged DNaseI I (+DNaseI) were slot blotted onto nitrocellulose and analyzed by Southern method with an [α32P]-dATP random primed pIM45 XbaI fragment probe. pIM45 DNA was included with 10 µg of 293 genomic DNA to show DNaseI I activity and as a positive hybridization control. B) Histogram comparing the levels of total DNA (black bars) and packaged DNA (gray bars). C) Graph showing the accumulation of total replicated DNA (-DNaseI I) from (A).

documented providing an ostensible explanation for the decreased Rep expression of MutR. It is not immediately clear why MutE has a similar phenotype, however this mutation may affect interactions between the TR and the cellular transcription complex. The lack of detectable Rep expression from MutD could be due low transcription template availability resulting from inefficient replication, or by Rep mediated repression of the p5 and p19 promoters thought to occur at low Rep concentrations.

Like the Rep proteins, which demonstrated a strict helper function requirement, capsid expression was not detected in the absence of Ad (Fig 4-7B). In the presence of Ad, all of the viruses synthesized readily detectable capsid protein. Given that wild type, MutE, MutY, and MutR showed robust replication and Rep expression, capsid protein synthesis was expected. In contrast, although rep is absent (Fig. 4-7A) and there is a low level of genomic template (Fig. 4-6), MutD capsid proteins were abundant after a 24-hour lag period. RNA analysis of the mutant panel showed that the kinetics and accumulation of mRNA's was roughly equivalent to replicated DNA levels (Fig. 4-8). The unexpected capsid protein expression from MutD suggests that cellular factors alone can support expression from the p40 promoter. It is possible, however, that Rep is present in concentrations not detected in our assay, yet sufficient to transactivate p40. Slightly more confusing is how the low RNA level of MutD was still able to support active capsid protein synthesis. This result suggests that a fairly large proportion of AAV mRNA is unavailable to the ribosome or inefficiently translated.

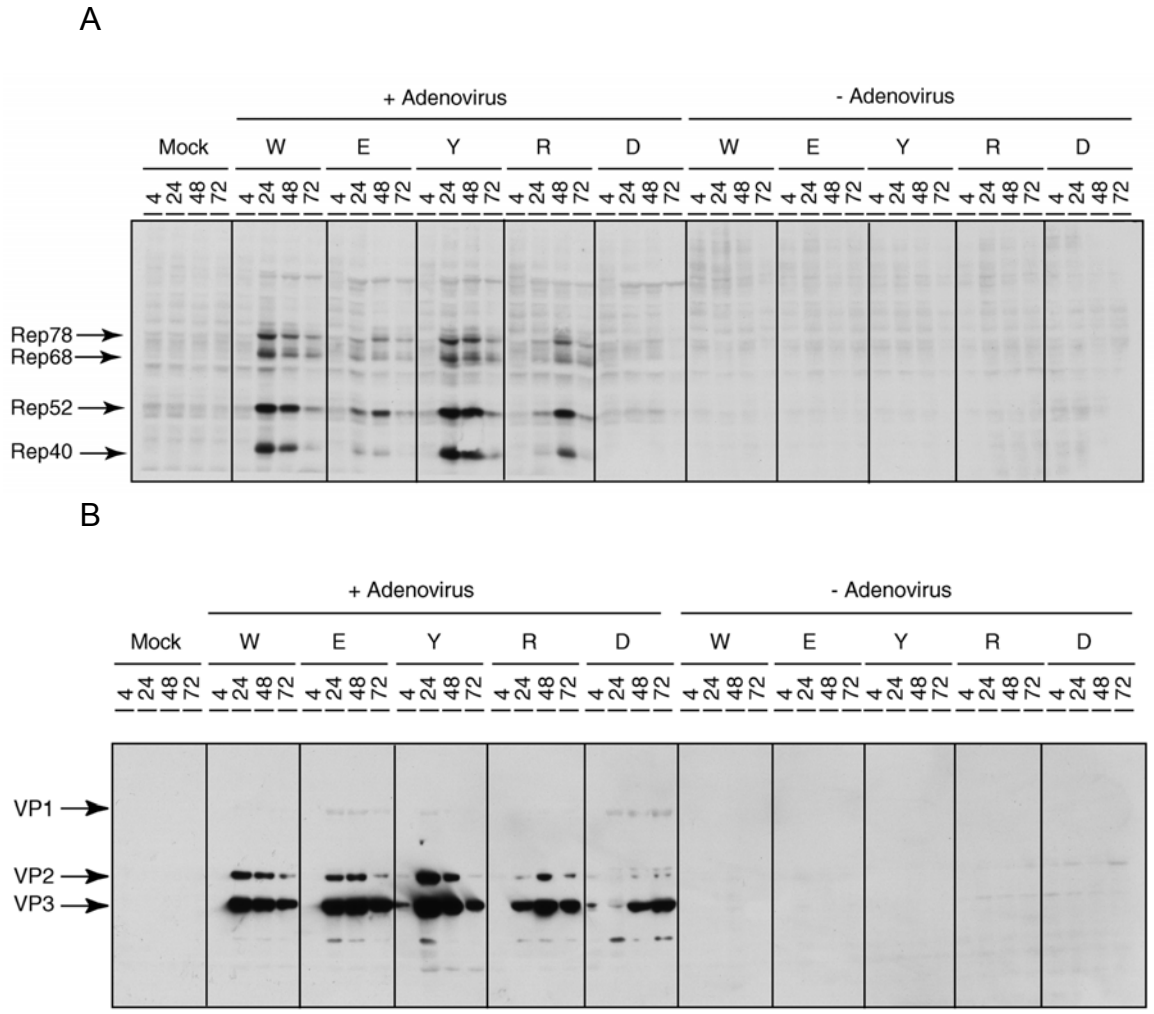

Figure 4-7. Western blot of radio-immunoprecipitation extracts prepared from wild type and mutant virus panel time course infection. In each case, 10 µg of total protein was separated by 8% SDS-PAGE, transferred to nitrocellulose and probed with the appropriate antibody. A) Regulatory proteins were detected with 1F antibody. B) Structural proteins were detected with B1 antibody. W, Wild type; E, MutE; Y, MutY; R, MutR, D; MutD.

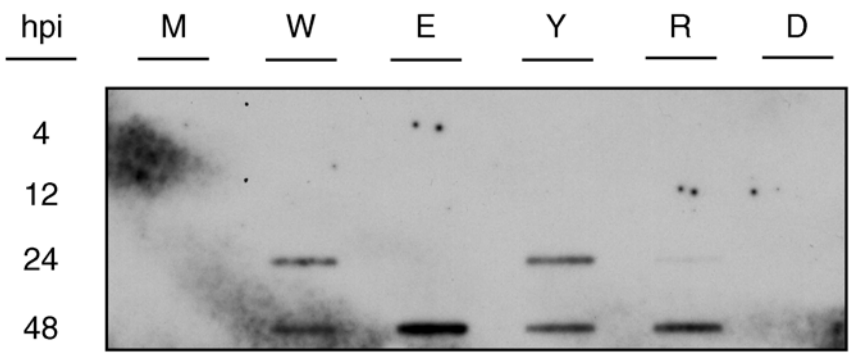

Figure 4-8. RNA expression of the wild type and the AAV mutant panel in 293 cells. Cells were infected at an AAV MOI=5 and Ad5 at an MOI = 1. Cells were harvested at the time points indicated. Total RNA was extracted using a Qiagen RNA extraction protocol, slot blotted to nitrocellulose and probed an [α^{32}P]-dATP random primed pIM45 XbaI fragment probe. W, Wild type; E, MutE; Y, MutY; R, MutR, D; MutD.

Characterization of the Detroit 6 Cell Line and Development Of A PCR Based Provirus-Chromosome 19 Integration Assay

AAV2 can preferentially integrate into the p19.2ter region in human chromosome 19 when Rep is present(25). The Detroit 6 human cell line is known to harbor an AAV2 provirus in tandem repeat fashion that can efficiently be rescued with adenovirus superinfection (9). This cell line was incorporated into our experiments as a positive control for AAV integration. To ensure that the clonal Detroit 6 cell line used in these experiments had not spontaneously deleted any provirus sequence and contained rescue competent AAV terminal repeats, cells were infected with and without Ad5, incubated for 48 hours, and harvested. Low molecular weight DNA was extracted by the Hirt procedure and digested with restriction enzymes that cut AAV2 DNA in a diagnostic manner (Fig 4-9A). The digestion products were separated on a 1% agarose gel, transferred to nitrocellulose, and probed with an [α-^{32}P] dATP random prime labeled pIM45 XbaI fragment probe (Fig. 4-9B). In the absence of Ad, no virus signal was detected indicating the Detroit 6 cell line does not harbor an AAV episome, and also demonstrates that genomic contamination of the Hirt extract was negligible. In the presence of Ad, a banding pattern consistent with a 4.7 kb provirus was detected. These results suggest that a full-length provirus without significant mutations in the TR region is fully capable of efficient excision and replication from Detroit 6 DNA.

Having established that the Detroit 6 cell line would serve as an appropriate control, we adapted a successful PCR based approach to detect the existence of a provirus integrated in the AAVS1 region (5, 28). Primers specific for the AAV

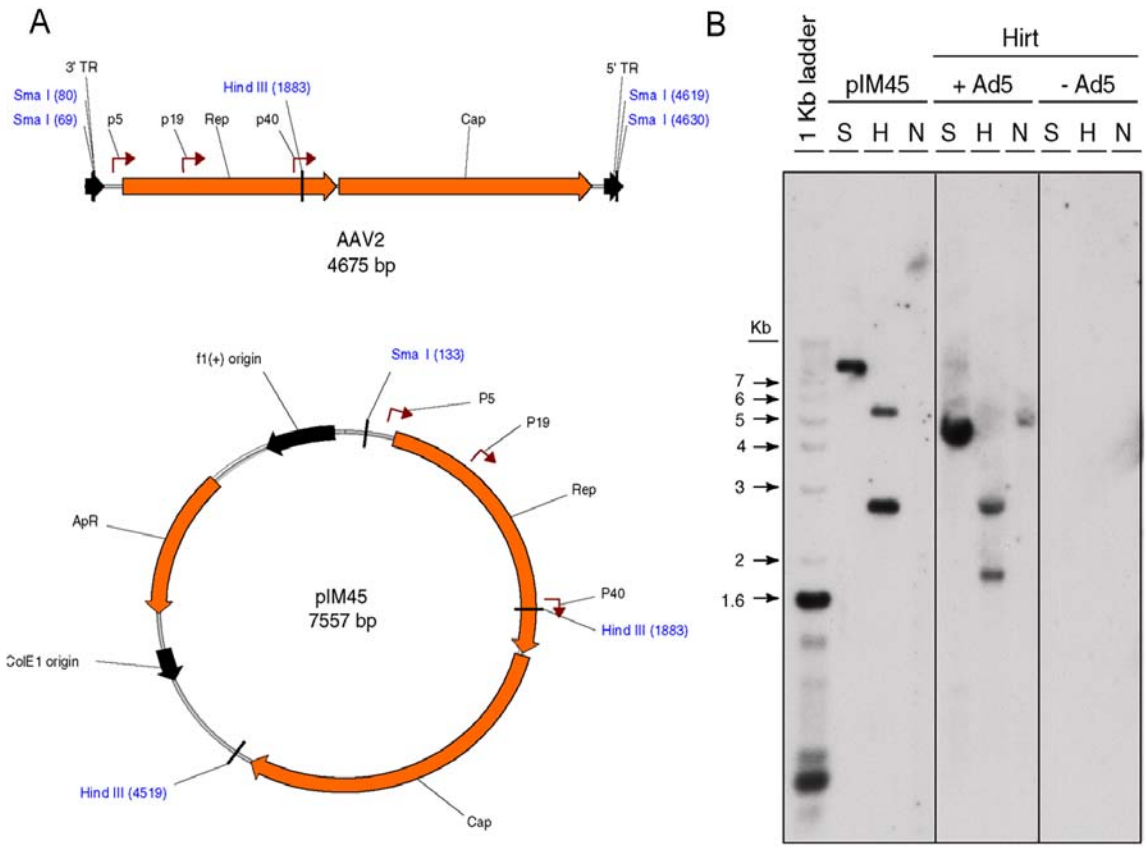

Figure 4-9. Rescue and replication of wild type AAV from the Detroit 6 cell line. (A) Vector Nti clone maps of restriction endonuclease sites in AAV2 and pIM45. (B) Detroit 6 cells were infected with or without Ad and harvested 48 hours post-infection. Low molecular weight DNA was extracted by the Hirt method, digested with the indicated enzyme, separated on a 1% agarose gel and probed with an [α-^{32}P] dATP random prime labeled pIM45 XbaI fragment probe. S, SmaI; H; Hind III; N, no enzyme.

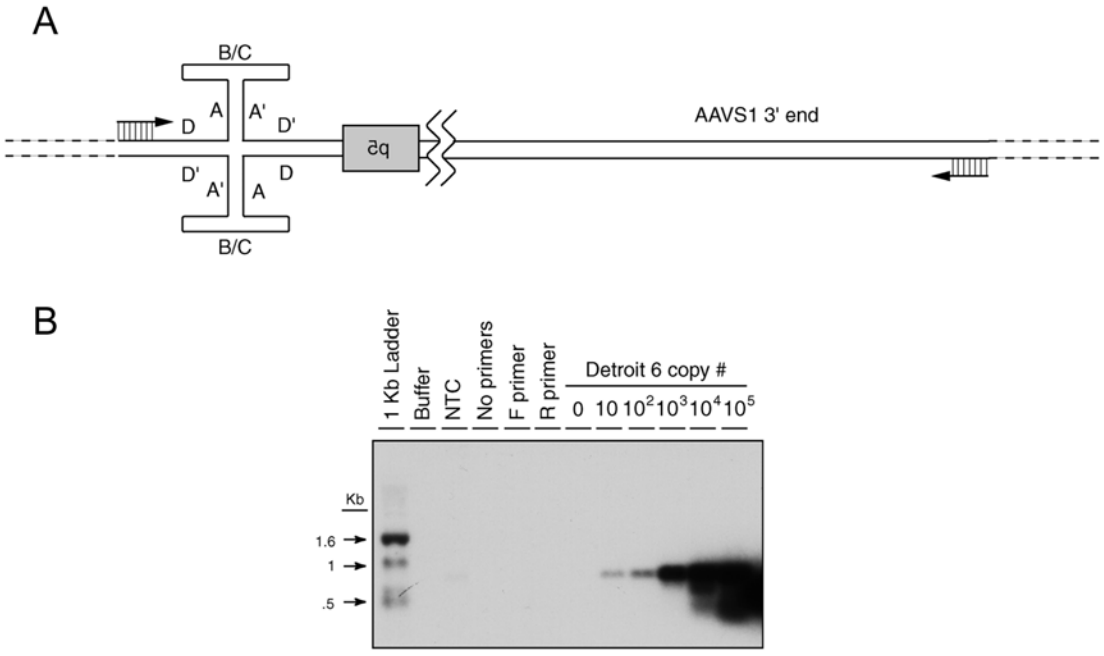

Figure 4-10. Characterization of a PCR based integration assay. A) Schematic of Detroit 6 AAV provirus and downstream AAVS1 sequence. They gray box indicates the duplicated p5 promoter in reverse orientation. The arrows indicate primer-binding regions on the AAV D-stem and the far 3' end of the AAVS1 region. The double wavy line indicates intervening sequence removed for clarity. B) PCR reactions were separated on a 1% agarose gel, transferred to nitrocellulose, and probed with an [α-^{32}P] dATP random prime labeled pIM45 XbaI fragment probe. The number of Detroit 6 genomes included in each reaction is indicated. Reactions were supplemented with the appropriate number of AAV2-free 293 cell line genomes to maintain a constant 10^5 total genomes per reaction. Buffer, no template, primers, or genomic DNA; NTC, no template control; F, forward; R, reverse.

D-stem and a downstream region of the AAVS1 chromosomal integration site were designed and included in a reaction buffer containing genomic template DNA extracted from Detroit 6 cells. A schematic of the primer binding positions and expected amplicon is diagrammed in (Fig. 4-10A). As the integration frequency of AAV2 is a relatively inefficient process (~ .1%), for future experiments it was important to estimate the sensitivity of the assay. To this end, Detroit 6 DNA was serially diluted keeping the total number of genomic copies constant by adding back an appropriate amount of provirus-free 293 genomic DNA. Products from this PCR assay were separated on a 1% agarose gel, transferred to nitrocellulose and examined by southern analysis using an [α-^{32}P]-dATP labeled pIM45 XbaI fragment probe. Under the given reaction conditions it was consistently possible to detect a 750 bp product down to 10 copies of provirus containing DNA per reaction with a linear range of almost 5-orders of magnitude (Fig. 4-10B). To demonstrate primer specificity and the absence of reagent contamination, buffer only, no template, and left, right and both primer only controls were included. These lanes showed no product accumulation and validated our assay.

Integration Is Prevented By Mutations In The RBE and Nicking Site

In order to examine the kinetics of proviral integration a time course infection using the mutant panel in the absence of adenovirus was performed. 293 cells were infected with the mutant panel at an AAV MOI=100 and harvested at 4, 24, 48, 72 hours post infection. Total cellular DNA was extracted and included in the PCR assay described in the previous section. Amplification products were slot blotted onto nitrocellulose and analyzed by hybridization with

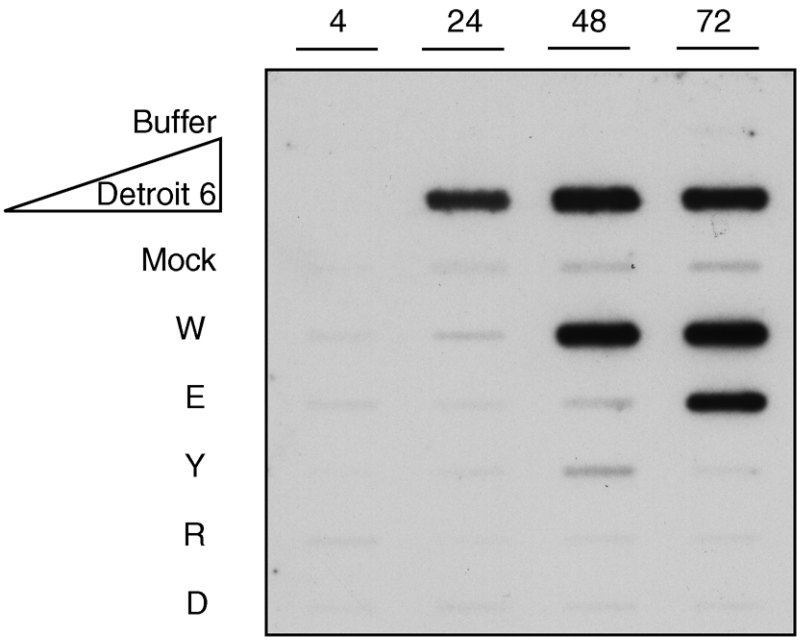

Figure 4-11. Integration of wt and mutant TR containing constructs. Hela cells infected with wild type and mutant AAV viruses and harvested a 4, 24, 48, and 72 hours post infection. 200ng genomic DNA extracted from infected HeLa cells was included in each PCR reaction. Amplification products were slot blotted onto nitrocellulose and probed with an [α-^{32}P] dATP random prime labeled pIM45 XbaI fragment probe. Buffer row contains all reaction products except template DNA. Detroit 6 row contains 0, 10. 100, 500 ng genomic DNA extracted from Detroit 6 cells. W, wild type; E, MutE; Y, MutY; R, MutR; D, MutD.

an [α-^{32}P] dATP random prime labeled pIM45 XbaI fragment probe. As shown in Fig 4.11, the first detectable integration event was observed with wild-type virus at 48 hours post infection. In contrast, all of the mutant viruses appeared to be defective for integration when compared to wild type. MutE was capable of integration, however this activity was delayed until 72 hours post infection. MutY, MutR, and MutD appeared to be completely defective for integration within the time the cells were harvested. Although the delay in MutE proviral integration suggests that there is a nicking requirement for integration, that MutR was completely defective suggests that Rep association with the RBE is more important during integration than *trs* cleavage. This hypothesis is supported by MutY, which contained the most efficiently cleaved TR but was unable to integrate into a proviral status.

Discussion

The purpose of these experiments was to address to contribution of nicking of the terminal repeat of AAV2 to the processes of rescue, replication, transcription, packaging and integration. We confirmed the results from previous studies that identified specific transversion mutations in the TR that increased and decreased nicking (2). *In vitro* replication from a plasmid template showed corresponding accumulation of replication products after transfection into HeLa cells.

Virus Replication

The *in vivo* DNA replication phenotypes of mutations in the TR that affected Rep nicking and binding did not precisely correspond to the *in vitro* results. We found that low nicking efficiencies *in vitro* still supported AAV DNA replication

nearly equal to wild type *in vivo*. This suggested that the relatively high Rep expression levels produced during an infection are sufficient to overcome the decrease in nicking. MutY was predicted to replicate at higher levels than we observed, although it did accumulate DNA at a faster and to a greater extent than wild type. MutR replicated at higher levels than predicted, suggesting again that Rep expression levels were sufficient to overcome this defect. MutD showed low levels of monomer only observed after prolonged exposure to and confirms previous studies that suggested that the D-stem is critical for rescue and replication from a plasmid (30-32).

An AAV DNA binding protein known as the single-stranded D-stem binding protein (ssDBP) has been identified as a negative regulator of AAV DNA replication. It is a cellular protein called FKBP-52 that binds specifically to both the positive and negative DNA stand of the AAV TR D-stem (29). ssDBP is phosphorylated on tyrosine residues and in this form it binds to the TR and prevents AAV leading strand DNA replication. Addition of adenovirus or the tyrosine kinase inhibitor genestein causes dephosphorylation and resumes AAV DNA replication. The core binding sequence of ssDBP was determined by sequence analysis, and we hypothesized that by incorporating mutations that prevented binding, we might be able to generate an autonomously replicating dependovirus. The results from *in vivo* replication studies from a plasmid template as well as a viral infection determined this may not be true. The inability to generate an Ad independent AAV2 using this template suggests to us that

other required cellular factors bind to the D-stem. This is supported by the inability of this virus to efficiently replicate in the presence of Ad.

Rep and Cap Protein Expression

Protein expression levels were initially linked to the concentration of replicating DNA. This contrasted to later times during infection when there was no overt correlation between these two activities. In fact, there appeared to be a negative correlation between template and protein amounts. In particular, MutE and MutE showed delayed and reduced Rep expression yet had consistently higher levels of replicated DNA at later time points. Rep has been shown to both negatively and positively regulate each of the three AAV promoters and the TRs in a binding dependent manner suggesting a possible mechanism for lower protein expression levels for MutR. The results for MutE are more difficult to explain, because we currently have no data that suggests nicking is directly involved in transcriptional activation or regulation.

In general, capsid protein synthesis showed a progression similar to Rep expression levels. An exception to this was MutD that had clearly lower levels of replicated DNA and mRNA transcription, yet after a 24-hour lag period, begun synthesizing capsid proteins at nearly wild-type levels. Given that the overall transcript levels correlated to Rep expression and DNA replication, this suggests that p40 transcripts are fundamentally different than p5 or p19 transcripts. Even if sufficient protein was still available to minimally transactivate only the p40 promoter yet below limit of detection for a western blot assay, the very low transcript levels of MutD, suggest that AAV mRNA is composed to two subsets. The first is a large pool that is not suitable for translation/export even though it is

abundantly synthesized. The second is a much smaller pool of AAV mRNA that is likely to be efficiently exported and serve as a template for multiple rounds of translation.

DNA Packaging

All of the mutations incorporated in this study had some effect on DNA packaging. When rescue from a transfected double stranded plasmid was required, none of virus preparations were able to package more than 25% of the available DNA. In contrast, when cells were infected with single stranded virus that did not have to undergo rescue, at least 50% of the available DNA for the entire mutant panel was packaged. This suggests that inefficient terminal resolution will negatively affect the titers of virus preparations, something we observed. By normalizing for DNA replication *in vivo*, we determined that MutE, MutY, MutR, and MutD packaged comparatively less DNA than wild type. The reasons for this are not entirely clear but suggest that even relatively minor mutations in the TR affect insertion of genome into the capsid.

DNA Integration

By taking a synthetic approach to production, we were able to generate virus stocks having heterologous TRs that were entirely free of Ad contamination. This enabled us to examine the capacity for these viruses to integrate. We found that all of the mutations impaired DNA integration compared to wild type. Not surprisingly, when mutations in the RBE were included, this virus was completely defective for DNA integration suggesting that Rep bound to the TR, the AAVS1 RBE homolog or both, is critical for integration. Because RBE and trs sites exist in both the TR and the AAVS1 and because of the inherent DNA cleavage

associated with endonucleolytic cleavage, it has been suggested that nicking participates in provirus integration. Recently, Young et al. observed that a replication deficient recombinant AAV having a *trs* mutation was still capable of integration (37). Results from our in vitro integration assay support this observation as MutE had a similar phenotype. This suggests that cellular factors have a catalytic activity in the process of integration.

APPENDIX A
ADDITIONAL AAV CAPSID DATA

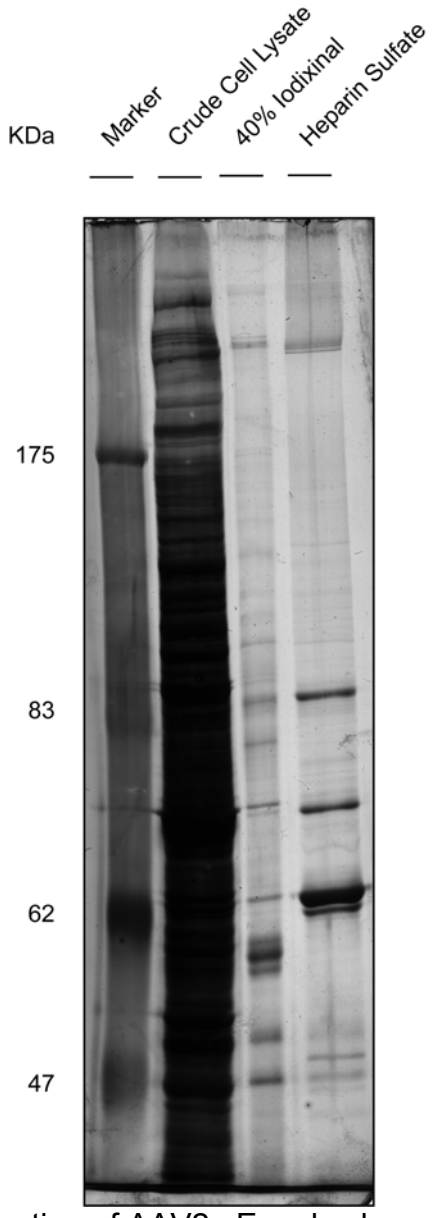

Figure A-1. Affinity Purification of AAV2. Equal volumes of fractions taken from various stages of virus purification were separated by 10% SDS-PAGE. Proteins were visualized by the silver stain method.

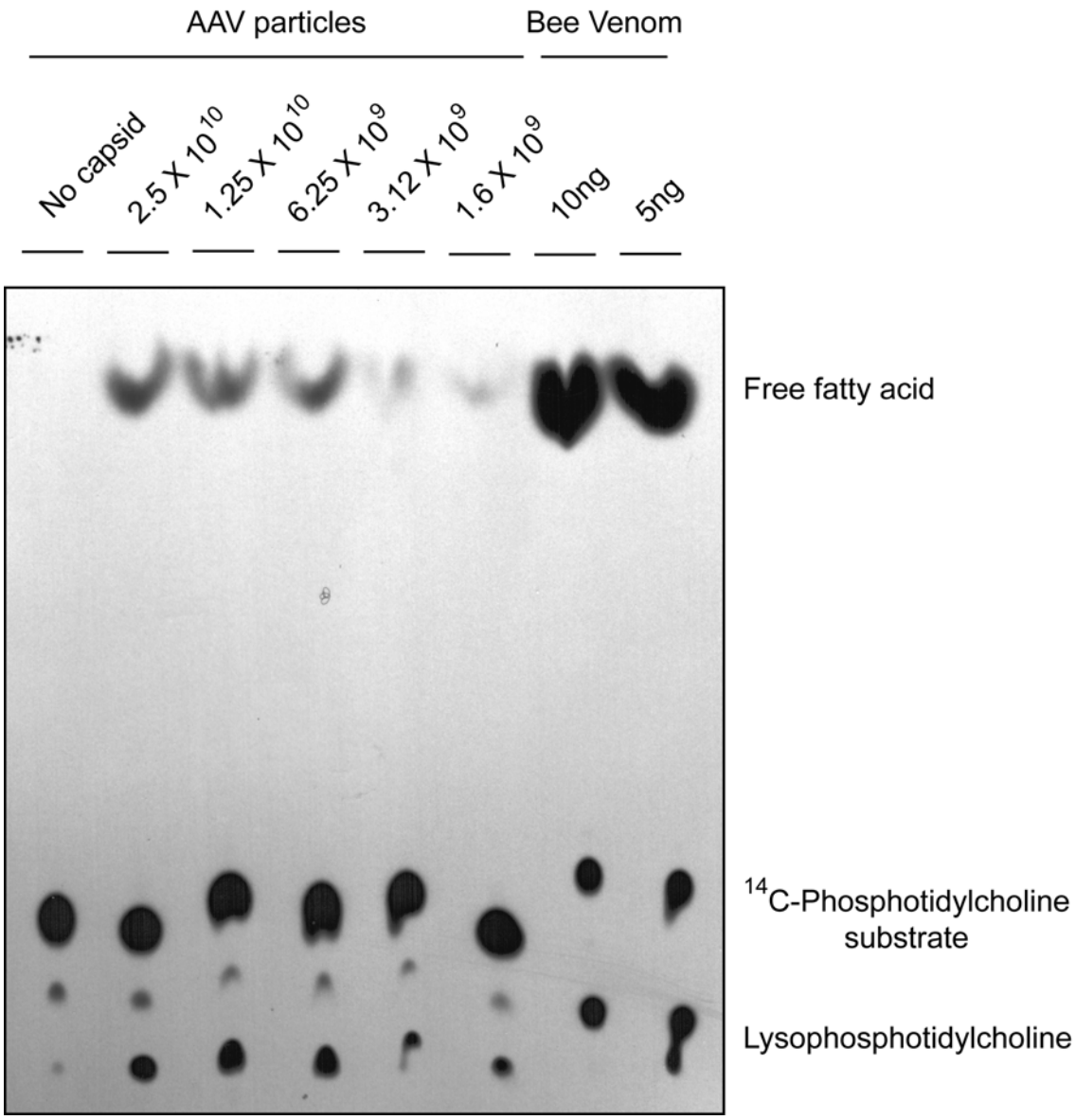

Figure A-2. The AAV capsid contains phospholipase A2-like activity. Wild type AAV2 capsid mixed micelle assays were performed on ^{14}C-phosphotidylcholine substrate under different enzyme concentrations after mild heat denaturation as described in the materials and methods. Products from the reaction were precipitated, dissolved in chloroform:methanol (2:1) and separated by silica gel thin layer chromatography. Silica plates were exposed to film for autoradiography.

LIST OF REFERENCES

1. **Bantel Schaal, U.** 1991. Infection with adeno-associated parvovirus leads to increased sensitivity of mammalian cells to stress. Virology **182:**260-268.

2. **Bantel Schaal, U., and H. zur Hausen.** 1984. Characterization of the DNA of a defective human parvovirus isolated from a genital site. Virology **134:**52-63.

3. **Barrijal, S., M. Perros, Z. Gu, B. L. Avalosse, P. Belenguer, F. Amalric, and J. Rommelaere.** 1992. Nucleolin forms a specific complex with a fragment of the viral (minus) strand of minute virus of mice DNA. Nucleic Acids Res. **20:**5053-5060.

4. **Bartlett, J. S., R. Wilcher, and R. J. Samulski.** 2000. Infectious entry pathway of adeno-associated virus and adeno-associated virus vectors. J. Virol. **74:**2777-2785.

5. **Batchu, R. B., D. A. Miles, T. M. Rechtin, R. R. Drake, and P. L. Hermonat.** 1995. Cloning, expression and purification of full length Rep78 of adeno-associated virus as a fusion protein with maltose binding protein in Escherichia coli. Biochem. Biophys. Res. Commun. **208:**714-720.

6. **Bauer, H. J., and G. Monreal.** 1986. Herpesviruses provide helper functions for avian adeno-associated parvovirus. J. Gen. Virol. **67:**181-185.

7. **Becerra, S. P., F. Koczot, P. Fabisch, and J. A. Rose.** 1988. Synthesis of adeno-associated virus structural proteins requires both alternative mRNA splicing and alternative initiations from a single transcript. J. Virol. **62:**2745-2754.

8. **Becerra, S. P., J. A. Rose, M. Hardy, B. M. Baroudy, and C. W. Anderson.** 1985. Direct mapping of adeno-associated virus capsid proteins B and C: a possible ACG initiation codon. Proc. Natl. Acad. Sci. USA **82:**7919-7923.

9. **Beck, S. E., L. A. Jones, K. Chesnut, S. M. Walsh, T. C. Reynolds, B. J. Carter, F. B. Askin, T. R. Flotte, and W. B. Guggino.** 1999. Repeated delivery of adeno-associated virus vectors to the rabbit airway. J. Virol. **73:**9446-9455.

10. **Bergelson, J. M., J. A. Cunningham, G. Droguett, E. A. Kurt-Jones, A. Krithivas, J. S. Hong, M. S. Horwitz, R. L. Crowell, and R. W. Finberg.** 1997. Isolation of a common receptor for Coxsackie B viruses and adenoviruses 2 and 5. Science **275:**1320-1323.

11. **Brister, J. R., and N. Muzyczka.** 2000. Mechanism of Rep-mediated adeno-associated virus origin nicking. J. Virol. **74:**7762-7771.

12. **Brister, J. R., and N. Muzyczka.** 1999. Rep-mediated nicking of the adeno-associated virus origin requires two biochemical activities, DNA helicase activity and transesterification. J. Virol. **73:**9325-9336.

13. **Buller, R. M., and J. A. Rose.** 1978. Characterization of adeno-associated virus-induced polypeptides in KB cells. J. Virol. **25:**331-338.

14. **Carter, B. J., B. A. Antoni, and D. F. Klessig.** 1992. Adenovirus containing a deletion of the early region 2A gene allows growth of adeno-associated virus with decreased efficiency. Virology **191:**473-476.

15. **Carter, B. J., C. J. Marcus Sekura, C. A. Laughlin, and G. Ketner.** 1983. Properties of an adenovirus type 2 mutant, Ad2dl807, having a deletion near the right-hand genome terminus: failure to help AAV replication. Virology **126:**505-516.

16. **Chamberlin, N. L., B. Du, S. de Lacalle, and C. B. Saper.** 1998. Recombinant adeno-associated virus vector: use for transgene expression and anterograde tract tracing in the CNS. Brain Res. **793:**169-175.

17. **Cheung, A. K., M. D. Hoggan, W. W. Hauswirth, and K. I. Berns.** 1980. Integration of the adeno-associated virus genome into cellular DNA in latently infected human Detroit 6 cells. J. Virol. **33:**739-748.

18. **Chiorini, J. A., S. Afione, and R. M. Kotin.** 1999. Adeno-associated virus (AAV) type 5 Rep protein cleaves a unique terminal resolution site compared with other AAV serotypes. J. Virol. **73:**4293-4398.

19. **Chiorini, J. A., F. Kim, L. Yang, and R. M. Kotin.** 1999. Cloning and characterization of adeno-associated virus type 5. J. Virol. **73:**1309-1319.

20. **Chiorini, J. A., M. D. Weitzman, R. A. Owens, E. Urcelay, B. Safer, and R. M. Kotin.** 1994. Biologically active Rep proteins of adeno-associated virus type 2 produced as fusion proteins in Escherichia coli. J. Virol. **68:**797-804.

21. **Clark, K. R., X. Liu, J. P. McGrath, and P. R. Johnson.** 1999. Highly purified recombinant adeno-associated virus vectors are biologically active and free of detectable helper and wild-type viruses. Hum. Gene Ther. **10:**1031-1039.

22. **Clark, K. R., F. Voulgaropoulou, and P. R. Johnson.** 1996. A stable cell line carrying adenovirus-inducible rep and cap genes allows for infectivity titration of adeno-associated virus vectors. Gene Ther. **3:**1124-1132.

23. **Conrad, C. K., S. S. Allen, S. A. Afione, T. C. Reynolds, S. E. Beck, M. Fee-Maki, X. Barrazza-Ortiz, R. Adams, F. B. Askin, B. J. Carter, W. B. Guggino, and T. R. Flotte.** 1996. Safety of single-dose administration of an adeno-associated virus (AAV)-CFTR vector in the primate lung. Gene Ther. **3:**658-668.

24. **Dechecchi, M. C., P. Melotti, A. Bonizzato, M. Santacatterina, M. Chilosi, and G. Cabrini.** 2001. Heparan sulfate glycosaminoglycans are receptors sufficient to mediate the initial binding of adenovirus types 2 and 5. J. Virol. **75:**8772-8780.

25. **Dechecchi, M. C., A. Tamanini, A. Bonizzato, and G. Cabrini.** 2000. Heparan sulfate glycosaminoglycans are involved in adenovirus type 5 and 2-host cell interactions. Virology **268:**382-390.

26. **DiGabriele, A. D., I. Lax, D. I. Chen, C. M. Svahn, M. Jaye, J. Schlessinger, and W. A. Hendrickson.** 1998. Structure of a heparin-linked biologically active dimer of fibroblast growth factor. Nature **393:**812-817.

27. **Donello, J. E., J. E. Loeb, and T. J. Hope.** 1998. Woodchuck hepatitis virus contains a tripartite posttranscriptional regulatory element. J. Virol. **72:**5085-5092.

28. **Douar, A. M., K. Poulard, D. Stockholm, and O. Danos.** 2001. Intracellular trafficking of adeno-associated virus vectors: routing to the late endosomal compartment and proteasome degradation. J. Virol. **75:**1824-1833.

29. **Duan, D., Q. Li, A. W. Kao, Y. Yue, J. E. Pessin, and J. F. Engelhardt.** 1999. Dynamin is required for recombinant adeno-associated virus type 2 infection. J. Virol. **73:**10371-10376.

30. **Duan, D., Y. Yue, Z. Yan, and J. F. Engelhardt.** 2003. Trans-splicing vectors expand the packaging limits of adeno-associated virus for gene therapy applications. Methods Mol Med **76:**287-307.

31. **Duan, D., Y. Yue, Z. Yan, J. Yang, and J. F. Engelhardt.** 2000. Endosomal processing limits gene transfer to polarized airway epithelia by adeno-associated virus. J. Clin. Invest. **105:**1573-1587.

32. **Dyall, J., P. Szabo, and K. I. Berns.** 1999. Adeno-associated virus (AAV) site-specific integration: formation of AAV-AAVS1 junctions in an in vitro system. Proc. Natl. Acad. Sci. USA **96:**12849-12854.

33. **Fisher, K. J., K. Jooss, J. Alston, Y. Yang, S. E. Haecker, K. High, R. Pathak, S. E. Raper, and J. M. Wilson.** 1997. Recombinant adeno-associated virus for muscle directed gene therapy. Nat. Med. **3:**306-312.

34. **Flotte, T., A. Agarwal, J. Wang, S. Song, E. S. Fenjves, L. Inverardi, K. Chesnut, S. Afione, S. Loiler, C. Wasserfall, M. Kapturczak, T. Ellis, H. Nick, and M. Atkinson.** 2001. Efficient ex vivo transduction of pancreatic islet cells with recombinant adeno-associated virus vectors. Diabetes **50:**515-520.

35. **Flotte, T. R., R. Solow, R. A. Owens, S. Afione, P. L. Zeitlin, and B. J. Carter.** 1992. Gene expression from adeno-associated virus vectors in airway epithelial cells. Am. J. Respir. Cell. Mol. Biol. **7:**349-356.

36. **Freese, A., M. G. Kaplitt, W. M. O'Connor, M. Abbey, D. Langer, P. Leone, M. J. O'Connor, and M. J. During.** 1997. Direct gene transfer into human epileptogenic hippocampal tissue with an adeno-associated virus vector: implications for a gene therapy approach to epilepsy. Epilepsia **38:**759-766.

37. **Fry, E. E., S. M. Lea, T. Jackson, J. W. Newman, F. M. Ellard, W. E. Blakemore, R. Abu-Ghazaleh, A. Samuel, A. M. King, and D. I. Stuart.** 1999.

The structure and function of a foot-and-mouth disease virus- oligosaccharide receptor complex. EMBO J **18:**543-554.

38. **Gao, G. P., M. R. Alvira, L. Wang, R. Calcedo, J. Johnston, and J. M. Wilson.** 2002. Novel adeno-associated viruses from rhesus monkeys as vectors for human gene therapy. Proc. Natl. Acad. Sci. USA **99:**11854-11859.

39. **Gavin, D. K., S. M. Young, Jr., W. Xiao, B. Temple, C. R. Abernathy, D. J. Pereira, N. Muzyczka, and R. J. Samulski.** 1999. Charge-to-alanine mutagenesis of the adeno-associated virus type 2 Rep78/68 proteins yields temperature-sensitive and magnesium-dependent variants [published erratum appears in J. Virol. 2000 Jan;74(1):591]. J. Virol. **73:**9433-9445.

40. **Giraud, C., E. Winocour, and K. I. Berns.** 1994. Site-specific integration by adeno-associated virus is directed by a cellular DNA sequence. .Proc.Natl.Acad.Sci.U.S.A. **91:**10039-10043.

41. **Girod, A., M. Ried, C. Wobus, H. Lahm, K. Leike, J. Kleinschmidt, G. Deleage, and M. Hallek.** 1999. Genetic capsid modifications allow efficient re-targeting of adeno- associated virus type 2 [published erratum appears in Nat. Med. 1999 Dec;5(12):1438]. Nat. Med. **5:**1052-1056.

42. **Girod, A., C. E. Wobus, Z. Zadori, M. Ried, K. Leike, P. Tijssen, J. A. Kleinschmidt, and M. Hallek.** 2002. The VP1 capsid protein of adeno-associated virus type 2 is carrying a phospholipase A2 domain required for virus infectivity. J. Gen. Virol. **83:**973-978.

43. **Green, M. R., and R. G. Roeder.** 1980. Definition of a novel promoter for the major adenovirus-associated virus mRNA. Cell **22:**231-242.

44. **Green, M. R., and R. G. Roeder.** 1980. Transcripts of the adeno-associated virus genome: mapping of the major RNAs. J. Virol. **36:**79-92.

45. **Grifman, M., M. Trepel, P. Speece, L. B. Gilbert, W. Arap, R. Pasqualini, and M. D. Weitzman.** 2001. Incorporation of tumor-targeting peptides into recombinant adeno- associated virus capsids. Mol. Ther. **3:**964-975.

46. **Grimm, D., A. Kern, K. Rittner, and J. A. Kleinschmidt.** 1998. Novel tools for production and purification of recombinant adenoassociated virus vectors. Hum. Gene Ther. **9:**2745-2760.

47. **Handa, A., S. Muramatsu, J. Qiu, H. Mizukami, and K. E. Brown.** 2000. Adeno-associated virus (AAV)-3-based vectors transduce haematopoietic cells not susceptible to transduction with AAV-2-based vectors. J. Gen. Virol. **81:**2077-2084.

48. **Hauswirth, W. W., and K. I. Berns.** 1977. Origin and termination of adeno-associated virus DNA replication. Virology **78:**488-499.

49. **Hermens, W. T., O. ter Brake, P. A. Dijkhuizen, M. A. Sonnemans, D. Grimm, J. A. Kleinschmidt, and J. Verhaagen.** 1999. Purification of recombinant

adeno-associated virus by iodixanol gradient ultracentrifugation allows rapid and reproducible preparation of vector stocks for gene transfer in the nervous system. Hum. Gene Ther. **10:**1885-1891.

50. **Hermonat, P. L., M. A. Labow, R. Wright, K. I. Berns, and N. Muzyczka.** 1984. Genetics of adeno-associated virus: isolation and preliminary characterization of adeno-associated virus type 2 mutants. J. Virol. **51:**329-339.

51. **Hileman, R. E., J. R. Fromm, J. M. Weiler, and R. J. Linhardt.** 1998. Glycosaminoglycan-protein interactions: definition of consensus sites in glycosaminoglycan binding proteins. Bioessays **20:**156-167.

52. **Hirt, B.** 1967. Selective extraction of polyoma DNA from infected mouse cell cultures. J. Mol. Biol. **26:**365-369.

53. **Hoggan, M. D., N. R. Blacklow, and W. P. Rowe.** 1966. Studies of small DNA viruses found in various adenovirus preparations: physical, biological, and immunological characteristics. Proc. Natl. Acad. Sci. USA **55:**1467-1474.

54. **Hoque, M., K. Ishizu, A. Matsumoto, S. I. Han, F. Arisaka, M. Takayama, K. Suzuki, K. Kato, T. Kanda, H. Watanabe, and H. Handa.** 1999. Nuclear transport of the major capsid protein is essential for adeno- associated virus capsid formation. J. Virol. **73:**7912-7915.

55. **Hunter, L. A., and R. J. Samulski.** 1992. Colocalization of adeno-associated virus Rep and capsid proteins in the nuclei of infected cells. J.Virol. **66:**317-324.

56. **Im, D. S., and N. Muzyczka.** 1990. The AAV origin binding protein Rep68 is an ATP-dependent site-specific endonuclease with DNA helicase activity. Cell **61:**447-457.

57. **Im, D. S., and N. Muzyczka.** 1992. Partial purification of adeno-associated virus Rep78, Rep52, and Rep40 and their biochemical characterization. J.Virol. **66:**1119-1128.

58. **Janik, J. E., M. M. Huston, K. Cho, and J. A. Rose.** 1989. Efficient synthesis of adeno-associated virus structural proteins requires both adenovirus DNA binding protein and VA I RNA. Virology **168:**320-329.

59. **Kaludov, N., K. E. Brown, R. W. Walters, J. Zabner, and J. A. Chiorini.** 2001. Adeno-associated virus serotype 4 (AAV4) and AAV5 both require sialic acid binding for hemagglutination and efficient transduction but differ in sialic acid linkage specificity. J. Virol. **75:**6884-6893.

60. **Kessler, P. D., G. M. Podsakoff, X. Chen, S. A. McQuiston, P. C. Colosi, L. A. Matelis, G. J. Kurtzman, and B. J. Byrne.** 1996. Gene delivery to skeletal muscle results in sustained expression and systemic delivery of a therapeutic protein. Proc. Natl. Acad. Sci. USA **93:**14082-14087.

61. **King, J. A., R. Dubielzig, D. Grimm, and J. A. Kleinschmidt.** 2001. DNA helicase-mediated packaging of adeno-associated virus type 2 genomes into preformed capsids. EMBO J. **20:**3282-3291.

62. **Klein, R. L., E. M. Meyer, A. L. Peel, S. Zolotukhin, C. Meyers, N. Muzyczka, and M. A. King.** 1998. Neuron-specific transduction in the rat septohippocampal or nigrostriatal pathway by recombinant adeno-associated virus vectors. Exp. Neurol. **150:**183-194.

63. **Kotin, R. M., and K. I. Berns.** 1989. Organization of adeno-associated virus DNA in latently infected Detroit 6 cells. Virology **170:**460-467.

64. **Kotin, R. M., M. Siniscalco, R. J. Samulski, X. D. Zhu, L. Hunter, C. A. Laughlin, S. McLaughlin, N. Muzyczka, M. Rocchi, and K. I. Berns.** 1990. Site-specific integration by adeno-associated virus. Proc. Natl. Acad. Sci. USA **87:**2211-2215.

65. **Kraulis, P. J.** 1991. MOLSCRIPT: a program to produce both detailed and schematic plots of protein structures. J. Appl. Cryst. **24:**946-950.

66. **Kronenberg, S., J. A. Kleinschmidt, and B. Bottcher.** 2001. Electron cryo-microscopy and image reconstruction of adeno-associated virus type 2 empty capsids. EMBO Rep **2:**997-1002.

67. **Laughlin, C. A., N. Jones, and B. J. Carter.** 1982. Effect of deletions in adenovirus early region 1 genes upon replication of adeno-associated virus. J. Virol. **41:**868-876.

68. **Leonard, C. J., and K. I. Berns.** 1994. Cloning, expression, and partial purification of Rep78: an adeno-associated virus replication protein. Virology **200:**566-573.

69. **Li, J., R. J. Samulski, and X. Xiao.** 1997. Role for highly regulated rep gene expression in adeno-associated virus vector production. J. Virol. **71:**5236-5243.

70. **Linden, R. M., E. Winocour, and K. I. Berns.** 1996. The recombination signals for adeno-associated virus site-specific integration. Proc. Natl. Acad. Sci. USA **93:**7966-7972.

71. **Liu, J., and S. C. Thorp.** 2002. Cell surface heparan sulfate and its roles in assisting viral infections. Med. Res. Rev. **22:**1-25.

72. **Lusby, E., K. H. Fife, and K. I. Berns.** 1980. Nucleotide sequence of the inverted terminal repetition in adeno-associated virus DNA. J. Virol. **34:**402-409.

73. **Mandel, R. J., S. K. Spratt, R. O. Snyder, and S. E. Leff.** 1997. Midbrain injection of recombinant adeno-associated virus encoding rat glial cell line-derived neurotrophic factor protects nigral neurons in a progressive 6-hydroxydopamine-induced degeneration model of Parkinson's disease in rats. Proc. Natl. Acad. Sci. USA **94:**14083-14088.

74. **McCarty, D. M., M. Christensen, and N. Muzyczka.** 1991. Sequences required for coordinate induction of adeno-associated virus p19 and p40 promoters by Rep protein. J. Virol. **65:**2936-2945.

75. **McCarty, D. M., D. J. Pereira, I. Zolotukhin, X. Zhou, J. H. Ryan, and N. Muzyczka.** 1994. Identification of linear DNA sequences that specifically bind the adeno-associated virus Rep protein. J. Virol. **68:**4988-4997.

76. **McCarty, D. M., J. H. Ryan, S. Zolotukhin, X. Zhou, and N. Muzyczka.** 1994. Interaction of the adeno-associated virus Rep protein with a sequence within the A palindrome of the viral terminal repeat. J. Virol. **68:**4998-5006.

77. **McLaughlin, S. K., P. Collis, P. L. Hermonat, and N. Muzyczka.** 1988. Adeno-associated virus general transduction vectors: analysis of proviral structures. J. Virol. **62:**1963-1973.

78. **McPherson, R. A., L. J. Rosenthal, and J. A. Rose.** 1985. Human cytomegalovirus completely helps adeno-associated virus replication. Virology **147:**217-222.

79. **Merritt, E. A., and D. J. Bacon.** 1997. Raster3D Photorealistic Molecular Graphics, p. 505-24, Methods In Enzymology, vol. 277.

80. **Mishra, L., and J. A. Rose.** 1990. Adeno-associated virus DNA replication is induced by genes that are essential for HSV-1 DNA synthesis. Virology **179:**632-639.

81. **Moskalenko, M., L. Chen, M. van Roey, B. A. Donahue, R. O. Snyder, J. G. McArthur, and S. D. Patel.** 2000. Epitope mapping of human anti-adeno-associated virus type 2 neutralizing antibodies: implications for gene therapy and virus structure. J. Virol. **74:**1761-1766.

82. **Mulloy, B., and R. J. Linhardt.** 2001. Order out of complexity--protein structures that interact with heparin. Curr. Opin. Struct. Biol. **11:**623-628.

83. **Muzyczka, N., and K. I. Berns.** 2001. Parvoviridae: The viruses and their replication, p. 2327-2360. *In* D. M. Knipe and P. M. Howley (ed.), Fields Virology, Fourth ed. Lippincott Williams and Wilkins, New York.

84. **Myers, M. W., and B. J. Carter.** 1980. Assembly of adeno-associated virus. Virology **102:**71-82.

85. **Nakai, H., S. R. Yant, T. A. Storm, S. Fuess, L. Meuse, and M. A. Kay.** 2001. Extrachromosomal recombinant adeno-associated virus vector genomes are primarily responsible for stable liver transduction in vivo. J. Virol. **75:**6969-6976.

86. **Ni, T. H., W. F. McDonald, I. Zolotukhin, T. Melendy, S. Waga, B. Stillman, and N. Muzyczka.** 1998. Cellular proteins required for adeno-associated virus DNA replication in the absence of adenovirus coinfection. J. Virol. **72:**2777-2787.

87. **Ni, T. H., X. Zhou, D. M. McCarty, I. Zolotukhin, and N. Muzyczka.** 1994. In vitro replication of adeno-associated virus DNA. J. Virol. **68:**1128-1138.

88. **Nicholls, A., K. Sharp, and B. Honig.** 1991. PROTEINS, Structure, Function and Genetics **11:**281.

89. **Nicklin, S. A., H. Buening, K. L. Dishart, M. de Alwis, A. Girod, U. Hacker, A. J. Thrasher, R. R. Ali, M. Hallek, and A. H. Baker.** 2001. Efficient and selective AAV2-mediated gene transfer directed to human vascular endothelial cells. Mol. Ther. **4:**174-181.

90. **Owens, R. A., M. D. Weitzman, S. R. Kyostio, and B. J. Carter.** 1993. Identification of a DNA-binding domain in the amino terminus of adeno-associated virus Rep proteins. J. Virol. **67:**997-1005.

91. **Pante, N., and M. Kann.** 2002. Nuclear pore complex is able to transport macromolecules with diameters of about 39 nm. Mol. Biol. Cell. **13:**425-434.

92. **Parks, W. P., M. Green, M. Pina, and J. L. Melnick.** 1967. Physicochemical characterization of adeno-associated satellite virus type 4 and its nucleic acid. J.Virol. **1:**980-987.

93. **Pereira, D. J., and N. Muzyczka.** 1997. The cellular transcription factor SP1 and an unknown cellular protein are required to mediate Rep protein activation of the adeno-associated virus p19 promoter. J. Virol. **71:**1747-1756.

94. **Qing, K., C. Mah, J. Hansen, S. Zhou, V. Dwarki, and A. Srivastava.** 1999. Human fibroblast growth factor receptor 1 is a co-receptor for infection by adeno-associated virus 2. Nat. Med. **5:**71-77.

95. **Qiu, J., and K. E. Brown.** 1999. A 110-kDa nuclear shuttle protein, nucleolin, specifically binds to adeno-associated virus type 2 (AAV-2) capsid. Virology **257:**373-382.

96. **Qiu, J., A. Handa, M. Kirby, and K. E. Brown.** 2000. The interaction of heparin sulfate and adeno-associated virus 2. Virology **269:**137-147.

97. **Quinn, C. O., and G. R. Kitchingman.** 1986. Functional analysis of the adenovirus type 5 DNA-binding protein: site-directed mutants which are defective for adeno-associated virus helper activity. J. Virol. **60:**653-661.

98. **Rabinowitz, J. E., F. Rolling, C. Li, H. Conrath, W. Xiao, X. Xiao, and R. J. Samulski.** 2002. Cross-packaging of a single adeno-associated virus (AAV) type 2 vector genome into multiple AAV serotypes enables transduction with broad specificity. J. Virol. **76:**791-801.

99. **Rabinowitz, J. E., and R. J. Samulski.** 2000. Building a better vector: the manipulation of AAV virions. Virology **278:**301-308.

100. **Rabinowitz, J. E., W. Xiao, and R. J. Samulski.** 1999. Insertional mutagenesis of AAV2 capsid and the production of recombinant virus. Virology **265:**274-285.

101. **Ren, J., X. Qu, J. B. Chaires, J. P. Trempe, S. S. Dignam, and J. D. Dignam.** 1999. Spectral and physical characterization of the inverted terminal repeat DNA structure from adenoassociated virus 2. Nucleic Acids Res. **27:**1985-1990.

102. **Ried, M. U., A. Girod, K. Leike, H. Buning, and M. Hallek.** 2002. Adeno-associated virus capsids displaying immunoglobulin-binding domains permit antibody-mediated vector retargeting to specific cell surface receptors. J. Virol. **76:**4559-4566.

103. **Rossmann, M. G., and J. E. Johnson.** 1989. Icosahedral RNA virus structure. Annu. Rev. Biochem. **58:**533-573.

104. **Ruffing, M., H. Heid, and J. A. Kleinschmidt.** 1994. Mutations in the carboxy terminus of adeno-associated virus 2 capsid proteins affect viral infectivity: lack of an RGD integrin-binding motif. J. Gen. Virol. **75:**3385-3392.

105. **Rutledge, E. A., C. L. Halbert, and D. W. Russell.** 1998. Infectious clones and vectors derived from adeno-associated virus (AAV) serotypes other than AAV type 2. J. Virol. **72:**309-319.

106. **Ryan, J. H., S. Zolotukhin, and N. Muzyczka.** 1996. Sequence requirements for binding of Rep68 to the adeno-associated virus terminal repeats. J. Virol. **70:**1542-1553.

107. **Samulski, R. J., K. I. Berns, M. Tan, and N. Muzyczka.** 1982. Cloning of adeno-associated virus into pBR322: rescue of intact virus from the recombinant plasmid in human cells. Proc. Natl. Acad. Sci. USA **79:**2077-2081.

108. **Samulski, R. J., L. S. Chang, and T. Shenk.** 1987. A recombinant plasmid from which an infectious adeno-associated virus genome can be excised in vitro and its use to study viral replication. J. Virol. **61:**3096-3101.

109. **Samulski, R. J., A. Srivastava, K. I. Berns, and N. Muzyczka.** 1983. Rescue of adeno-associated virus from recombinant plasmids: gene correction within the terminal repeats of AAV. Cell **33:**135-143.

110. **Samulski, R. J., X. Zhu, X. Xiao, J. D. Brook, D. E. Housman, N. Epstein, and L. A. Hunter.** 1991. Targeted integration of adeno-associated virus (AAV) into human chromosome 19 [published erratum appears in EMBO J. 1992 Mar;11(3):1228]. EMBO J. **10:**3941-3950.

111. **Sanlioglu, S., P. K. Benson, J. Yang, E. M. Atkinson, T. Reynolds, and J. F. Engelhardt.** 2000. Endocytosis and nuclear trafficking of adeno-associated virus type 2 are controlled by rac1 and phosphatidylinositol-3 kinase activation. J. Virol. **74:**9184-9196.

112. **Schlehofer, J. R., M. Ehrbar, and H. zur Hausen.** 1986. Vaccinia virus, herpes simplex virus, and carcinogens induce DNA amplification in a human cell line and support replication of a helpervirus dependent parvovirus. Virology **152:**110-117.

113. **Seisenberger, G., M. U. Ried, T. Endress, H. Buning, M. Hallek, and C. Brauchle.** 2001. Real-time single-molecule imaging of the infection pathway of an adeno-associated virus. Science **294:**1929-1932.

114. **Senapathy, P., J. D. Tratschin, and B. J. Carter.** 1984. Replication of adeno-associated virus DNA. Complementation of naturally occurring rep- mutants by a wild-type genome or an ori- mutant and correction of terminal palindrome deletions. J. Mol. Biol. **179:**1-20.

115. **Shi, W., G. S. Arnold, and J. S. Bartlett.** 2001. Insertional mutagenesis of the adeno-associated virus type 2 (AAV2) capsid gene and generation of aav2 vectors targeted to alternative cell- surface receptors. Hum. Gene Ther. **12:**1697-1711.

116. **Sieczkarski, S. B., and G. R. Whittaker.** 2002. Dissecting virus entry via endocytosis. J. Gen. Virol. **83:**1535-1545.

117. **Smith, R. H., and R. M. Kotin.** 2000. An adeno-associated virus (AAV) initiator protein, Rep78, catalyzes the cleavage and ligation of single-stranded AAV ori DNA. J. Virol. **74:**3122-3129.

118. **Smith, R. H., and R. M. Kotin.** 1998. The Rep52 gene product of adeno-associated virus is a DNA helicase with 3'-to-5' polarity. J. Virol. **72:**4874-4881.

119. **Smith, R. H., A. J. Spano, and R. M. Kotin.** 1997. The Rep78 gene product of adeno-associated virus (AAV) self-associates to form a hexameric complex in the presence of AAV ori sequences. J. Virol. **71:**4461-4471.

120. **Snyder, R. O., D. S. Im, T. Ni, X. Xiao, R. J. Samulski, and N. Muzyczka.** 1993. Features of the adeno-associated virus origin involved in substrate recognition by the viral Rep protein. J. Virol. **67:**6096-6104.

121. **Snyder, R. O., C. H. Miao, G. A. Patijn, S. K. Spratt, O. Danos, D. Nagy, A. M. Gown, B. Winther, L. Meuse, L. K. Cohen, A. R. Thompson, and M. A. Kay.** 1997. Persistent and therapeutic concentrations of human factor IX in mice after hepatic gene transfer of recombinant AAV vectors. Nat. Genet. **16:**270-276.

122. **Song, S., M. Morgan, T. Ellis, A. Poirier, K. Chesnut, J. Wang, M. Brantly, N. Muzyczka, B. J. Byrne, M. Atkinson, and T. R. Flotte.** 1998. Sustained secretion of human alpha-1-antitrypsin from murine muscle transduced with adeno-associated virus vectors. Proc. Natl. Acad. Sci. USA **95:**14384-14388.

123. **Srivastava, A., E. W. Lusby, and K. I. Berns.** 1983. Nucleotide sequence and organization of the adeno-associated virus 2 genome. J. Virol. **45:**555-564.

124. **Stauber, D. J., A. D. DiGabriele, and W. A. Hendrickson.** 2000. Structural interactions of fibroblast growth factor receptor with its ligands. Proc. Natl. Acad. Sci. USA **97:**49-54.

125. **Straus, S. E., E. D. Sebring, and J. A. Rose.** 1976. Concatemers of alternating plus and minus strands are intermediates in adenovirus-associated virus DNA synthesis. Proc. Natl. Acad. Sci. USA **73:**742-746.

126. **Summerford, C., J. S. Bartlett, and R. J. Samulski.** 1999. AlphaVbeta5 integrin: a co-receptor for adeno-associated virus type 2 infection. Nat. Med. **5:**78-82.

127. **Summerford, C., and R. J. Samulski.** 1998. Membrane-associated heparan sulfate proteoglycan is a receptor for adeno-associated virus type 2 virions. J. Virol. **72:**1438-1445.

128. **Trempe, J. P., E. Mendelson, and B. J. Carter.** 1987. Characterization of adeno-associated virus rep proteins in human cells by antibodies raised against rep expressed in Escherichia coli. Virology **161:**18-28.

129. **Urabe, M., Y. Hasumi, A. Kume, R. T. Surosky, G. J. Kurtzman, K. Tobita, and K. Ozawa.** 1999. Charged-to-alanine scanning mutagenesis of the N-terminal half of adeno- associated virus type 2 Rep78 protein. J. Virol. **73:**2682-2693.

130. **Veldwijk, M. R., J. Topaly, S. Laufs, U. R. Hengge, F. Wenz, W. J. Zeller, and S. Fruehauf.** 2002. Development and optimization of a real-time quantitative PCR-based method for the titration of AAV-2 vector stocks. Mol. Ther. **6:**272-278.

131. **Wang, K., S. Huang, A. Kapoor-Munshi, and G. Nemerow.** 1998. Adenovirus internalization and infection require dynamin. J. Virol. **72:**3455-3458.

132. **Wang, X. S., S. Ponnazhagan, and A. Srivastava.** 1996. Rescue and replication of adeno-associated virus type 2 as well as vector DNA sequences from recombinant plasmids containing deletions in the viral inverted terminal repeats: selective encapsidation of viral genomes in progeny virions. J. Virol. **70:**1668-1677.

133. **Wang, X. S., S. Ponnazhagan, and A. Srivastava.** 1995. Rescue and replication signals of the adeno-associated virus 2 genome. J. Mol. Biol. **250:**573-580.

134. **Wang, X. S., K. Qing, S. Ponnazhagan, and A. Srivastava.** 1997. Adeno-associated virus type 2 DNA replication in vivo: mutation analyses of the D sequence in viral inverted terminal repeats. J. Virol. **71:**3077-3082.

135. **Wang, X. S., and A. Srivastava.** 1997. A novel terminal resolution-like site in the adeno-associated virus type 2 genome. J. Virol. **71:**1140-1146.

136. **Ward, P., F. B. Dean, M. E. O'Donnell, and K. I. Berns.** 1998. Role of the adenovirus DNA-binding protein in in vitro adeno-associated virus DNA replication. J. Virol. **72:**420-427.

137. **Watson, G. L., J. N. Sayles, C. Chen, S. S. Elliger, C. A. Elliger, N. R. Raju, G. J. Kurtzman, and G. M. Podsakoff.** 1998. Treatment of lysosomal storage disease in MPS VII mice using a recombinant adeno-associated virus. Gene Ther. **5:**1642-1649.

138. **Weitzman, M. D., S. R. Kyostio, R. M. Kotin, and R. A. Owens.** 1994. Adeno-associated virus (AAV) Rep proteins mediate complex formation between AAV DNA and its integration site in human DNA. Proc. Natl. Acad. Sci. USA **91:**5808-5812.

139. **Wickham, T. J., E. J. Filardo, D. A. Cheresh, and G. R. Nemerow.** 1994. Integrin alpha v beta 5 selectively promotes adenovirus mediated cell membrane permeabilization. J. Cell Biol. **127:**257-264.

140. **Wickham, T. J., P. Mathias, D. A. Cheresh, and G. R. Nemerow.** 1993. Integrins alpha v beta 3 and alpha v beta 5 promote adenovirus internalization but not virus attachment. Cell **73:**309-319.

141. **Wistuba, A., A. Kern, S. Weger, D. Grimm, and J. A. Kleinschmidt.** 1997. Subcellular compartmentalization of adeno-associated virus type 2 assembly. J. Virol. **71:**1341-1352.

142. **Wistuba, A., S. Weger, A. Kern, and J. A. Kleinschmidt.** 1995. Intermediates of adeno-associated virus type 2 assembly: identification of soluble complexes containing Rep and Cap proteins. J. Virol. **69:**5311-5319.

143. **Wobus, C. E., B. Hugle-Dorr, A. Girod, G. Petersen, M. Hallek, and J. A. Kleinschmidt.** 2000. Monoclonal antibodies against the adeno-associated virus type 2 (AAV-2) capsid: epitope mapping and identification of capsid domains involved in AAV-2-cell interaction and neutralization of AAV-2 infection. J. Virol. **74:**9281-9293.

144. **Wonderling, R. S., S. R. Kyostio, and R. A. Owens.** 1995. A maltose-binding protein/adeno-associated virus Rep68 fusion protein has DNA-RNA helicase and ATPase activities. J. Virol. **69:**3542-3548.

145. **Wonderling, R. S., and R. A. Owens.** 1997. Binding sites for adeno-associated virus Rep proteins within the human genome. J. Virol. **71:**2528-2534.

146. **Wu, J., M. D. Davis, and R. A. Owens.** 1999. Factors affecting the terminal resolution site endonuclease, helicase, and ATPase activities of adeno-associated virus type 2 Rep proteins. J. Virol. **73:**8235-8244.

147. **Wu, P., W. Xiao, T. Conlon, J. Hughes, M. Agbandje-McKenna, T. Ferkol, T. Flotte, and N. Muzyczka.** 2000. Mutational analysis of the adeno-associated virus type 2 (AAV2) capsid gene and construction of AAV2 vectors with altered tropism. J. Virol. **74:**8635-8647.

148. **Xiao, W., K. H. Warrington, Jr., P. Hearing, J. Hughes, and N. Muzyczka.** 2002. Adenovirus-facilitated nuclear translocation of adeno-associated virus type 2. J Virol **76:**11505-11517.

149. **Xiao, X., J. Li, and R. J. Samulski.** 1998. Production of high-titer recombinant adeno-associated virus vectors in the absence of helper adenovirus. J. Virol. **72:**2224-2232.

150. **Xiao, X., W. Xiao, J. Li, and R. J. Samulski.** 1997. A novel 165-base-pair terminal repeat sequence is the sole cis requirement for the adeno-associated virus life cycle. J. Virol. **71:**941-948.

151. **Xie, Q., W. Bu, S. Bhatia, J. Hare, T. Somasundaram, A. Azzi, and M. S. Chapman.** 2002. The atomic structure of adeno-associated virus (AAV-2), a vector for human gene therapy. Proc. Natl. Acad. Sci. USA **99:**10405-10410.

152. **Xu, L., T. Daly, C. Gao, T. R. Flotte, S. Song, B. J. Byrne, M. S. Sands, and K. Parker Ponder.** 2001. CMV-beta-actin promoter directs higher expression from an adeno-associated viral vector in the liver than the cytomegalovirus or elongation factor 1 alpha promoter and results in therapeutic levels of human factor X in mice. Hum. Gene Ther. **12:**563-573.

153. **Yalkinoglu, A. O., R. Heilbronn, A. Burkle, J. R. Schlehofer, and H. zur Hausen.** 1988. DNA amplification of adeno-associated virus as a response to cellular genotoxic stress. Cancer Res. **48:**3123-3129.

154. **Yan, Z., T. C. Ritchie, D. Duan, and J. F. Engelhardt.** 2002. Recombinant AAV-mediated gene delivery using dual vector heterodimerization. Methods Enzymol. **346:**334-357.

155. **Yan, Z., Y. Zhang, D. Duan, and J. F. Engelhardt.** 2000. Trans-splicing vectors expand the utility of adeno-associated virus for gene therapy. Proc. Natl. Acad. Sci. USA **97:**6716-6721.

156. **Yang, Q., A. Kadam, and J. P. Trempe.** 1992. Mutational analysis of the adeno-associated virus rep gene. J. Virol. **66:**6058-6069.

157. **Yang, Q., M. Mamounas, G. Yu, S. Kennedy, B. Leaker, J. Merson, F. Wong-Staal, M. Yu, and J. R. Barber.** 1998. Development of novel cell surface CD34-targeted recombinant adenoassociated virus vectors for gene therapy. Hum. Gene Ther. **9:**1929-1937.

158. **Young, S. M., Jr., and R. J. Samulski.** 2001. Adeno-associated virus (AAV) site-specific recombination does not require a Rep-dependent origin of replication within the AAV terminal repeat. Proc. Natl. Acad. Sci. USA **98:**13525-13530.

159. **Zadori, S., J. Szelei, M.-C. Lacoste, Y. Li, S. Gariepy, P. Raymond, M. Allaire, I. Nabi, and P. Tijssen.** 2001. A viral phopholipase A_2 is required for parvovirus infectivity. Developmental Cell **1:**291-302.

160. **Zhou, C., Q. Yang, and J. P. Trempe.** 1999. Enhancement of UV-induced cytotoxicity by the adeno-associated virus replication proteins. Biochim. Biophys. Acta. **1444:**371-383.

161. **Zhou, X., and N. Muzyczka.** 1998. In vitro packaging of adeno-associated virus DNA. J. Virol. **72:**3241-3247.

162. **Zhou, X., I. Zolotukhin, D. S. Im, and N. Muzyczka.** 1999. Biochemical characterization of adeno-associated virus rep68 DNA helicase and ATPase activities. J. Virol. **73:**1580-1590.

163. **Zolotukhin, S., B. J. Byrne, E. Mason, I. Zolotukhin, M. Potter, K. Chesnut, C. Summerford, R. J. Samulski, and N. Muzyczka.** 1999. Recombinant adeno-associated virus purification using novel methods improves infectious titer and yield. Gene Ther. **6:**973-985.

164. **Zolotukhin, S., M. Potter, W. Hauswirth, J. Guy, and N. Muzyczka.** 1996. A humanized green fluorescent protein cDNA adapted for high level expression in mammalian cells. J. Virol. **70:**4646-4654.

165. **Zolotukhin, S., M. Potter, I. Zolotukhin, Y. Sakai, S. Loiler, T. J. Fraites, Jr., V. A. Chiodo, T. Phillipsberg, N. Muzyczka, W. W. Hauswirth, T. R. Flotte, B. J. Byrne, and R. O. Snyder.** 2002. Production and purification of serotype 1, 2, and 5 recombinant adeno-associated viral vectors. Methods **28:**158-167.

BIOGRAPHICAL SKETCH

Shaun Rueben Opie was born in New Plymouth, New Zealand, on May 23rd, 1972. His parents are Dr. John and Dona Opie and he has one younger sister, Katie. As a result of multiple international moves he attended the Prince of Wales high school in Vancouver, Canada, Our Lady of Mercy grammer school in Liverpool, England, and graduated from Lewisburg High School in Pennsylvania, USA in 1990. He attended Bucknell University, Pennsylvania, where he trained in Drosophila genetics in the laboratory of Dr. John Tonzetitch and received a Bachelor of Science degree in Biology in 1994. After a year-long interlude as a rock-climbing guide in Arizona, Shaun entered graduate school in the Department of Molecular Genetics and Microbiology at the University of Florida in August, 1995. There he pursued his dissertation research in the laboratory of Dr. Nicholas Muzyczka. He plans to pursue a career in genetic medicine.